Renewable and Sustainable Energy Reviews 16 (2012) 5951–5993

Contents lists available at SciVerse ScienceDirect

Renewable and Sustainable Energy Reviews

journal homepage: www.elsevier.com/locate/rser

An overview on heat transfer augmentation using vortex generators and nanofluids: Approaches and applications

H.E. Ahmed [a], H.A. Mohammed [b,*], M.Z. Yusoff [c]

[a] Department of Mechanical Engineering, College of Engineering, University of Anbar, Anbar, Iraq
[b] Department of Thermofluids, Faculty of Mechanical Engineering, Universiti Teknologi Malaysia, 81310 UTM Skudai, Johor Bahru, Malaysia
[c] Centre of Advanced Computational Engineering, College of Engineering, Universiti Tenaga Nasional, Jalan IKRAM-UNITEN, 43000 Kajang, Selangor, Malaysia

ARTICLE INFO

Article history:
Received 23 September 2011
Received in revised form
28 May 2012
Accepted 4 June 2012
Available online 10 August 2012

Keywords:
Heat transfer augmentation
Vortex generators
Nanofluids
Applications

ABSTRACT

The subject of heat transfer enhancement has significant interest to develop the compact heat exchangers in order to obtain a high efficiency, low cost, light weight, and size as small as possible. Therefore, energy cost and environmental considerations are going on to encourage attempts to invent better performance over the existence designs. Streamwise vortices can be generated using small flow manipulators or protrusions such as wings and winglets configurations. Single-pair, single row, or two dimensional array of vortex generators (VGs) can be punched, mounted, attached or embedded in the boundary layer of flow channel. VGs generate longitudinal and transverse vortices, while longitudinal vortices are more efficient for heat transfer enhancement than transverse vortices. A dramatic augmentation in thermal performance of the thermal system can be achieved but pressure drop penalty is existed. Several parameters have been overviewed in this paper, which have pronounced effect on the convective heat transfer coefficient and pressure drop penalty. These parameters are: attack angle of VG, geometry of VG, standard and novel types of VG, spacing between the VG tips, number of pairs of VGs in the flow direction, rectangular or circular array arrangement of VGs, common-flow upper (CFU) or common-flow down (CFD) configuration of VG, pointing up (PU) or pointing down (PD) arrangement of VG with flow direction, Re number, channel aspect ratio, number of tubes of fin-tube heat exchanges (HE), circular or oval tubes of fin-tube HE, and location of VG respect to the tube of HE or from leading edge of the channel. This paper gives an overview about the early studies done in order to improve the performance of thermal systems with minimal pressure losses to derive systems with less negative impact on the environment and high level of energy economic. This study also provides an outlook for future work using nanofluids with vortex generators.

This article is also summarizes the recent experimental and numerical developments on the thermal conductivity measurements of nanofluids, thermal conductivity enhancement, convection and conduction heat transfer, some applications, main problems and suggestions for future works.

Contents

* Corresponding author. Tel.: +6 07 55 34716; fax: +6 07 55 66 159.
E-mail addresses: hamdi_engi@yahoo.com (H.E. Ahmed), hussein.dash@yahoo.com (H.A. Mohammed).

1364-0321/$ - see front matter © 2012 Elsevier Ltd. All rights reserved.
http://dx.doi.org/10.1016/j.rser.2012.06.003

1. Introduction

Compact heat exchangers are widely used in such fields as automobile industries, power systems, heating and air conditioning, chemical engineering, electronic chip cooling and aerospace, etc. This subject has received considerable attention to get high efficiency, low cost, small size, and light weight. For the vehicle industries, an additional benefit can be considered such as a small size for the radiator tends to get a small frontal area of vehicle which in turn leads to diminish the drag force and subsequently minimizes the fuel consumption.

Several engineering applications had held an enormous attention to improve heat transfer performance of the compact heat exchangers in gas–gas and gas–liquid side. For the gas, it is well known that the thermal conductivity of the gas is inherently lower than that of liquid needs to improve its convective heat transfer coefficient. The traditional heat exchangers are generally improved by serve enhancement techniques with concentration on many types of surface augmentation. The augmentation of heat transfer can be done by disrupting the boundary layer growth, increasing the turbulence intensity, and generating secondary flows [1,2]. Fig. 1 shows several types of the compact heat exchangers.

Longitudinal vortex generators (LVGs) are one of the passive methods. It can be mounted on channel surfaces to generate longitudinal vortices which create a secondary flow and disrupt the growth of the boundary layer, disturb the fluid flow and create fluid swirling. It in turn causes a heavy exchange of core and wall fluid and thereby improves the heat transport between the flowing fluid and channel walls. VGs have been extensively studied to their high heat transfer performance [3].

The enhancement of heat transfer by using VGs depends on many parameters such as their shape, their geometries, their position from the leading edge of the test duct, and angles of attack. The geometrical parameters of VGs have more effects on the heat transport. Four basic configurations of VGs are: delta wing, rectangular wing, delta–winglet and rectangular winglet as shown in Fig. 2 [4]. The vortex generators VGs usually take configurations of tiny protrusions which may be incorporated into the main surface of the channel by punching, stamping, attaching, mounting and embossing [1]. Although the heat transfer surface area may be not changed before and after the set up of VG. The fluid flow can be significantly disturbed because of the longitudinal vortices generated by VG. Winglets have been successfully used in order to improve the convective heat transfer rate of modern thermal systems because they can generate intensive longitudinal vortices with less penalties in pressure drop [2].

2. Vortex generators

The vortex may be divided into transverse vortex (TV) and longitudinal vortex (LV) according to its rotating axis direction. The axes of TVs lie perpendicular to the main flow direction, while LVs have their axes parallel to the main flow direction, thus they are also called streamwise vortices. In general, the LVs have been reported to be more effective than TVs on heat transfer enhancement [5]. A transverse vortices TV and longitudinal vortices LV are generated as a mainstream flows across the VG. The axis of the longitudinal vortices is parallel to the main flow direction whereas the axis of the transverse vortices is normal to the flow direction. Generally, the effect of longitudinal vortices is more effective than transverse vortices on heat transfer performance [1].

The fluid flow and heat transfer characteristics in flow channels have been extensively studied in the past decades. This is due

Nomenclature

C_f	fanning friction coefficient
C_p	specific heat (J/kg K)
d	nanoparticle diameter (nm)
f	Darcy's friction factor
h	heat transfer coefficient (W/m^2 K)
k	thermal conductivity (W/kg K)
k_B	Boltzmann's constant
$k_{c,j}$	effective dielectric constant
Nu	Nusselt number, $Nu=hD/k$
ΔP	pressure drop, Pa
Pe	Peclet number, $Pe=Lu/\alpha$
Pr	Prandtl number, $Pr=C_p\mu/k$
Re	Reynolds number, $Re=Du/\nu$
St	Stanton number
T	temperature (K)
u	mean fluid velocity (m/s)

Greek symbols

β	attack angle
φ, ε	volume fraction
ϕ	nanoparticle volume fraction
ρ	density (kg/m^3)
μ	dynamic viscosity (kg/m s)
ν	kinematic viscosity (m^2/s)

Subscript

eff	effective
f	base fluid
fr	freezing point of the base liquid
in	inner
nf	nanofluid
np	nanoparticle
o	base case
out	outer
p	particle
s	solid

Abbreviation

CFD	common-flow down
CFU	common-flow up
CHE	compact heat exchanger
CNT	carbon nanotube
C-MWNT	carbon multi-walled nanotubes
ETC	effective thermal conductivity
LV	longitudinal vortices
PCM	phase change material
HTE	heat transfer enhancement
TV	transverse vortices
VG	vortex generator

to its wide applications in compact heat exchangers, solar collector, laser curtain seals, and cooling of electrical devices. However, in these applications, gases were used instead of liquids as heat transfer medium. Gases inherently have lower heat transfer rate than liquids. Therefore, heat transfer enhancement techniques that improve heat transfer rate are of particular interest. Many previous investigators have studied the techniques of heat transfer augmentation theoretically and experimentally.

Heat transfer enhancement by VG is one passive method to generate streamwise vortices that create high turbulence in fluid flow over heat transfer surfaces. It was found that the only effective way to increase the heat transfer coefficient is to decrease the thermal resistance of the sublayer adjacent to the wall immediately where the viscous effects of the sublayer are dominant. This can be done by increasing the turbulence of the fluid flow in the main stream so that the turbulent eddies can penetrate deeper into this layer. The thermal resistance can be reduced and the heat transfer can be augmented by using VG that can be punched or attached to the internal surface of the channel wall. The vortex generator can be regarded as a special kind of extended surface, which can be stamped on or punched out from the fin. VG not only disturbs the flow field, disrupt the growth of the boundary layer, but also makes fluid swirling and causes a heavy exchange of core and wall fluid, leading to the enhancement of heat transfer between the flowing fluid and the channel walls.

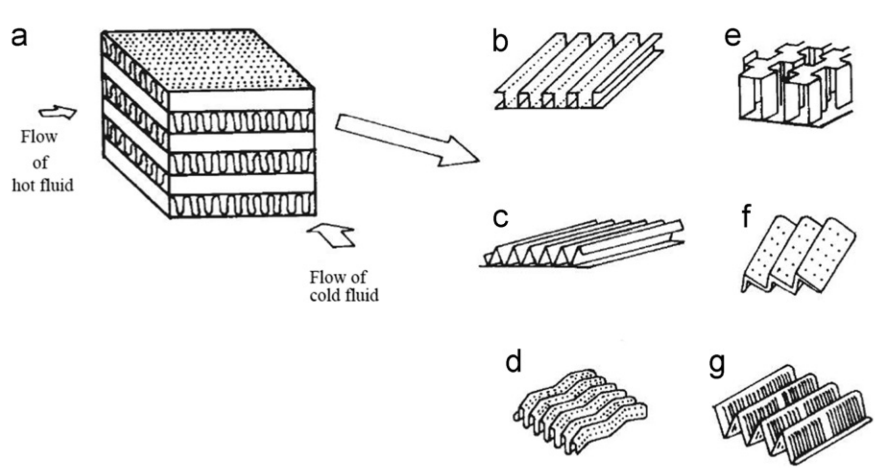


Fig. 1. (a) Plate-fin heat exchanger and its surface geometries, (b) plain rectangular fins, (c) plain triangular fins, (d) wavy fins, (e) offsets strip fins, (f) perforated fins and (g) louvered fins [3].

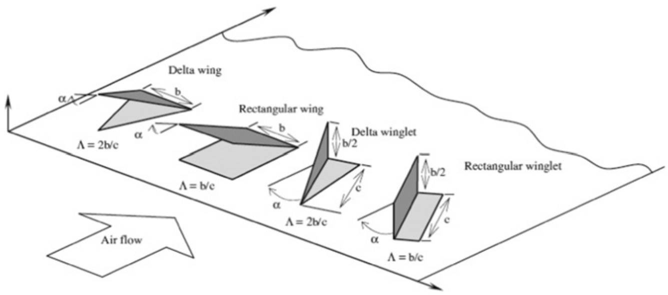


Fig. 2. Longitudinal vortex generators types: (a) delta wing, (b) rectangular wing, (c) delta winglet pair and (d) rectangular winglet pair [30].

In the tube bank fin heat exchangers, the airside resistance generally comprises more than 90% of the total thermal resistance. Therefore, special surfaces are employed to effectively improve the airside heat transfer performance. VGs can be applied on the fin surface to generate longitudinal vortices in the main flow; hence the heat transfer of the fin surface is enhanced [6].

The techniques used to investigate the flow phenomena associated with VGs are classically IR imaging, particle image velocimetry (PIV), five hole pressure probes and the naphthalene sublimation technique which relates mass transfer to heat transfer by evoking the heat and mass transfer analogy. Hernon et al. [7] studied the phenomena associated with the VGs using the technique of hotwire and PIV images and made a comparison between them. They found some of the key observations from the instantaneous PIV are that at any given time the vortices shed from each delta winglet can vary in size, strength, and location from the wall. These variations cause the two counter rotating vortices to sweep across the lower wall while at the same time they move towards and away from the wall causing compression and extension of the underlying boundary layer. All of these complex unsteady flow phenomena may results in enhanced heat transfer.

In the development of recent industrial world, the reduction in the heat exchanger volume and augmentation in their performance for heat transfer had a great interest of many researchers. In addition, there are always economical factors need to be considered to reduce the costs of heat transfer process. The need for high performance thermal systems due to the increase in the pressure drop associated with the augmentation in heat transfer becomes necessary.

Henze and Wolfersdorf [8] examined the effects of longitudinal vortices induced by tetrahedral VG. They highlighted that the highest VG shows the highest heat transfer enhancement. The convection heat transfer coefficient increases as *Re* number increases while the heat transfer enhancement related to the smooth channel flow is decreasing. They found that the effect of turbulence is less remarked for regions which are affected by vortices.

3. Applications of vortex generator

Heat exchangers are widely used in many industrial areas such as chemical engineering, radiator of car, locomotive powered by internal combustion engine, geothermal, fossil, process plant, power system, air-conditioning, refrigeration, internally cooled gas turbine blades, air-cooled solar collectors, electronic chip cooling, wastewater aeration tanks, chemical mixers, nuclear reactors cores, aerospace, and other engineering applications. An efficient heat exchanger in such systems could results in the lesser consumption of the energy resource, which provides both economical and environmental benefits. Increasing demands are being placed on heat exchanger performance for reasons of compactness, economy in manufacturing and operating costs, energy conservation and even for ecological reasons. The importance of these issues continues to motivate the study of enhancement techniques. Universal types of heat exchangers incorporating plate-fins or fin-circular/flat tubes are designed for the above industrial processes and systems, and for these types the flow is channeled between plates [3,9–13]. VGs are used with the louvered fins to provide advantages over continuous fin designs because each louver initiates new boundary layer growth producing higher convective heat transfer than that of a continuous fin [14].

According to 2002 estimate by the US Department of Energy (EIA) heating ventilation, air conditioning, and refrigeration (HVACR) systems accounted for 55% of the energy used in residential buildings and 45% in the commercial buildings. This usage amounts to an annual expenditure of roughly 32 trillion dollars for energy consumed by HVACR systems alone. In the liquid-to-air and phase-change heat exchangers typical to HVACR systems, the air-side thermal resistance is the largest single contributor to the overall thermal resistance. For example, the air side can comprise 75% of the thermal resistance in an evaporator and 95% in condenser for typical refrigeration applications. With rising energy costs and new legislation aimed at efficiency and environmental protection, heat exchanger performance will continue to be very important. Achieving even a 10% performance enhancement in this type of heat exchanger geometry could have profound implications on the HVACR systems where it is commonly used [15].

The need of high performance of thermal systems in many engineering applications has stimulated enormous interesting to find various methods to improve heat transfer rate in the system. The conventional heat exchangers are generally improved by various augmentation techniques which focus on many types of surface augmentation. There are two enhancement technologies of convective heat transfer for compact heat exchangers. One is to extend heat transfer surface area like a fin, the other is to increase heat transfer coefficients between solid surface and fluid such as using turbulators as vortex generators. In cooling channel and channel heat exchanger design, rib, fin, wing turbulators are often employed in order to increase the convective heat transfer rate leading to the compact heat exchanger and in turn leads to meet the desired of high efficiency and low cost with the volume as small as possible and the weight as light as possible. The use of wing turbulators completely results in the change of the flow field and hence the variation of the local convective heat transfer coefficient. Winglets have been successfully used for enhancement of heat transfer of modern thermal systems because they can generate longitudinal vortices and help to disrupt the main flow with less penalty of pressure loss [2,5,16–18].

Vortex induced heat transfer enhancement is a passive augmentation method that relies on the intentional generation of secondary, streamwise vortices to enhance heat transfer. The method may be utilized in many liquid-to-air and refrigerant-to-air heat exchanger applications. Streamwise vortices can be introduced using small flow manipulators such as those shown in Fig. 2. VG is used with the flat-plate compact heat exchangers to improve their thermal performance.

For the array of VGs, regular arrays of longitudinal vortices embedded in turbulent boundary layer occur frequently behind evenly spaced pro-turbulences, and behind vortex generator rows installed to increase mixing. VG array embedded in turbulent boundary layer causes periodic variations in the skin friction with corresponding increase in heat transfer [19].

The most common practical application is the introduction of the vortex into a boundary layer to suppress separation. These

flows also occur naturally when horseshoe vortices form near the junction of a blunt body and a wall on which a turbulent boundary layer is developing. A typical example is the junction between a gas-turbine blade and its endwall, where the enhanced mixing due to the vortices can lead to locally high heat transfer rates along the endwall [20].

The subject of heat transfer is of serious interest in heat exchanger applications. The process industries call for more and more compact designs of heat exchangers. Flow interruption created in flow at periodic intervals is a popular means for heat transfer enhancement in compact heat exchangers. One relevant application using such flow configurations is the heat transfer between the flowing fluid and plates in the case of plate-fin heat exchangers [21]. Since global energy consumption is starting to impact negatively on the environment, as well as causing depletion of the existing fuel stocks, energy utilization has come under close scrutiny. Energy cost and environmental considerations continue to motivate attempts to derive better performance over the existing designs [22].

3.1. Circular and non-circular ducts

Li et al. [23] illustrated that the vortex intensity and vortex flow length are strongly affected by the rib dimensions in laminar flow of water tube.

Kenan et al. [24] studied experimentally the tapes with double-sided delta-winglets under different geometrical and flow parameters in a test pipe. They pointed out that the winglet height has the most effective parameter on the friction factor, while the most effective parameter affects the amplitude of the pressure fluctuations is the *Re* number.

Several studies have been performed to study the influence of pair/row of VG mounted on a rectangular channel wall on heat transfer performance. Pauley and Eaton [19] studied array of one transverse row of VG with several spacing between the edge of VG which varied from 2 cm to 14 cm and different angle of attack which varied from 6° to 24°. They have found that one row of VG causes a tremendous heat transfer augmentation over large areas. They found that the peak augmentation in the Stanton number (*St*) was approximately 30% and the minimum value was 8% below the undisturbed level for all cases with different VG spacing. They observed that the downstream where the vortices have lifted themselves out of the boundary layer, the peaks in heat transfer augmentation became less pronounced and 7–18% level of heat transfer augmentation was seen across the channel. They pointed out that the co-rotating array produces 13% augmentation in heat transfer over the entire surface which is somewhat higher than observed for the alternating array. Wroblewski and Eibeck [20] found that a peak enhancement in heat transfer performance was 25% in the region near the downwash side of DWVG mounted in a turbulent boundary layer when the attack angle is 12°. Kim and Yang [25] found that the common flow-down (CFD) cases showed better heat transfer characteristics than the common flow-up (CFU) cases when a pair of DWVG was embedded in turbulent boundary layer of rectangular channel. They obtained, at $\beta=45^\circ$, an enhancement in heat transfer rate for the CFD by 7% and 3% more than those of $\beta=20^\circ$ and 30° respectively. The secondary velocity vectors at $\beta=30^\circ$ for the CFD and CFU is shown in Fig. 3.

Depaiwa et al. [2] examined the effect of existence of ten pairs of rectangular winglet vortex generators (RWVG) at the entrance of a rectangular solar air heater channel. The attack angle of VGs was varied from 30° to 60° pointing upstream (PU) and pointing downstream (PD) of the flow while Reynolds number was varied from 5000 to 23,000. They found that the larger attack angle leads to higher heat transfer rate and flow loss than the lower one. They displayed that the PD-RWVG yields higher heat transfer rate than PU-RWVG. They reported that convective heat transfer coefficient is strongly affected by the attack angle of VG.

Qiuwang et al. [26] achieved experiments on the heat transfer and pressure drop in horizontal narrow rectangular channels with mounted LVGs. Two and three rows of VG pairs were examined with different arrangements. They found that the LVGs could greatly improve the heat transfer rate by 10–45% and the heat transfer performance of channel with LVGs on two sides are better than those on one side.

Jian et al. [27] performed tests to investigate fluid flow and convective heat transfer characteristics in a narrow rectangular channel with and without four pairs of LVGs. For laminar flow regime, VG causes heat transfer enhancement of about 100.9% and flow resistance increase of only 11.4%., while for turbulent flow regime, VG causes heat transfer enhancement of above 87.1% and flow resistance increase of 100.3%. They concluded that LV can obviously enhance heat transfer of single-phase water, and increase flow resistance mildly.

Min et al. [3] tested the influence of RWPVG attached on the rectangular channel wall on heat transfer characteristics. *Re* number was ranged from 5000 to 17,500 with various valued of β. They modified the shape of rectangular wing MRWP as shown in Fig. 4. Their results revealed that the average *Nu* number increases with the

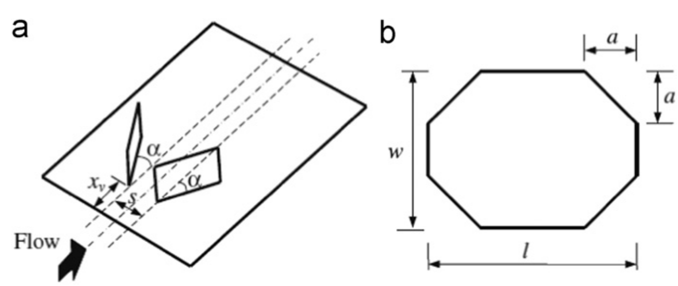


Fig. 4. Schematic view of modified VG: (a) layout of CFD wings and (b) modified rectangular wing [3].

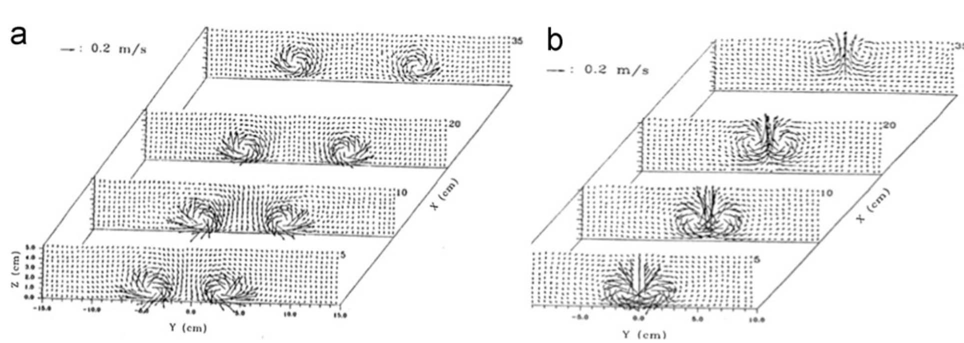


Fig. 3. (a) Secondary velocity vectors with CFD and (b) secondary velocity vectors with CFU, at $\beta=30^\circ$ [25].

attack angle and 55° angle shows the highest average *Nu* number which was 46–55% compared with plain channel in the range of their study. MRWP have higher heat transfer enhancement and lower friction factors in comparison with RWP.

Promvonge et al. [17] and Chompookham et al. [18] performed tests to investigate the heat transfer characteristics in a rectangular channel fitted with combined wedge ribs turbulators and winglet type VGs for the turbulent regime. *Re* number was varied from 5000 to 22,000. The results of Promvonge et al. [17] revealed that the combined ribs and DWVG give significant increase in heat transfer rate over the smooth channel. The increase in *Nu* number is around 240% over the smooth channel when in-line ribs and WVG are used. The *Nu* number obtained from combined ribs and DW pair of VGs was found to be much higher than those from the ribs only. This is around 50% greater than that of the rib alone. The rib along with the WVGs of higher attack angle value provides higher heat transfer than that of lower attack angle value. The larger the attack angle value leads to higher friction loss than the lower one. The friction factor of the combined WVG and ribs was found to be higher than that of the rib alone around 25–125%. While the results of Chompookham et al. [18] found that the combined staggered rib and the WVGs with attack angle of 30° should be applied instead of using the rib/WVGs alone to obtain higher heat transfer performance of about 40–65%. The friction factor values obtained from combined the ribs and WVGs are found to be much higher than those from the rib or WVGs alone.

Promvonge et al. [28] showed that the larger attack angle of the DW leads to higher heat transfer and friction loss than the lower one. They observed that the largest attack angle (60°) of the PU-DW gives the highest *Nu* number and friction factor while the lowest attack angle of the PD-DW yields the best thermal performance.

Aris et al. [29,30] investigated experimentally and numerically the use of wing type surface protrusions in the form of 3-D delta wing tabs adhered to the fin surface, thin wings punched-out of the fin material and TiNi shape memory alloy delta wings which changed their angles of attack based on the fin surface temperature. The 3-D tabs in a staggered arrangement gave an augmentation in the heat transfer by about 37% compared to a plain fin stack. While the punched-out delta wings in the staggered and inline arrangements provided enhancements of 30% and 26%, respectively. The pressure drop through the fin stack was by approximately 19% in the de-activate position. Their CFD results were in good agreement with their experimental work and previous reports. While Aris et al. [30] obtained maximum heat transfer improvements of up to 90% and 80% by the single and double wings, respectively, in the laminar-transition air flow. The pressure drop penalty across the test section, when the wings were activated, increased between 7% and 63% of the losses at their de-activated positions, for the single and double VG, respectively.

Mochizuki et al. [31] studied the fluid flow characteristics in a rectangular channel with DWPVG mounted in a turbulent flow regime. They reported that the mean velocity profile averaged over the spanwise direction has acceleration near the wall and deceleration away from the wall.

Numerically, Charbel et al. [32] performed a 3-D simulation to study the heat transfer in turbulent vortical flows. Vorticity is generated by inclined vortex generators in a turbulent circular pipe flow with different configurations that fall into three categories which are, rows of trapezoidal vortex generators in different arrangements; the vortex generators are fixed at certain distance from the tube wall, and vortex generator rows between which a row of small protrusions are inserted on the tube wall. They pointed out that the longitudinal variation of local *Nu* number computed on different high-efficiency vortex mixer cross sections shows the advantage of using protrusions between two successive vortex generator rows in which they increase the local heat transfer by increasing the temperature gradients and vorticity very close to the heated wall. Saraç and Bali [33] performed experiments to investigate the heat transfer and pressure drop characteristics of a decaying swirl flow in a horizontal pipe. The decaying swirl flow is produced by inserting VGs with propeller-type for *Re* number ranged from 5000 to 30,000. Their results indicate that the *Nu* number increases ranged from 18.1% to 163% depending on *Re* number, the position of VG, the angle of attack and the number of vane. They observed a decrease in *Nu* number when the angle of attack increases. They attributed that to an increase in the vane angle would increase the swirl period.

Wu and Tao [5,34] investigated the heat transfer characteristics in a rectangular channel with a pair of RWVG mounted on the lower wall of the channel. *Re* number was ranged from 800 to 3000. They remarked that the thickness of RWVG can cause less heat transfer enhancement in the region near to the VG. They found that the pressure drop in the rectangular channel with RWVG increases rapidly with the increase of the attack angle of the LVG. They observed that the thickness of LVG has little influence on average friction factor of the channel. The LVGs can improve the synergy between the velocity and temperature fields not only in the region near LVG but also in the large downstream region of LVG. LVs enable to enhance the global heat transfer of the channel. Whereas TVs can only enhance the local heat transfer of the channel. The attack angle of 45° of VG always provides better effectiveness of heat transfer enhancement. They found that *Nu* number decreases with the LVG's location away from the inlet of the channel and decreases too with the space between the LVG pair decreases. They have seen that *Nu* number increased with the increasing the area of LVG pair and the results of *Nu* number at $\beta=45^\circ$ is slightly higher than that of $\beta=60^\circ$. As the attack angle of DWVG increases from 15° to 60°, the convective heat transfer coefficient increases from 8–11% to 21–34%. They observed that the heat transfer was improved better with the increasing of the length of RWVG and decreasing the height of RWVG when the area of LVG was fixed. They found that the DWVG is more effective than RWVG on *Nu* number at the same area of LVG. The geometry of VG plays an important role in the enhancement of heat transfer [34].

Yang et al. [35] studied the effects of the common-flow-up pair produced by vortex generators in a rectangular channel flow on fluid flow and heat transfer. They displayed that the distortion of thermal boundary layer is not as strong as the distortion of hydraulic boundary layer. The influence of the common-flow-up pair on heat transfer enhancement is maintained at the downstream location 30 times as large as the chord length of the vortex generators.

Biswas and Chattopadhyay [36] solved numerically the complete Navier–Stokes and energy equations and have seen that the delta-wing VG has a strong effect on the heat transfer performance when punched on the rectangular channel wall. They observed that the heat transfer is enhanced by about 45.4% over the smooth channel case at a non-dimensional axial distance of 4 from the inlet and at attack angle of 20°. They found that the improvement was 26.4% in *Nu* number for $\beta=30^\circ$ over the case of $\beta=20^\circ$ at the same location. At the exit of the channel and $Re=1815$, *Nu* number was 98.38% greater than that when $Re=500$. Zhu et al. [37] studied the heat transfer performance for fully developed flow in a rectangular channel using RWVG on one wall and rib-roughness elements on the other wall. They used the SOLA-algorithm to solve the time-dependent Navier–Stokes equations directly for the primitive variables by advancing the solution explicitly in time. They displayed that $\overline{Nu}/Nu_o$ was 3.42

when $Re=10^5$ and $\beta=45^\circ$. Maximum augmentation obtained by Zhu et al. [37] was 450% using this arrangement of VG and ribs. The f/f_o is 32.0 at Re number equal to 15×10^4 and $\beta=45^\circ$. Ahmed et al. [12] examined several types of VG embedded in laminar and turbulent boundary layer of rectangular channel. They stated that the delta-wing shows the generation of counter rotating longitudinal vortices along their leading edges that diverge slightly depending on the aspect ratio of the wing. They have seen that the longitudinal vortices follow somewhat the wing inclination angle until they are redirected by the duct wall. Kaniewski et al. [38] found that one pair of RWVG attached on lower wall of rectangular channel can increase the global mixing by more than 50% for laminar flow.

Rütten and Krenkel [39] tested the effect of existence of delta–winglet pair punched on the upper heated wall of rectangular channel in a flow form of CFU. While another pair of VG was punched on the lower cold wall in a flow form of CFD (facing one another). They stated that this arrangement of VG enhances the mixing of cold and warm fluid in the channel. The configuration of the VG in the channel and the temperature distribution is shown in Fig. 5.

While Hiravennavar et al. [40] studied the influence of the existence of DWVG pair of non-zero thickness embedded in the hydrodynamically developed and thermally developing laminar rectangular channel flow. They have found that heat transfer enhancement increases by 33% when single winglet is used and by 67% when a winglet pair is utilized compared to the plain channel. It was observed that as Re number increases from 790 to 1580 the heat transfer increases by 37.6% at the end of the channel. They obtained an increase in Nu number by about 0.83–12.49% when W/H (thickness of VG/height of the channel) varied from 0.0622 to 0.2485. Biswas et al. [41] examined the presence of delta-wing and delta-winglet pair VGs on heat transfer performance embedded in laminar boundary layer of rectangular channel. This geometric configuration of the channel is considered from their viewpoint as a representative of single element of either a compact gas–liquid fin-tube crossflow heat exchange or a plate-fin crossflow heat exchanger. They have seen that the delta-wing VG is more effective than the winglet-pair but the use of winglets appears to be a more attractive augmentation technique. They reported that the channel may not be allowed to be so long ($X\geq8.0$). They stated that another row of VGs may be mounted before this length. They found that the combined spanwise average friction coefficient due to the winglet pair is less than that due to the wing.

Deb et al. [42] have made an effort to investigate the heat transfer characteristics in laminar and turbulent flows through a rectangular channel containing built-in DWVGs. This channel is considered as a representative of single element of a plate-fin heat exchanger. They found that a significant enhancement is observed for the cases with built-in DWVGs over the corresponding cases without any obstacle. For example, they found that the enhancement is about 16% at the exit of the channel when Re number equal to 5000. They also obtained a turbulent intensity by about 10% at the inlet of the channel for the cases of $Re=5000$ and $Re=15{,}000$, $\beta=12^\circ$ and with aspect ratio of 1.6. The effect of the Re number on the distribution of combined spanwise-average-skin-friction in the channel with built-in winglet pair is shown in Fig. 6.

Sohankar [43] investigated the heat transfer augmentation in a rectangular channel with two angled ribs as a V-shaped VG. The VGs are attached on the bottom wall of the channel and their angles in respect to the main flow direction are between 10° and 30°. Re number is ranged from 200 to 2000. They observed that the heat transfer becomes steady at lower Re number while it becomes unsteady at higher Re number values. They found that the vortex strength increases with Re number and it decays in the streamwise direction. The peak values of Nu number they observed occurs on the lower wall upstream of the VGs where the horseshoe vortices form.

Munish et al. [44,45] stated that in order to obtain the heat transfer augmentation with RWVG the price of increase in

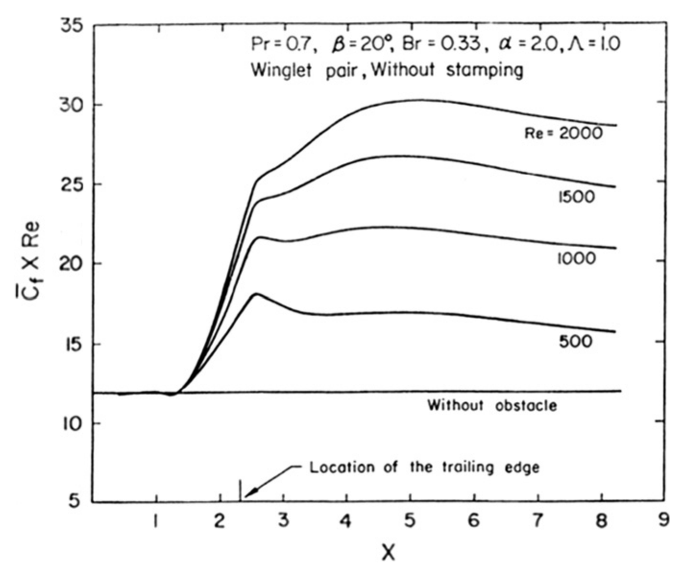


Fig. 6. Effect of the Re number on the distribution of combined spanwise-average-skin-friction in the channel with built-in winglet pair [42].

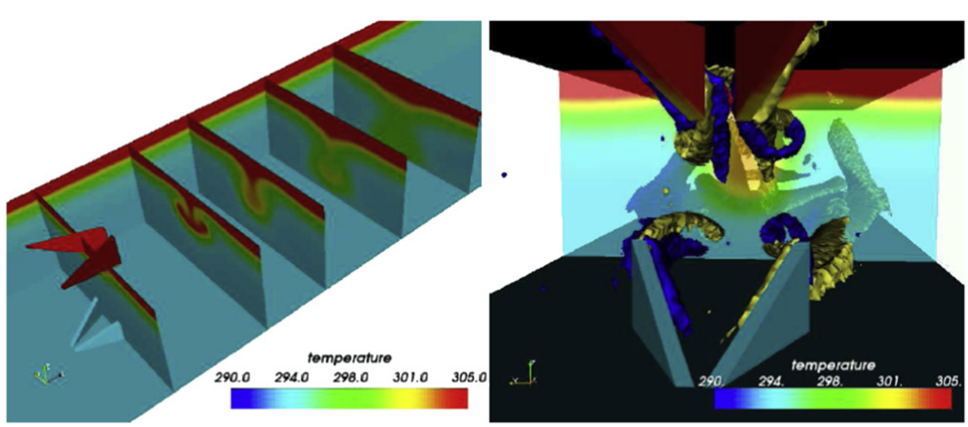


Fig. 5. Vortices generated by VGs and their impact on the temperature field [39].

pressure drop has to be paid. The pumping power increases with the increase of the attack angle of VG. A higher angle of attack a higher pressure drop. The pressure drop increases from 18.7% to 31.3% when the attack angle of VG increases from 20° to 37° compared to the plain duct. For the constant area of VG, the pressure drop decreases from 23% to 18.7% with an increase in length from 0.894 to 1.23.

3.2. Flat plate-fin heat exchanger

A plate-fin heat exchanger with triangular fins is a good choice because of excellent compactness and cost effectiveness when compared to traditional shell and tube heat exchangers or plate heat exchangers. The performance can be further increased by using LVGs that produce longitudinal vortices that strongly enhance the heat transfer by mixing the fluid from the wall into the free stream and vice-versa.

Nakod et al. [46] studied experimentally the effect of the finned surfaces and surfaces with VGs on the local heat transfer coefficient between impinging circular air jet and flat plate as shown in Fig. 7. VGs are in the form of equilateral triangle arranged in many circular rows. They observed an augmentation in heat transfer higher than that of the finned surfaces. This augmentation was as high as 110% for a single row of six VGs and $Re=25{,}000$ compared to the smooth surface. They reported that the effect of increase in the number of rows of VGs, arrangement of VGs in a row, radius of pitch circle of VGs and number of VGs in a row is to decrease the Nusselt number compared to the single row of six VGs. They found that the optimum configuration of the VGs is single row of six VGs. The inclination angle does not affect the heat transfer in case of the VGs.

Joardar and Jacobi [47] investigated experimentally the effectiveness of 1500 delta-wings VGs mounted in full-scale wind-tunnel testing of a compact heat exchanger typical to those used in automotive systems. They reported that an average heat transfer increases over the baseline case of 21% for dry surface conditions and 23.4% for wet surface conditions with pressure drop penalty smaller than 7%. Gentry and Jacobi [48] studied the effect of delta-wing VG on heat transfer embedded in a laminar boundary layer of a flat-plate. Reynolds number was ranged from 600 to 1000 and the attack angle of VG was from 10° to 55°. They found that the heat transfer was enhanced up to 50% compared to the plain flat-plate. They reported that the VG geometry and angle of attack play important roles to predict how and where the vortex is started and how its position relative to the boundary layer evolves as it flows down the plate.

Chen and Shu [49] showed that the presence of delta-wing vortex generator mounted on heated plate installed on the bottom wall of a duct in fan flows has little overall effect on the near-wall averaged axial mean velocity and axial vorticity, but increases the turbulent kinetic energy. They concluded that the delta-wing vortex generator in fan flows has little effect on the heat transfer augmentation.

Kotcioğlu et al. [21] and Tiggelbeck et al. [50] investigated the heat transfer characteristics in a plate fins channel using the four basic types of VG and RWP of VG respectively. Kotcioğlu and his group studied the arrangement of the wings as an array of rows with attack angle which was varied from 7° to 20° positively and negatively with the main flow direction in a rectangular channel. They pointed out that the mixing effect in the intermediate region between wing cascades improves the heat transfer characteristics as the inclination angle of winglet increases. They indicated that the *Nu* number increases with the *Re* number and the dependence of *Re* number on the friction factor is strong. The results of Tiggelbeck et al. [50] imply that the winglets give better performance in heat transfer than the wings and a DWP performs slightly better than a RWP at higher attack angles greater than 30°. They showed that DWPVG enhanced heat transfer by 46% at $Re=2000$ and 120% at $Re=8000$ over the heat transfer on a plate. Their results showed that the maximum heat transfer for the case with RWP of VG occurs at a β between 45° and 65° and this maximum is smaller than that of DWP of VG. While at $\beta=90°$ a sharp decrease in *Nu* number was observed. *Nu* number increases almost linearly with *Re* number as shown in Fig. 8. The friction coefficient for channel with VGs starts slowly increasing whereas the friction coefficient for a smooth channel still decreases.

Wu and Tao [51] made an experimental and numerical study to investigate the average convective heat transfer on the top and bottom surfaces of a plain plate and four plates with a pair of delta winglet longitudinal vortex generator punched directly from the plates with attack angles ranged from 15° to 60°. The average Nusselt number of the plate with attack angle of 60° is slightly higher than that of plate with attack angle of 45° yet may bring larger pressure drop. They obtained a deviation of 10% between their numerical data and experimental results which validates their numerical model.

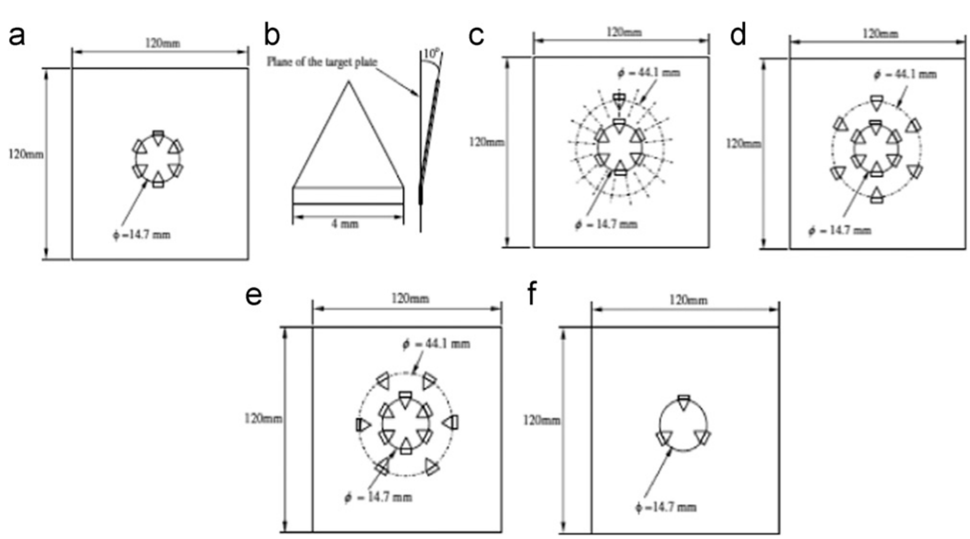


Fig. 7. Details of vortex generators [46]. (a) Arrangement of single row of six vortex generators. (b) Vortex generator. (c) Arrangement of two rows of vortex generators (same circumferential pitch). (d) Two rows of vortex generators (inline arrangement). (e) Two rows of vortex generators (staggered arrangement). (f) Arrangement of single row of three vortex generators.

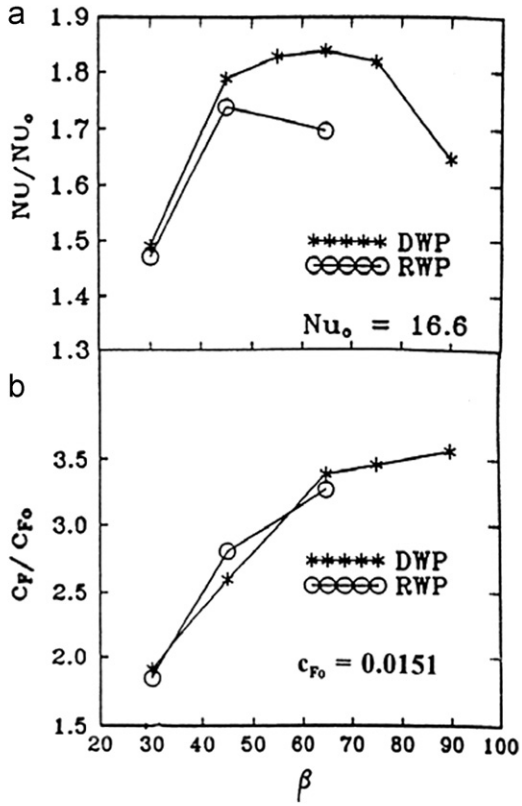


Fig. 8. (a) Complete fin area-averaged *Nu* number, *Nu*, normalized with Nu_o and (b) the friction coefficient normalized with C_{Fo} as function of β [51].

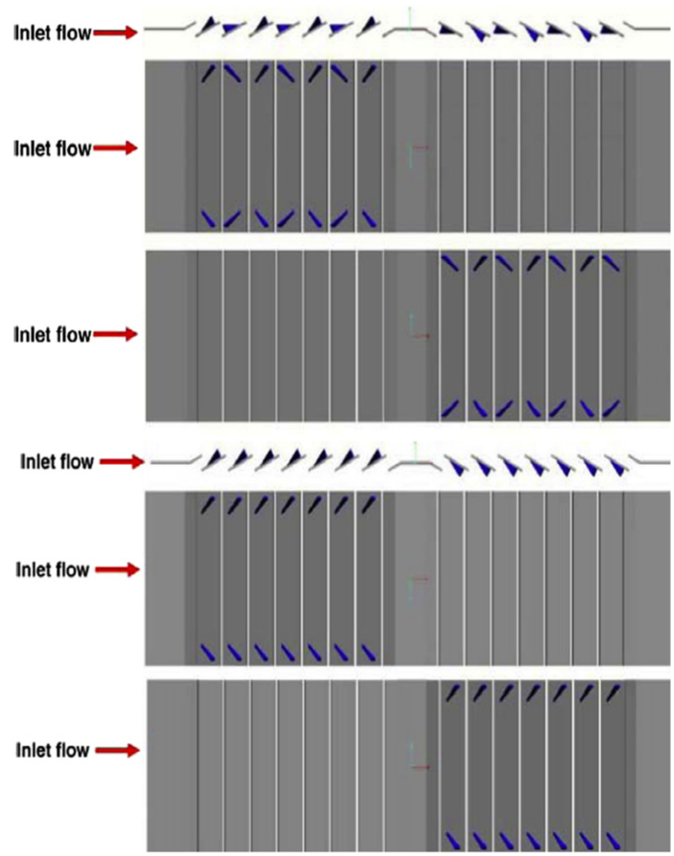


Fig. 9. Side, top, and bottom view of VG winglet [14].

Experiments to study the enhancement of heat transfer in louvered fin heat exchanger using winglets placed on louvered was performed by Sanders and Thole [14]. They tested the effect of attack angle, aspect ratio, direction, and the shape of winglet in a laminar regime. They highlighted that the best heat transfer augmentation is found with RW pair of VG and it is around 3%, 36% and 38% at *Re* numbers of 230, 615 and 1016, respectively. They reported that in an attempt to optimize these winglet parameters, heat transfer augmentations as high as 39% were achieved with associated friction factor increment as high as 23%. The maximum augmentation in heat transfer obtained is 25% when the winglet direction and orientation were alternated on every other louver, while the maximum value is around 33% when all winglets were placed in the VG-B orientation with alternating direction as shown in Fig. 9. The RW pair of VG yields higher friction factor values than the VG-B winglet. The friction factor significantly increases as the angle of attack and the winglet size increase.

Guobing and Qiuling [52] performed a new shape of VG of curved trapezoidal winglet CTW and compared with traditional vortex generators; rectangular winglet, trapezoidal winglet and delta winglet. They showed that DWP is the best in laminar and transitional flow region, while CTWP has the best thermohydraulic performance in fully turbulent region due to the streamlined configuration and then the low pressure drop, which indicates the advantages of using this kind of VGs for heat transfer enhancement. The CTWP showed that smaller attack angle, larger curvature and larger angle of inclination gives better thermohydraulic performance under the same conditions. An appropriate spacing between the leading edges of CTWP should be considered for different flow regions. They concluded that double rows of CTWP do not show better thermohydraulic performance due to the larger pressure drop and the spacing between the two rows of CTWP should also be optimized.

Numerically, Li-Ting et al. [53] reported that the flat-plate channel with DWP has better overall performance than RWP. The CFD and CFU configurations of DWP have almost the same overall performance. The CFD configuration has a better overall performance than the CFU configuration for RWP.

Munish et al. [44,45] and Akcayoglu [54] performed their investigation about the HTE in a plate-fin heat exchanger with triangular fins as insert using a winglet pair of VG. They observed an enhancement in heat transfer when a RW type VG is mounted on triangular fins. The attack angle of VG was varied from 20° to 37° and *Re* number was ranged from 100 to 200. A constant wall temperature is considered as a thermal boundary condition and the air is taken as a working fluid. They confirmed that the average *Nu* number increases with an increase in the angle of attack and *Re* number. For the same area of LVGs, the increase in the length of the LVGs brings more HTE than increasing the height [44]. While in [45], the HTE was 13% over the case of without winglet pair even at the exit when $Re=200$, $\beta=20^\circ$. They observed that the performance of the winglet pair increases as *Re* number increases from 200 to 500 and increases with the increase in the height of the winglet pair. Akcayoglu [54] studied the effect of double rows DW pair of VG in CFD and CFU configuration mounted on the duct's slant surface. They found that the second flow is stronger behind the second pair of VG than behind the first pair but becomes weaker far from the second pair in the case of CFD. They observed that both configurations are able to create a counter-rotation. They showed a large vortex formation area and a great induced vorticity field between vortex pairs for CFU arrangement compared to the CFD arrangement.

Ferrouillat et al. [55] studied the effect of DWP and RWP VG on the performance of compact heat exchanger. They stated that for different turbulent models used, that DWP is more efficient than

RWP in terms of compactness criterion. In addition, they found that the optimum heat transfer and mixing efficiencies can be obtained when the distance between VG rows is around 7–10 times the channel heights.

Ahmed and Lars [56] showed that the temperature fluctuations, turbulent kinetic energy and unsteadiness effects are stronger in the region of a plate–fin heat exchanger where the longitudinal vortices are more active.

Leu et al. [57] performed a combined numerical and experimental study of the heat transfer and fluid flow characteristics in the 3-row plate–fin and circular tube heat exchanger with inclined block shape VG mounted behind the tubes. They stated that the proposed heat transfer enhancement technique is able to generate longitudinal vortices and to improve heat transfer performance in the wake region. They pointed out that this kind of VGs not only produces longitudinal vortices, but also aid the fluid into the wake re-circulation zone. They found that as the attack angle increased, the strength of the longitudinal vortex intensified and both the Colburn and friction factors increased. They demonstrated that the case of $\beta=45^{\circ}$ provides the best heat transfer augmentation with 8–30% increase in Colburn factor across the range of *Re* from 400 to 3000, while the Fanning friction factor is only increased by 11–15%. This gave the greatest area reduction ratio by 25% as shown in Fig. 10.

3.3. Tube-fin heat exchanger

An augmentation of heat transfer in a compact plain-fin-and-tube heat exchanger with presence of winglet VGs have been studied by [4,9–11,16,22,58,59]. Torii et al. [9] found that the heat transfer was enhanced by 30% and 10% for *Re* number ranging from 350 to 2100 with the using of DWVGs of the common flow up CFU for staggered tube banks heat exchanger. While the augmentation was 20% and 10% for in-line tube banks for the same range of *Re* number. Zhang et al. [10] found that VGs should be mounted as near as possible to the tube wall in the case of three-row flat tube bank fin, and vortices generated by the upstream VGs converge at wake region of flat tube. They have seen that the friction factor decreases as *Re* number increases. Yoo et al. [16] stated that the overall average heat transfer coefficient of fin-flat tube heat exchanger with DWVGs is increased by 75% compared to that of fin-flat tube without DWVGs and is increased by 45% compared to that of the fin-circular tube heat exchanger without DWVGs. They observed that the pressure drop of the fin-flat tube bank with VGs is increased by 80% compared to that of the fin-flat tube bank without VGs, but is increased by 50% compared to that of the fin-circular tube bank without VGs. Zhang et al. [10] studied the effect of the pitch of in-line delta-winglet VGs on local and average *Nu* number of the finned three-row flat tube bank. The *Re* number ranged from 500 to 5000. They reported the following: the pitch of in-line VG has a large effect on heat transfer, VGs with small pitch can enhance the heat transfer of the fin surface downstream, and the effect of the pitch on heat transfer performance depends on the attack angle of VG for identical mass flow rate.

Allison and Dally [22] demonstrated that, when the VGs placed directly upstream of the tube of the fin and tube radiator, the winglet surface has 87% of heat transfer capacity of the louvered fin surface. They found that 39° attack angle of VG gives the best flow structure. While Jalil et al. [58] examined four different shapes of winglet VGs around heated cylinder with attack angle varied from 20° to 32° and *Re* number ranged from 7200 to 14,400. They concluded that the heat transfer was augmented by about 14% when winglets were used and this enhancement increases with the *Re* number and the attack angle of VG while the pressure drop was slightly increased; the local pressure coefficient increases when the winglet is used; the local pressure drop increases as the attack angle of VG increases; the pressure drop is relatively proportional with the *Re* number. They reported that the position of VG plays an important role on the performance of heat transfer. They showed that the trapezoidal winglet gives a better enhancement in heat transfer rate compared to the

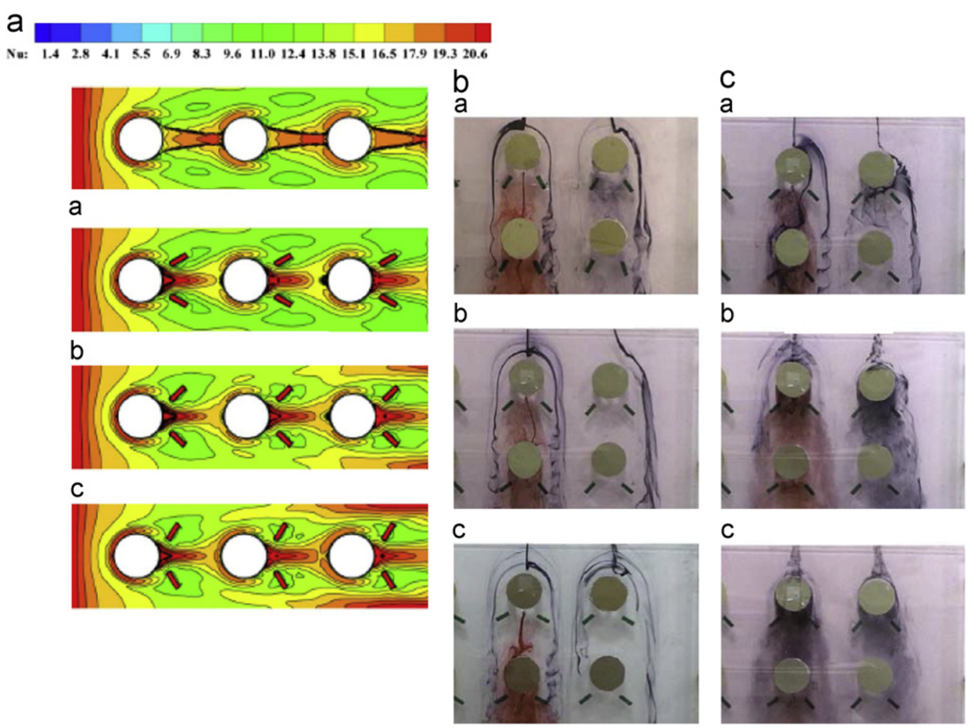


Fig. 10. (a) Local *Nu* number distribution across the fin surface at $Re_{Dh}=3000$ ((a) VG_0, (b) VG_{30}, (c) VG_{45}), (b) flow visualization for three different span angles at $Re_{Dh}=500$ ((a) VG_{30}, (b) VG_{45}, (c) VG_{60}), and (c) flow visualization for span angle of 45° at three different Re_{Dh} ((a) Re_{Dh}=500, (b) Re_{Dh}=1500, (c) Re_{Dh}=2500) [57].

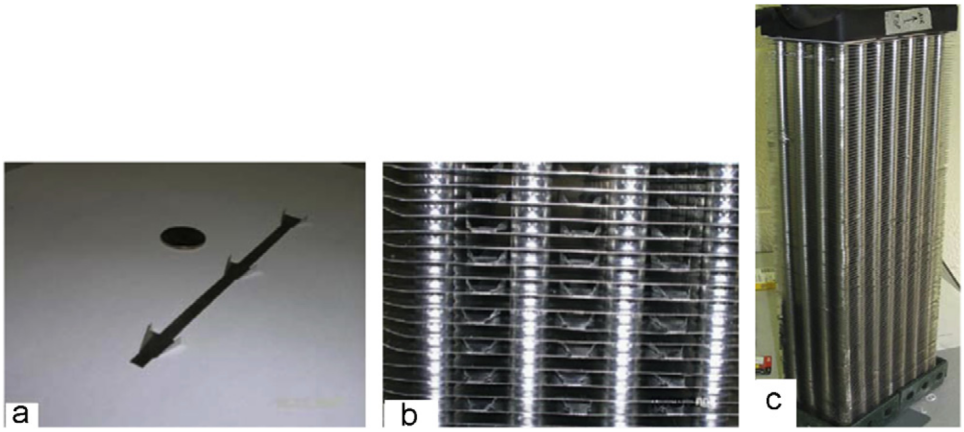


Fig. 11. VG implementation: (a) winglets are manufactured as strips with six winglets, (b) VG in fin-spaces of the heat exchanger provides approximately 3500 winglet VGs in CFU configuration and (c) heat exchanger geometry showing actual evaporator [59].

rectangular, triangular and circular winglets. Joardar and Jacobi [59] examined delta-winglet pairs arranged as a single-row VG placed at the leading tube and three-row-inline VG array placed at alternate tubes as shown in Fig. 11. They found that the 3VG array yields higher pressure drop penalty which decreases rapidly with increase in *Re* number. They reported that when the heat transfer is augmented by using VG, the size of heat exchanger can be minimized to get the same heat duty. So the available size reduction could be redeemed by reducing the flow length which leads to reduce the pressure penalty and can reduce cost and allow more compactness.

Kwak et al. [60] and Tang et al. [61] found that the increase of VG attack angle or length, or decrease of VG height may enhance the performance of vortex-generator fin of the fin-and-tube heat exchanger.

Shi et al. [4] studied the optimal fin spacing for three-row flat tube bank fin mounted VGs. They observed that for commonly used fin materials and fin thickness, the optimal fin spacing is about 2 mm in industrial application. Wang et al. [11] showed that, for the same height of winglet, the delta-winglet exhibits intensely vertical motion and flow unsteadiness. They interpreted that this leads to a better flow mixing phenomenon. They showed that the corresponding pressure drops of the DW pair of VG are lower than those of the annular winglet at the same *Re* number. The pressure drop penalty of VG is relatively proportional with *Re* number.

Numerically, many researchers have studied the heat transfer augmentation in inline/staggered circular tube heat exchangers with several types of VG mounted on the channel walls such as [13,16,42–48]. Gorji et al. [13] studied the heat transfer on staggered circular tube heat exchanger with VG embedded in hydrodynamically developed and thermal developing laminar boundary layer. For an incompressible fluid, they have seen that the average *Nu* number increases with presence of airfoil obstacle by about 20–30% and these obstacles are effective to increase the heat transfer. They reported that the more *Re* number the better effect on *Nu* number. Their results revealed that a triangular obstacle with three attack angles improve the heat transfer compared to the plain case. The downstream reattachment lengths were found to depend only on the triangle's angle of attack [62]. Joardar and Jacobi [15] studied the effect of three arrangements of DWVG on heat transfer performance of seven-row inline-tube heat exchanger. These arrangements are: single pair, three inline array, and three staggered array mounted in laminar boundary layer. It was observed that the CFU arrangement of DWVG has high effectiveness on the heat transfer enhancement. At a constant tube-wall temperature, the 3-VG-inline-array configuration achieved enhancement up to 32% over

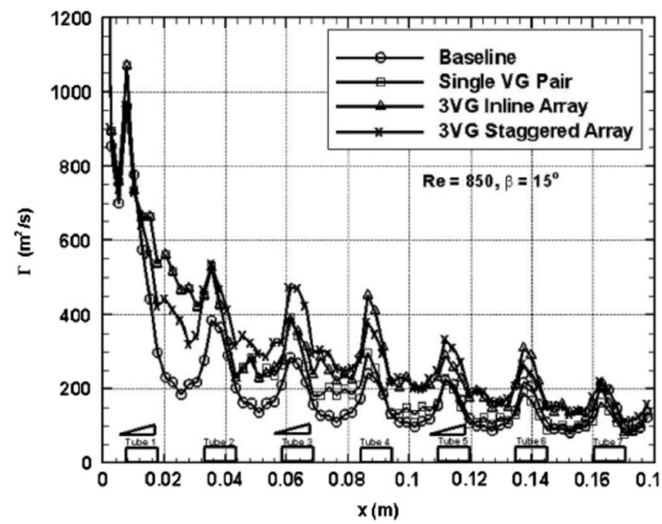


Fig. 12. Local heat flux distribution ($z=0$) at different axial locations on the VG fin for four configurations [15].

the baseline case. The local heat flux on the VG mounted fin ($z=0$) for four arrangements are shown in Fig. 12.

Lei et al. [63] found, that the heat transfer coefficient increases as the attack angle of VG increases when *Re* number was ranged from 600 to 2600 and the attack angle was varied from 10° to 50°. The DWVG with an attack angle of 20° and aspect ratio of 2 provides the best performance over the range of *Re* number. Their results implied that the VG placed in CFU orientation are more effective flow at lower *Re* numbers than at high *Re* numbers. They found that the heat transfer coefficient increases with the increase in *Re* number. The results show that the DWVG in CFU configuration can enhance heat transfer performance without an excessive amount of pressure drop penalty. This pressure drop penalty increases with the increase of attack angle and the increasing tendency is strengthened gradually.

Gorji and Soleimani [64] revealed that heat exchangers with triangle obstacle improve the heat transfer in comparison with heat exchangers without obstacle. The upstream location of flow separation and the downstream reattachment lengths are found to depend only on the triangle's angle of attack. Ünal and Gören [65] performed 3-D computational simulations of the flow around a circular cylinder fitted with VGs. Their numerical calculations emphasized the effectiveness and the performance enhancing character of the VGs. Li et al. [66] performed a 3-D numerical simulation on laminar heat transfer and flow characteristics of a slit fin-and-tube heat exchanger with

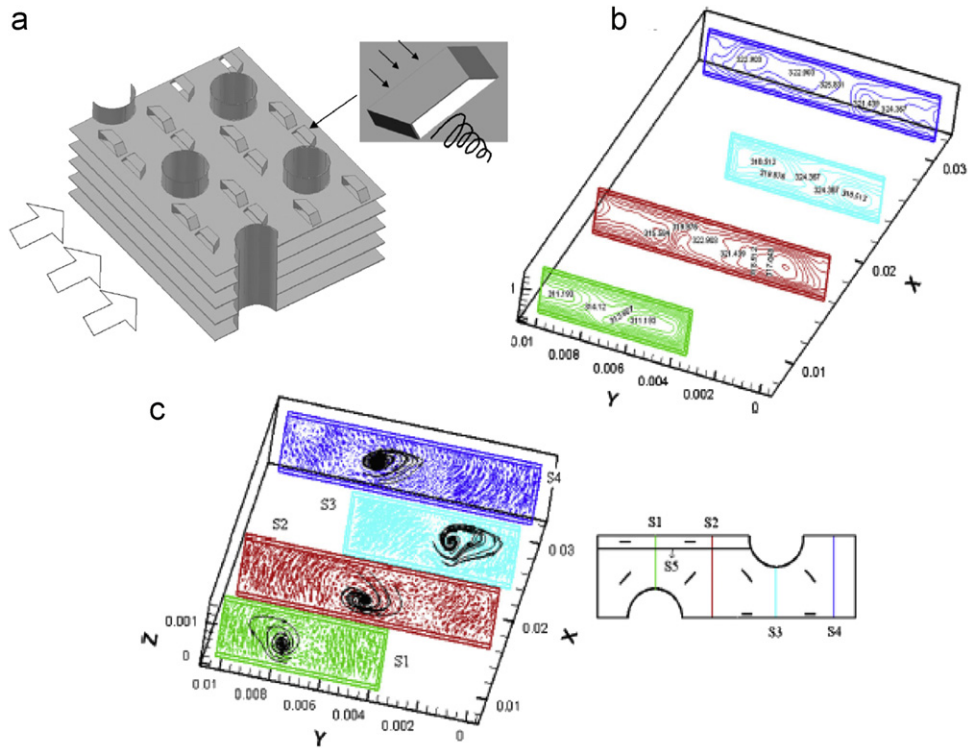


Fig. 13. (a) Schematic diagram of core region of a slit fin-and-tube heat exchanger with LVGs, (b) streamlines generated by LVGs and (c) temperature distribution in four y–z sections at $Re=1051.3$ [66].

LVGs. The core of the compact heat exchanger, the streamlines and the temperature distribution at four y–z sections with the using of LVGs is shown in Fig. 13.

They found a significant heat transfer enhancement with the modest pressure drop penalty. The same study was performed by Zeng et al. [67] to examine the effect of DW pairs of VG on the thermal performance of fin-and-tube surface. They observed that the intensity of heat transfer can be greatly increased with the increase of the VG attack angle and the length and height of VG accompanying with the increase in pressure drop. Wu and Tao [68] displayed that the heat transfer enhancement of delta-winglet with an attack angle of 45° is larger than that of 30° while the pressure drop associated is also greater for the range of *Re* number of 800–2000.

Tiwari et al. [69] and Chu et al. [70] found that the average *Nu* number for the three-row fin-and-oval-tube heat exchanger with LVGs increases by 13.6–32.9% over the baseline case, and the corresponding pressure loss increased by 29.2–40.6%. They displayed that LVGs with placement of downstream, angles of attack 30° and two tube-row provide the best heat transfer performance.

Other researchers have investigated the heat transfer enhancement (HTE) in many-row oval (flat) tube heat exchangers using different types of VGs such as [6,71–73]. Chang et al. [6] examined the influence of the attack angle and the aspect ratio of a DWVG which is punched near the leading edge of the fin of a compact heat exchanger (CHE) on heat transfer enhancement. The VG was embedded in a thermally and hydrodynamically developing laminar boundary layer with angle of attack ranged from 20° to 45°. They displayed that the winglet with $\beta=30°$ and aspect ratio of 2 provides the best ratio of HTE. They highlighted that when the dimensionless distance of DWP from the leading edge changes from 1.46 to 0.63, a little HTE has. Chen et al. [71] punched LVGs in form of winglets in staggered arrangements to enhance heat transfer in finned oval tube heat exchanger elements at $Re=300$ and $\beta=30°$. They demonstrated that the staggered arrangement of the winglets has more effective than the inline arrangement for heat transfer enhancement. In the staggered arrangement, which is away from the tube, has more effective for heat transfer than winglets which is near the tube. They also found that the temperature distribution in the flow passage is intensively distorted by the staggered longitudinal vortices. The vector-plots of the secondary flow and corresponding 2D streamlines in eight cross-sections of several configurations of VGs at $Re=300$ are shown in Fig. 14.

Chen et al. [73] added a new idea to augment the heat transfer in a flat-tube bank fin surfaces where VGs are mounted on both surfaces of the fin. Their results revealed that using this configuration of VGs, the height of VGs can be reduced and still obtain satisfactory THE. They found that if VGs on one surface of the fin is determined, the locations where VGs are mounted on other surface of the same fin are very important. While Song et al. [72] studied the relationship between the intensity of the secondary flow produced by VGs which are mounted on a three-row flat tube bank fin surfaces and the strength of convective heat transfer. The results revealed that the averaged absolute vorticity flux normal to the main flow direction can reflect the intensity of the secondary flow. In most cases, the secondary flow cannot change greatly the boundary layer characteristics especially for the internal flow at beginning region of boundary layer. The averaged absolute vorticity flux can account for only the secondary flow effects on convective heat transfer but cannot quantify the effects of developing boundary layer on convective heat transfer.

Lemouedda et al. [74] performed a numerical investigation to study the performance of the finned-tubes using DWVGs. They demonstrated that VGs increase the level of vorticity especially behind the tubes and increase the mixing inside the finned tubes. This process enhances the heat transfer rate. They found that the tubes are exposed to stronger mean flow where the first pair of VG is in CFU configuration with mainstream flow compared with CFD configuration. This leads to increase the local heat transfer

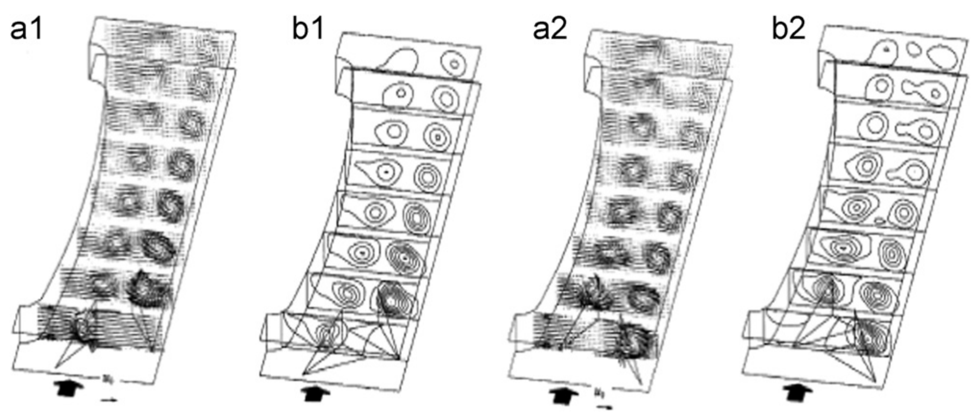


Fig. 14. Secondary flow and the corresponding 2D streamlines on eight cross-sections in several configurations at $Re = 300$: (a) velocity vectors and (b) temperature distribution [70].

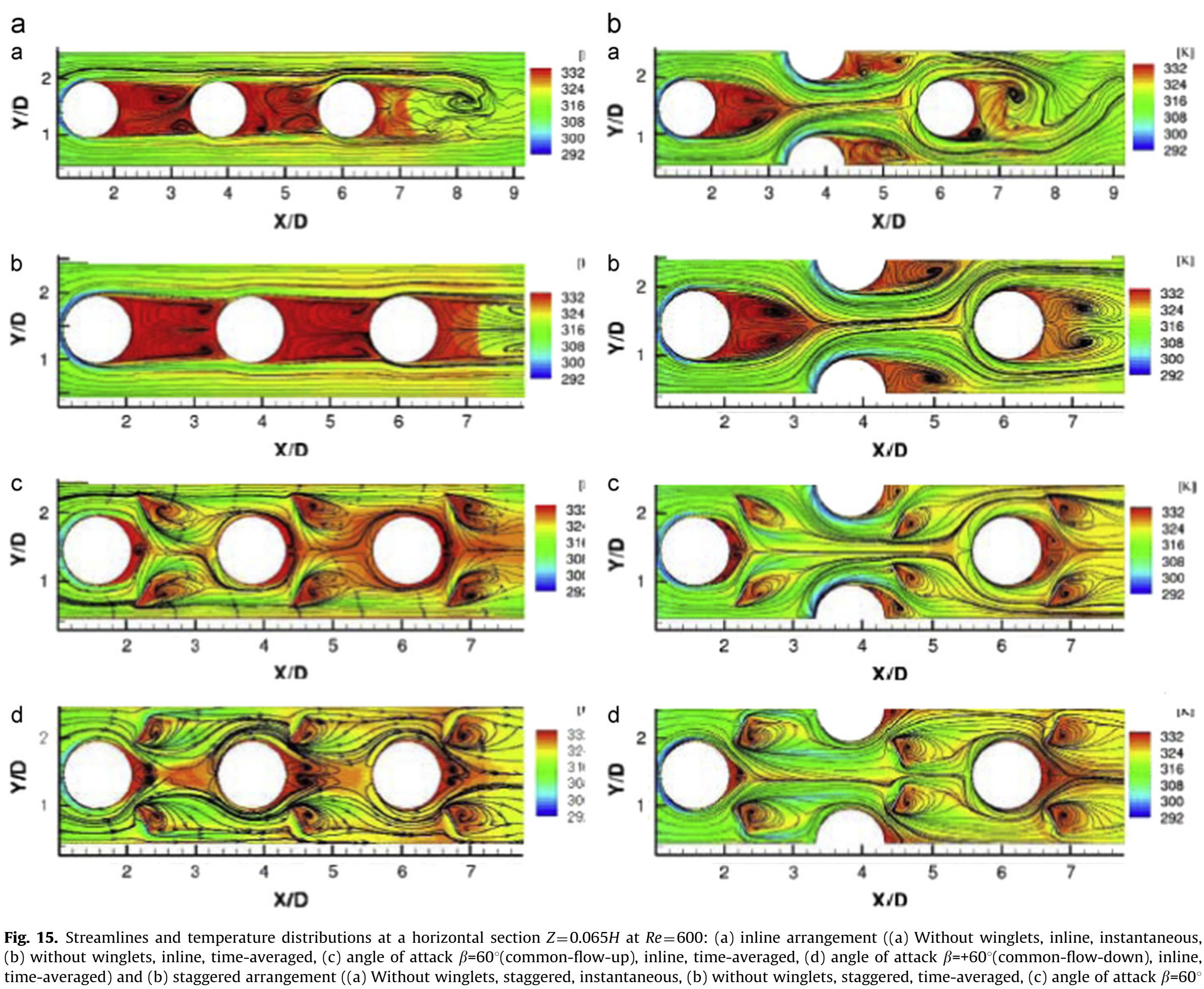


Fig. 15. Streamlines and temperature distributions at a horizontal section $Z = 0.065H$ at $Re = 600$: (a) inline arrangement ((a) Without winglets, inline, instantaneous, (b) without winglets, inline, time-averaged, (c) angle of attack β=60°(common-flow-up), inline, time-averaged, (d) angle of attack β=+60°(common-flow-down), inline, time-averaged) and (b) staggered arrangement ((a) Without winglets, staggered, instantaneous, (b) without winglets, staggered, time-averaged, (c) angle of attack β=60° (common-flow-up), staggered, time-averaged, (d) angle of attack β=+60° (common-flow-down), staggered, time-averaged) [74].

accompanied by increase in pressure drop. They have seen that increase the number of DWVGs will increase the heat transfer rate which is also accompanied by increasing the pressure drop. The optimal design they obtained is 14% higher than that without VGs. The streamlines and temperature distributions at $Z = 0.065H$ and $Re = 600$ can be seen in Fig. 15. They stated that this increases the flow resistance leading to higher pressure losses and hence to higher power input required.

O'Brien et al. [75] showed that the addition of single pair of winglet to the oval-tube geometry yields significant heat transfer

enhancement averaged 38% higher than the oval-tube without VG. While the corresponding increase in friction factor was very modest, less than 10% at $Re_{Dh}=500$ and less than 5% at $Re_{Dh}=5000$. They demonstrated that the highest mean heat transfer coefficient can be observed for the case of circular-tube with winglets located on the downstream side of the cylinder, oriented at 45° angle to the flow.

3.4. Heat sink

Dake and Majdalani [76] designed thin winglet-type VG mounted on the leading edge of heat sink fins as shown in Fig. 16. This idea is applied for PCs, routers and servers. An experimental simulation of the interfin channel reveals that certain VGs, when placed upstream, can outperform others in their ability to fill the channel with pairs of strong vortices. Multiple pairs can also be generated to further accentuate the heat transfer using dual VGs. They summarized their results as follows: the flat shape of VG provides the most stable structure; the trapezoidal design induces the most oval shaped vortices with the spacing being a function of the width of the tip; the curved shape tends toward smaller; faster rotating vortices with the separating rotational center; the double delta design provides the least productive vortices exhibiting small outer diameter and widely spaced centers. Their results show that the lower angle of attack produces the widest vortex spread, presence of the common-downwash region, and recirculation zones in each case.

Kai-Shing et al. [77,78] stated that the enhancement using VG mounted in a heat sink are relatively effective when the flow is in the developing region whereas they become quite less effective in the fully developed region especially when the fin pitch is small or operated at a lower frontal velocity. They suggested that the vortex generators operated at a higher frontal velocity and at a larger fin pitch are more beneficial than that of plain fin geometry. The semi-circular VG has the highest heat transfer coefficients and pressure drops at developing region. They obtained a reduction of 31.1% in the heat dissipation area at a frontal velocity of 5 m/s within a developing region while for fully developed region the area reduction was of 1.8–11.5% at a frontal velocity 3–5 m/s. The results suggest that the vortex generators operated at a higher frontal velocity is more beneficial than that of plain fin geometry. The triangular attack vortex generator is regarded as the optimum enhancement design for it could reduce 12–15% surface area at a frontal velocity around 3–5 m/s.

3.5. Electronic chips

Investigations have been done to study the augmentation in heat transfer in air cooling of a staggered array of rectangular electronics modules using DWVGs. Chomdee and Kiatsiriroat [79,80] observed that the VGs could enhance the heat transfer coefficient by 10–30% and reduce the thermal wake function and the module temperature when VGs integrated in front of all modules. They encouraged that the attack angle should not be more than 10°. They monitored that when VGs integrated in front of first row only, the heat transfer enhancement is distinct only at the first row. They observed that a higher attack angle results higher pressure drop in the fluid flow. They advised that the attack angle should not be more than 10°.

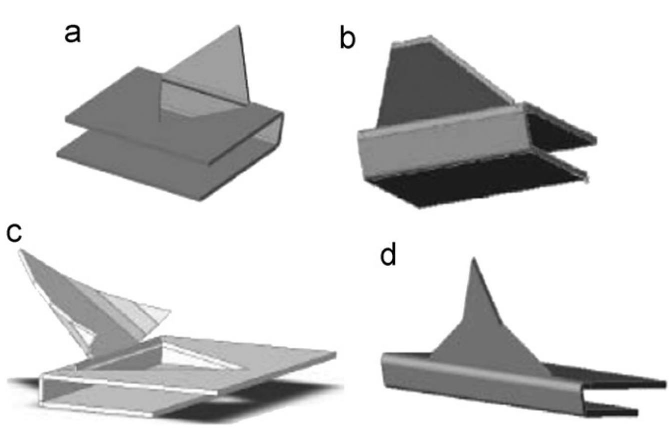


Fig. 16. Shapes of vortex generators [76]. (a) Flat triangular design. (b) Trapezoidal design. (c) Curved design. (d) Double delta design.

3.6. Mini-channels and microchannels

Qiuwang et al. [26] carried out experiments on the heat transfer and pressure drop in horizontal narrow rectangular channels with mounted LVGs for water flow to enhance heat transfer in cooling channels of plate-type fuel elements in reactor cores. They displayed that the LVGs could greatly improve the heat transfer rate by 10–45%, and the heat transfer performance of channel with LVGs on two sides are better than those on one side.

Jian et al. [27] stated that single-phase heat transfer of water can be enhanced greatly with acceptable increasing flow resistance after using several pairs of LVG as disturbing elements in narrow rectangular channel. For laminar flow regime, heat transfer augmentation was around 100.9% and flow resistance was increased only 11.4%, whereas heat transfer augmentation was over 87.1% and the flow resistance was increased 100.3% for the turbulent flow regime. They found the performance of heat transfer enhancement became better with increasing *Re* numbers in turbulent regime.

Chao et al. [81] showed that heat transfer is enhanced in rectangular microchannel using LVGs compared with the smooth microchannel, with large pressure drop. They found that changing the direction of attack angle of one pair of LVGs in the streamwise direction can delay the occurrence of laminar-to-turbulent transition to some extent.

3.7. Refrigeration

In most domestic and commercial refrigeration systems, frost forms on the air-side surface of the air-to-refrigerant heat exchanger. Frost-tolerant design typically employ a large fin spacing in order to delay the need for a defrost cycle. Unfortunately, this approach does not allow for a very high air-side heat transfer coefficient, and the performance of these heat exchangers is often air-side limited. Sommers and Jacobi [82] stated that LVG is an effective technique for thinning the thermal boundary layer and enhancing heat transfer, but its efficacy in a frosting environment is essentially unknown. They studied an array of delta-wing VGs applied to a plain-fin-and-tube heat exchanger as shown in Fig. 17. They indicated that the air-side thermal resistance is reduced by 35–42% when VG is used. While the heat transfer coefficient increases by 60–93% when *Re* number is ranged from 500 to 1300.

The heat transfer performance of the air-cooled condensers used in binary geothermal power plants can be developed by replacing the circular tubes with oval tubes and adding strategically located VGs (winglets) in the fins [83]. They indicated that the addition of winglets increases the heat transfer coefficient by about 35% approximately, compared to plain tubes. Corresponding increase in friction factor is in the range of 5–10% for *Re* number based on the hydraulic diameter in the range of 500–5000.

4. Nanofluids

Advances in high power technology are demanding size reduction of thermal systems resulting in constrained spaces for increased heat

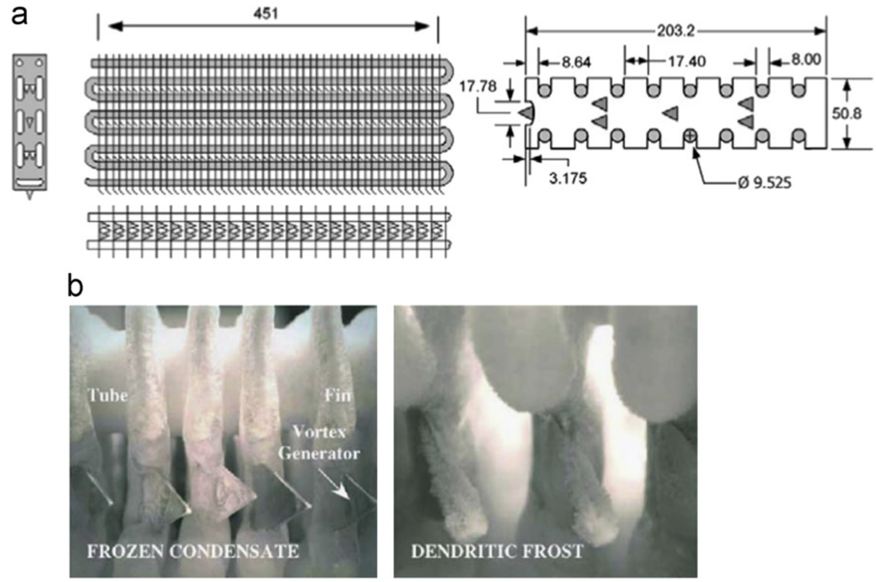


Fig. 17. (a) Heat exchanger geometry and VG configuration and (b) frost deposition on delta-wing type VGS [82].

transfer. This has led to thermal management problems in emerging systems which have defied solution by conventional cooling methods. Due to recent developments in nanotechnology, a new class of heat transfer fluids called nanofluids was discovered [84]. The nanofluid is a solid–liquid mixture in which metallic, nonmetallic or polymeric nanoparticles are suspended. The suspended ultrafine particles change transport properties and heat transfer performance of the nanofluid, which exhibits a great potential in enhancing heat transfer. However, the usual slurries, with suspended particles in the order of millimeters or even micrometers may cause some severe problems. The abrasive action of the particles causes the clogging of flow channels, erosion of pipelines and their momentum transfers into an increase in pressure drop in practical applications. Furthermore, they often suffer from instability and rheological problems. In particular, the particles tend to settle rapidly. Thus, although the slurries give better thermal conductivities, they are not practical. The nanofluid appears with development of nanoscience and nanotechnology. The great potential of nanofluids in enhancing heat transfer means chances and challenges in thermal science and engineering. Since the concept of the nanofluid is newly proposed, so there are many questions which remain unclear and need to be solved [85,86].

Several important factors such as the type, shape and size of nano-particles, clustering and settling of nano-particles, and temperature of the nanofluids have not been studied widely. In addition, lack of agreement between experimental results and theoretical models is still the main issue of authors.

Many authors reviewed the literature of nanofluids like [86–93] and reviewed and discussed the enhancement of convection heat transfer using nanofluids, experiments to synthesize the nanofluids, techniques of measuring the thermal conductivity and absolute viscosity of nanofluids, problems and challenges of nanofluids and the applications of nanofluids. In this review of literature, we focus on recent investigations which show new and precise empirical correlations for nanofluids properties with low deviations with related experimental results and new applications for nanofluids particularly in micro-scale heat exchangers.

4.1. Synthesis of nanofluids

The synthesis of the nanofluids is the first key to enhance the thermal conductivity (k) of nanofluids. The convenient of nanofluid does not mean a simple liquid–solid mixture. Nanofluids are produced by dispersing nanometer-sized solid particles into base-liquid such as water, ethylene glycol (EG), oil, etc. The major problem in the preparation of the nanofluid is the agglomeration (clustering) of the nanoparticles. The nanotechnology opens wide opportunities to produce nanometer scale particle with different shapes. There are mainly two techniques for the preparation of nanofluids; the single (one)-step process and two-step process.

The single-step process is direct evaporation approach. Preparation of nanofluid using this process is done by making and dispersing nanoparticles directly into the base fluid. This process is used to produce non-agglomerating copper nanoparticles which remain uniformly dispersed and stably suspended in EG. This process is favorable because it prevents the oxidation of the nanoparticle especially for nanofluids which have high-conductivity metals such as copper.

When the nanoparticles are made and then dispersed in the base fluid later it is known as two-step process. This process is extremely utilized to synthesize nanofluids considering the available commercial nanopowders. The advantage of this process is that the inert gas condensation technique has been developed to economically produce nanoparticles. Whereas the disadvantage of this process is essentially when the nanoparticles tend to agglomerate before the nanoparticles dispersed in base fluid. So, one of the challenges to solve the agglomeration problem of the nanoparticles is the development of an innovative method to avoid the agglomeration which generally occurs in all nanopowders [94–96].

Liu et al. [97] prepared the nanofluids phase change materials (PCMs) wherein TiO_2 nanoparticles using the two-step procedure. The nanoparticles were uniformly dispersed in saturated $BaCl_2$ aqueous solution with pH 8. For stabilization, a supersonic oscillator was used to improve the dispersion of nanoparticles in fluid. They did not use any thickening agents to help suspending and prevent phase separation.

Zhu et al. [98] synthesized and developed stable CuO nanofluids using a wet chemical method in a large-scale. They found that the concentration of copper acetate and reaction time affected the size and shape of clusters of primary nanoparticles. Nanofluids with different microstructures could be obtained through changing the synthesis parameters. The thermal

conductivity of CuO nanofluids increased with the increase of particle loading. It is expected that this method can be extended to synthesize other nanofluids.

Sudhan and Meenakshi [99] developed the one-pot method for preparing silver nanofluids by reducing silver nitrate using sodium hypophosphite as reducing agent and ethylene glycol as base fluid by means of conventional heating. This is advantageous over other conventional methods; economical and one-step. The non-agglomerated and stably suspended silver nanofluids are obtained in a short time and the synthesized silver nanofluid has superior thermal conductivity. Hence, the silver nanofluid resulted, as they mentioned, may be used as an effective coolant in automobile industry in place of the conventional fluids that are currently in use.

4.2. Mechanisms of nanofluids

Keblinski et al. [100] explored four possible explanations for anomalous increase in the thermal conductivity with the decrease in the grain size. These mechanisms are Brownian motion of the particles, molecular level layering of the liquid at the liquid/particle interface, the nature of heat transport in the nanoparticles, and the effects of nanoparticle clustering. They showed that the key factors in understanding thermal properties of nanofluids are the ballistic, rather than diffusive, nature of heat transport in the nanoparticles, combined with direct or fluid-mediated clustering effects that provide paths for rapid heat transport.

Based on Green–Kubo linear response theory, Nie et al. [101] utilized the exact expression for the heat flux vector of the base fluid plus nanoparticle system to estimate the contribution of nanoparticle Brownian motion to thermal conductivity. They found that the contribution is too small to account for abnormally high reported values. They also found the possibility of convection caused by Brownian particles is also unlike. They demonstrated a layer structure can form around the nanoparticles and the structure does not further induce fluid–fluid phase transition in the bulk fluid. For the models of an asymmetric hard sphere mixture representing the single spherical nanoparticles and a mixture of rods and hard spheres representing aggregates, both suspended in the fluid, they observed that for the very low volume fraction cases, the compressibility slightly changes. This shows that the speed of phonon transition is unchanged due to the addition of nanoparticles of any type. The results indicate that, besides the enhancement due to the high thermal conductivity of nanoparticles themselves, fluid molecules make no evident contribution to the enhancement of thermal conductivity which is attributed to the presence of the nanoparticles at volume fractions less than 5%.

Ma and Liu [102] demonstrated that having the highest conductivity, being electromagnetically drivable, the liquid metal with low melting point is expected to be an idealistic base fluid for making super conductivity solution which may lead to the ultimate coolant in a wide variety of heat transfer enhancement area.

4.3. Thermal conductivity measurement techniques

The importance of thermal conductivity measurement is potential because *k* is responsible for heat transfer enhancement. Plenty of investigations have been done and developed in this area to get a reasonable accuracy. The temperature oscillation technique, the steady-state parallel-plate technique, and the transient hot wire method have been used to measure the thermal conductivity of nanofluids [103,104]. The last one has been utilized widely due to its high accuracy. The schematic diagram of the transient hot-wire set-up for measuring the thermal conductivity of nanofluids is shown in Fig. 18.

Because of the electrical conductivity for all nanofluids, the hot wire should be surrounded by such material as epoxy adhesive which has an excellent electrical insulation to avoid applying the hot wire directly to the nanofluid [106]. There is no significant negative effect of the insulation layer on the performance of this method. The principle of this method is using a thin metallic wire embedded in the liquid to measure its thermal conductivity. This wire is employed as a heat source and a temperature sensor. The wire is heated by applying a power supply through it. The principle idea of this method is measuring the temperature/time response of the wire to an abrupt electrical pulse. A higher conductivity of surrounding nanofluid, a lower temperature will be raised in the wire. The advantage of this method is faster than the other techniques, and it has a simple design compared to other techniques.

Xie et al. [103] measured thermal conductivity of nanosized SiC (26 nm) suspensions using the same method. Their experimental results illustrated that the thermal conductivities of the suspensions containing a small amount of solid particles are higher than those of the base liquids. For low volume fraction, they found that thermal conductivities increase almost-linearly with the volume fraction of the particles. The *k* increased by about 15.8% at 4.2vol% of particles. For different systems containing the same kind of particles, the thermal conductivity ratios are independent of the base liquids, but the absolute value of the thermal conductivity of the suspension is proportional to that of the base liquids. Wang and Xu [107] measured the thermal conductivity of nanofluids consisted of Al_2O_3 (28 nm) and CuO (23 nm) suspended with distilled water as a base fluid by a steady-state parallel method. They demonstrated that the predicted thermal conductivities of nanoparticle–fluid mixtures are much lower than their measured data. They indicated that there

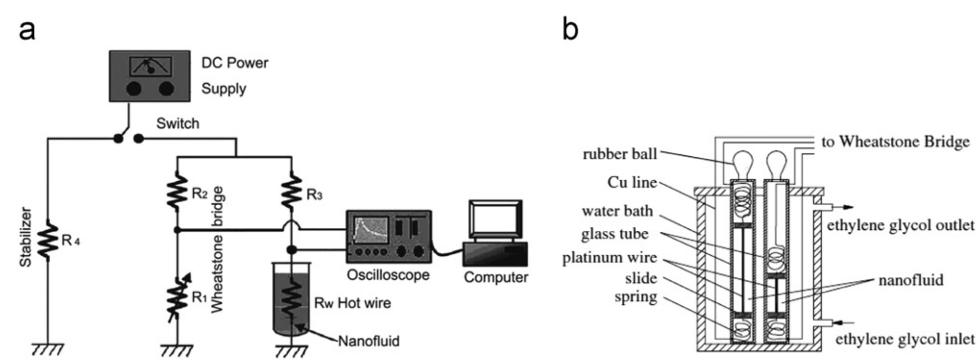


Fig. 18. (a) Schematic diagram of the transient hot-wire apparatus for measuring the thermal conductivity of nanofluids [105] and (b) schematic diagram of transient hot wire instrument [54].

is a deficiency in models when they employed for nanoparticle–fluid mixtures.

Asseal et al. [104] obtained a 34% of enhancement of the thermal conductivity for 0.6vol% of carbon multi-walled nanotubes (C-MWNTs) suspended in water using the transient hot-wire method. Hu et al. [108] measured thermal conductivity of AlN-ethanol nanofluids by a hot-disk method from 0.5% to 4% volume fraction at temperatures of 273.15 K and 297.15 K. The hot-disk thermal constant analyzer system is shown in Fig. 19.

They reported that 20% increase in thermal conductivity of ethanol with the addition of 4 vol% at 273.15 K and a strong temperature dependence of the thermal conductivity. Li et al. [109] measured the thermal conductivity of Al_2O_3 (47 nm)/water nanofluid with 0.5–6 vol% using the transient hot wire and the steady-state cut-bar method at room temperature. They concluded that the enhancement in thermal conductivity of the nanofluid exists and is independent of the measurement technique. Chen et al. [110] applied small angle X-ray scattering (SAXS) to the characterization of SiO_2 nanoparticles (10–30 nm) uniformly dispersed in a water-base fluid. They observed that thermal conductivity for 16 vol% of nanoparticles shows a linear increase with increasing the average particle size. They suggested that thermal resistance at the solid–liquid interface may be critical to the thermal conductivity of nanofluids with small particle sizes.

A transient Hot Wire Technique for measuring the thermal conductivity in liquids is implemented in an in-house made computer controlled experimental set-up was presented by Codreanu et al. [111]. The aim of this technique is that the thermodynamic state of the material under test is not changed during the measuring process due to the small heat disturbance and thermal properties can be assigned to the equilibrium temperature attained prior to the disturbance. They reported that the Quick Start Development System from Analog Devices offers a very convenient, rapid, low cost, highly sensitive and accurate solution for implementation of the Hot Wire Technique. The high resolution of the converter ensures a good precision of measurements. Fig. 20 illustrates the experimental set-up and the testing cell configuration.

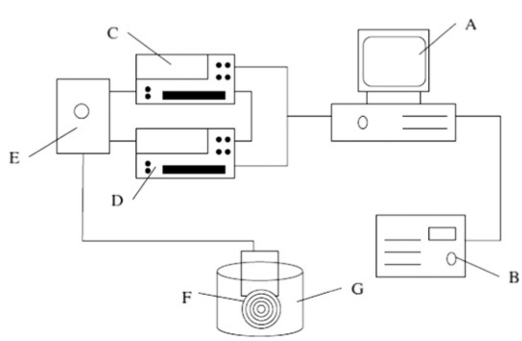


Fig. 19. Hot-disk thermal constant analyzer system, (A) computer, (B) computation device, (C) Keithley 2000, (D) Keithley 2400, (E) Hot-disk bridge, (F) sensor, and (G) samples [108].

Table 1 shows the experimental results of the enhanced thermal conductivity of nanofluids measured by different technique methods.

4.4. Thermal conductivity enhancement

In 1990, Bonnecaze and Brandy [121] developed a general method to predict the effective thermal conductivity of an infinite, statistically homogeneous suspension of particles in an arbitrary (ordered or disordered) configuration. The method follows closely that of 'stokesian dynamics' and captures both far-field and near-field particle interactions accurately with no convergence difficulties. The results are found to be in excellent agreement with the accepted values. The effective conductivities of spherical particles in cubic arrays are calculated for particle to matrix conductivity ratios of infinity 10 and 0.01. Xuan and Li [94] observed that the volume fraction, shape, dimensions and properties of the nanoparticles affect the thermal conductivity of nanofluids. They revealed that the nanofluid shows great enhancement in the heat transfer process. The k_{nf}/k_f of the Cu–H_2O nanofluids remarkably increases with the volume fraction of ultra-fine particles. This increase is found to be varied from 1.24 to 1.78 times when the volume fraction of particles increases from 2.5% to 7.5%.

Suspensions of micron-sized silicon-carbide (SiC) particles with various aspect ratio ranged from 1 to 10 distributions are prepared and measured by Cherkasova and Shan [122]. They inferred that the thermal conductivity results are above the Maxwell prediction when anisotropic particle are used. They noticed, when the volume fraction remains constant, the thermal conductivity enhancement goes from 16.5% up to 39.5% as the volume-averaged aspect ratio increases from 4.8 to 9.6. They observed that any possible contamination of the suspension by the grinding material itself should only increase the conductivity with grinding time which is opposite to the observed trend. Kondaraju et al. [123] investigated the effective thermal conductivity of Cu (100 nm)/water nanofluid and Al_2O_3 (80 nm)/water nanofluid by developing the Eulerian–Lagrangian based direct numerical simulations (DNS) model. Their results exhibit an increase in the thermal conductivity of nanofluids with the

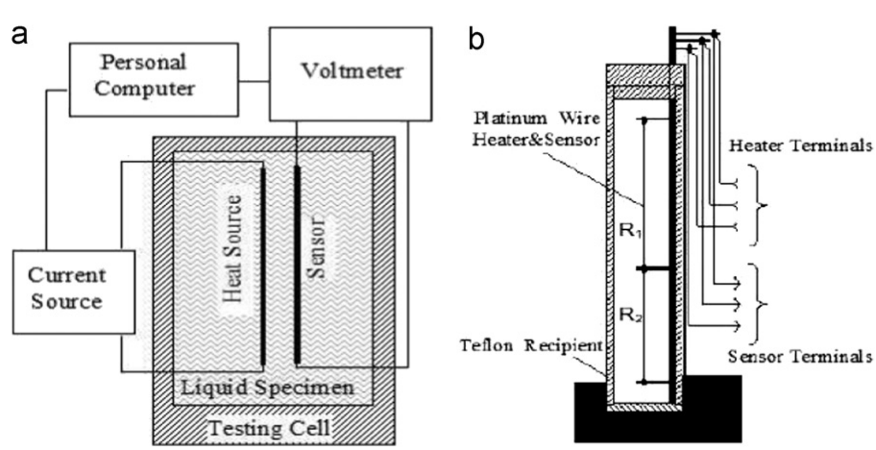


Fig. 20. (a) Basic configuration of the experimental set-up measuring the thermal conductivity of liquids and (b) the testing cell configuration [111].

Table 1
Illustration of the techniques used for measuring *k*.

Nanofluid/Ref.	Diameter/length	Volume fraction	Method used to measure *k*	Max. enhancement in *k*
$TiO_2/BaCl_2$ aqueous [97]	20 nm	0.167–1.13%	THW	15.65%
SiC/water [103]	26 nm 600 nm	4.2%	Transient hot wire	20%
C-MWNTs/water	D_{out}=40 nm, D_{in}=15 nm	0.6%	THW	34%
C-DWNTs/water [104]	D_{out}=5 nm, D_{in}=2.5 nm l=10 μm			38%
Al_2O_3/water	28 nm	2.4–8%	Steady-state	40%
CuO/water [107]	23 nm		Parallel-plate	
ALN/ethanol [108]	20 nm	0.5–4%	Hot-disk	20%
Al_2O_3/water [109]	47 nm	0.5, 2, 4, 6%	THW Steady-state cut-bar	$k_{THW} < k_{steady\text{-}state}$ at 4 vol% $k_{THW} \geq k_{steady\text{-}state}$ at 2.6 vol%
SiO2/water	12 nm	0.45–4%	3ω	
Al_2O_3/water [112]	30 nm	0.5–1.5%		
Al_2O_3/water	45 nm	4%	3ω	13.3%
Al_2O_3/EG [113]				
ALN/ethanol [114]	20 nm	0.5%-4%	Hot-disk	20%
Cu_2O/water	200.5 nm	0.02–0.05	THW	24%
$CuSO_4$/water [115]		mol/L		
CuO/water	29 nm	3.3–9.32%	THW	16% (20–40 °C)
Al_2O_3/water [116]	36 nm, 47 nm	3.14–9%		16% (20–40 °C)
Al_2O_3/water	47 nm	0.8%	Transient hot wire	6.52%
CuO/water [117]				24.6%, and 2–4 times at 30–60 °C
Silver-water [118]	100–500 nm	1000 ppm 5000 ppm 10 000 ppm	Transient hot wire	10% 16% 18%
Hybrid sphere of alumina/iron oxide CNTs [119]	∅70 nm, 2μm	0.2%	3ω	21%
$Al_{70}Cu_{30}$/EG [120]	20–40 nm	0.2–2 vol%	Modified thermal comparator	Twofold

increase of volume fraction. They proposed that the temperature two-way coupling term should be considered for predicting the thermal conductivity of nanofluids. The results also show larger thermal conductivity for nanofluids where the coagulation of particles is not considered. The coagulation of nanoparticles in fluids is inevitable and thus numerical models should consider it for an accurate prediction of thermal conductivity.

Yu and Choi [124] developed the Hamilton–Crosser model for suspensions of nonspherical particles to include the effect of a solid/liquid interface. The solid/liquid interface is described as a confocal ellipsoid with a solid particle. Their new model for the three-phase suspensions is mathematically expressed of the equivalent thermal conductivity and equivalent volume fraction of anisontropic complex ellipsoids as well as empirical shape factor which is expressed as follows respectively:

$$k_{pj} = \left\{1 + \frac{k_p - k_s}{k_p[rd(j,0) - d(j,t)] - k_s[rd(j,0) - d(j,t) - r]}\right\} k_s \quad (1)$$

$$f_e = \frac{\sqrt{(a^2+t)(b^2+t)(c^2+t)}}{abc} f = rf \quad (2)$$

$$\psi = \frac{2e(t)[1-e^2(t)]^{1/6}}{e(t)\sqrt{1-e^2(t)} + \arcsin e(t)} \quad (3)$$

This model correctly predicts the magnitude of the thermal conductivity of nanotube-in-oil nanofluids. But at present, this model is not able to predict the nonlinear behavior of the nanofluid thermal conductivity. Shukla and Dhir [125] presented numerical results obtained from Molecular Dynamics Simulations of a solid–liquid system comprising of Lennard–Jones atoms used to study the liquid layering on solid nanoparticles. They found that close to the solid surface the liquid atoms from ordered layers which display higher thermal conductivity compared to the bulk liquid. They also presented a model for thermal conductivity of nanofluids based on the theory of Brownian motion of a free particle as follows:

$$\lambda_{particle} = \lambda_{liquid} + \frac{11}{32\pi^2}\,\frac{\phi k_B{}^2 T}{a^4 \mu} \quad (4)$$

where μ is the viscosity of the liquid. This relationship agrees qualitatively with the experimental results in that contribution of nanoparticles to the increase in thermal conductivity rises with an increase in particle volume fraction and fluid temperature.

Kumar et al. [126] derived a model of thermal conductivity based on the statistical mechanics in the first term and Brownian motion based on critical size and optimum effective volume fraction in the second term as follows:

$$\frac{k_{eff}}{k_f} = \left[\frac{k_p + (n-1)k_f - (n-1)\alpha_e(k_f - k_p)}{k_p + (n-1)k_f + \alpha_e(k_f - k_p)}\right] + \frac{C\alpha_e(T - T_o)}{\mu_{nf} k_f r_c^4} \quad (5)$$

where $\alpha_e = \alpha(1 + h/r_c)^3$, h is the liquid layer thickness and r_c is the critical particle size. The lesser the particle size, the higher the liquid layer thickness.

Putnam et al. [127] claimed that it is not observed an anomalous enhancement of the thermal conductivity that has been reported in previous studies of nanofluids. The largest increase in thermal conductivity that they noticed is $1.3 \pm 0.8\%$ for nanoparticles having 4 nm in diameter and volume fraction <1 for Au nanoparticles suspended in ethanol. Murshed et al. [128] conducted a combined experimental and theoretical study on the effective thermal conductivity of titanium oxide and aluminum oxide nanoparticles suspended in DIW and EG. They emphasized that the effective thermal conductivity is substantially higher than the values of the base fluids. They proposed models for nanofluids which show a good agreement with the experimental results and give better predictions for the effective thermal conductivity. They found that the effective thermal conductivity of nanofluids increases with the nanoparticle concentration.

Wang et al. [129] proposed a fractal model for predicting the effective thermal conductivity of liquid with dilute suspension of nonmetallic nanoparticles. This model predicts well the trend for

variation of the effective thermal conductivity with dilute suspension of nanoparticles, and fits successfully with their experimental data for CuO (50 nm)/DIW nanofluid with volume fraction less than 0.5%. Their calculated results show that the predictive calculation of effective thermal conductivity is complicated. Emami et al. [130] derived a general simple equation for thermal conductivity of all suspensions, including nanofluids, based on distance between particles. The Brownian motion approach should be used to calculate this distance in the nanofluids. The interactions between nanoparticles that were neglected in the derivation of Brownian motion relations may yield an incorrect calculated distance. An adjustable parameter was used to correct this distance as follows:

$$\Lambda^{Brow} = \left[\frac{8k_B T}{\pi m \varsigma^2}(2\varsigma\bar{t} - 3 + 4e^{-\varsigma\bar{t}} - e^{-2\varsigma\bar{t}})\right]^{1/2} - d_p \quad (6)$$

Han et al. [119] synthesized a new type of complex nanoparticle-hybrid sphere (∅70 nm, 2 μm)–CNT particle, consisting of numerous CNTs attached to an alumina/iron oxide sphere as shown in Fig. 21. These hybrid nanoparticles are dispersed to poly-alpha-olefin with sonication and a small amount of surfactant to form stable nanofluids. The thermal conductivity of the fluids was measured by a 3ω-wire method over a temperature range 10–90 °C. They states that for such hybrid nanoparticles, heat is expected to transport rapidly from one CNT to another through the center sphere and thus leading to less thermal contact resistance between CNTs when compared to simple CNTs dispersed in fluids. CNTs have an extremely high thermal conductivity, but thermal resistance between the CNTs and the fluid has limited their performance in nanofluids. Their experimental results refer that the effective thermal conductivity of the fluids is increased by about 21% at room temperature for particle concentration of 0.2 vol%.

Corcione [131] presented empirical correlation for predicting the effective thermal conductivity of nanofluids, based on a high number of experimental data available in the literature. It is found that the k_{nf}/k_f increases as the nanoparticle volume fraction and the temperature are increased, and the nanoparticle diameter is decreased as shown in Fig. 22. The wide range of the thermal conductivity equation of validity (i.e., 10–150 nm nanoparticle diameter, 0.002–0.09 volume fraction and 294–324 K temperature), makes such equation useful by the engineering point of view. The model formulas of thermal conductivity of [131–134] are as follows, respectively:

$$\frac{k_{eff(M)}}{k_f} = \frac{k_p + 2k_f - 2\varphi(k_f - k_p)}{k_p + 2k_f + \varphi(k_f - k_p)} \quad (7)$$

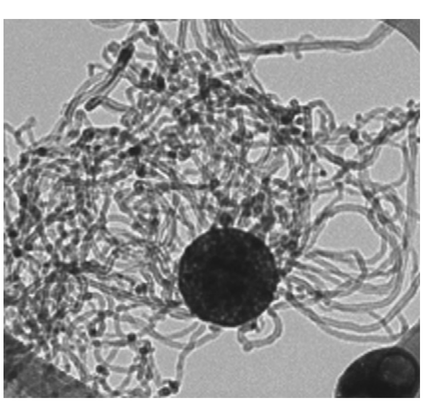


Fig. 21. TEM image of a sample hybrid sphere/CNT particle produced by the aerosol method. The central spheres are polydisperse with a broad size range from 10 to 300 nm, having a geometric mean diameter of 70 nm [119].

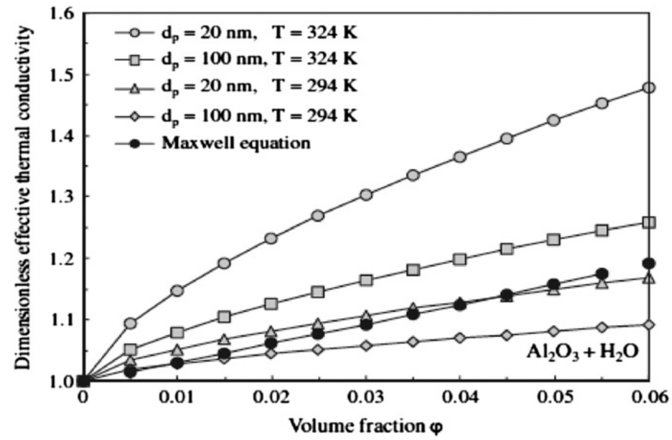


Fig. 22. Distributions of $k_{eff(M)}/k_f$ vs. φ for Al_2O_3–H_2O, with d_p and T as parameters [131].

$$\frac{k_{eff}}{k_f} = 1 + 4.4 Re^{0.4} Pr^{0.66} \left(\frac{T}{T_{fr}}\right)^{10} \left(\frac{k_s}{k_f}\right)^{0.03} \varphi^{0.66} \quad (8)$$

$$\frac{k_{eff}}{k_f} = 1 + 64.7 \times \phi^{0.7460} \left(\frac{d_f}{d_p}\right)^{0.3690} \left(\frac{k_s}{k_f}\right)^{0.7476} \times Pr^{0.9955} \times Re^{1.2321} \quad (9)$$

where

$$Pr = \frac{\mu}{\rho_f \alpha_f} \quad (10)$$

$$Re = \frac{\rho_f B_c T}{3\pi\mu^2 l_{BF}} \quad (11)$$

where l_{BF} is the mean free path of water, B_c is Boltzman constant. $k_{eff(M)}$ in Eq. (7) is the effective thermal conductivity of the nanofluid according to Maxwell.

Meibodi et al. [135] proposed a model of thermal conductivity of the suspension considering Brownian motion and interfacial layer as well as a new mechanism considering nanoparticles as liquid-like particles. Unlike Beck et al. [136], they pointed out that this model can be used for estimating of upper and lower limits of nanofluid thermal conductivity without any adjustable parameter. They concluded that the most important factor for thermal conductivity enhancement of nanofluids is distance between nanoparticles. At very low particle concentration, thermal conductivity can be calculated using Brownian approach. For micro-particles and/or high particle volume fractions can be calculated using effective diameter. They reported that Brownian motion and vibration of nanoparticle mechanisms can be considered for thermal conductivity of nanofluids, but these mechanisms display minor roles for enhancement of thermal conductivity in nanofluids.

The self-consisted scheme is generalized to predict the thermal conductivity of nanofluids containing spherical nanoparticles with a conductive interface was done by Hadjov [137]. He assumed that a flux jump in the particle–fluid interface in the opposite to the assumption for temperature jump in the case of thermal barrier resistance. An upper and lower bound to the homogenized suspension thermal conductivity according to the particle packing is. The model takes into account the enhanced conductivity and thickness of this thin layer. The suspension thermal conductivity is dependent on the kind of particle packing. This packing depends on the particle surface state and size distribution. In the same area of research, Xue [138] presented a novel model of the effective thermal conductivity for nanofluids

considering the interface effect between the solid particles and the base fluid in nanofluids. The results of effective thermal conductivity of nanotube/oil nanofluid and Al_2O_3/water nanofluid are in good agreement with the experimental data. Their model can interpret the anomalous enhancement of the effective thermal conductivity of nanotube/oil nanofluid and its nonlinearity with nanotube loading. His formula of thermal conductivity is

$$9\left(1-\frac{\upsilon}{\lambda}\right)\frac{k_e-k_m}{2k_e+k_m}+\frac{\upsilon}{\lambda}\left[\frac{k_e-k_{c,x}}{k_e+B_{2,x}(k_{c,x}-k_e)}+4\frac{k_e-k_{c,y}}{2k_e+(1-B_{2,x})(k_{c,y}-k_e)}\right]=0 \tag{12}$$

where $\lambda=abc/[(a+t)(b+t)(c+t)]$, $k_{c,j}$ is the effective dielectric constant component, and $B_{2,j}$ is the depolarization factor component of the elliptical particle along the j-symmetrical axis.

Koo and Kleinstreuer [139] theoretically found that the impact of nanoparticle Brownian motion is much more significant than the thermo-phoretic and osmo-phoretic motion effects. They observed that Brownian motion effect on thermal conductivity decreases with particle size. At very dilute nano-suspensions $<0.5\%$, particle interaction is negligible, while it may be profound for $>1\%$. The thermophoretic and osmo-phoretic motion effects were found to be independent of particle size, which is not the case for Brownian-motion included elevated thermal conductivities of dilute nanofluids. Their formula of thermal conductivity due to osmo-phoresis is

$$k_{OS}=\frac{1}{3\pi}\,\frac{\alpha_d^2 k}{\mu_c}\,\frac{3k_c}{k_d+2k_c}\rho_d c_d \nabla T \tag{13}$$

With viscous effects is

$$k_{OS}=\frac{1}{3\pi}\,\frac{\alpha_d^2 k}{\mu_c}\,\frac{3k_c}{k_d+2k_c}(1\times 10^5\rho_1 c_1)\nabla T \tag{14}$$

where k_c and k_d are the thermal conductivities of the continuous and discrete phases, respectively, ∇T is the temperature gradient in the spherical particle.

As a continuous work, Raykar and Singh [140] proposed a theoretical model employing a differential effective medium with Brownian motion to predict effective thermal conductivity (ETC) of CNT nanofluids. They inferred that ETC is influenced significantly by Brownian motion and enhancement is higher in dilute nanofluids. They predict that in future it is expected that the terms for the third phase (surfactants), dispersibility factors, and dynamic interfacial resistance are also incorporated using proper mathematical descriptions to predict the ETC of nanofluids. The combined static and dynamic mechanisms based model for predicting the ETC of nanofluids is presented also by Murshed et al. [141]. The model shows a good agreement with the experimental data of several types of nanofluids and gives better predictions compared to the classical and recently models. This is because they took into account the effects of particle size, nanolayer, Brownian motion, and particle surface chemistry and interaction potential which are the static and dynamic mechanisms responsible for the enhanced effective thermal conductivity of nanofluids. Their combined model of ETC of nanofluids is

$$\begin{aligned}k_{eff-nf}=&\left\{k_f\frac{\phi_p\omega(k_p-\omega k_f)[2\gamma_1^3-\gamma^3+1]+(k_p+2\omega k_f)\gamma_1^3\left[\phi_p\gamma^3(\omega-1)+1\right]}{\gamma_1^3(k_p+2\omega k_f)-(k_p+\omega k_f)\phi_p\left[\gamma_1^3+\gamma^3-1\right]}\right\}\\&+\left\{\phi_p^2\gamma^6 k_f\left(3\Lambda^2+\frac{3\Lambda^3}{4}+\frac{9\Lambda^3}{16}\frac{k_{cp}+2k_f}{2k_{cp}+3k_f}+\frac{3\Lambda^4}{2^6}+\ldots\right.\right\}\\&+\left\{\frac{1}{2}\rho_{cp}c_{p-cp}d_s\left[\sqrt{\frac{3K_BT(1-1.5\gamma^3\phi_p)}{2\pi\rho_{cp}\gamma^3 r_p^3}}+\frac{G_T}{6\pi\eta\gamma r_p d_p}\right]\right\}\end{aligned} \tag{15}$$

where d_s is the distance between two particles, c_p is the specific heat, K_B is the Boltzmann's constant, r is the particle radius, and η is the viscosity. For smaller sized nanoparticles and low volume fractions, dynamic mechanisms such as particle Brownian motion, particle interactions and surface chemistry are significant in enhancing the thermal conductivity of nanofluids. However, the major contributions to the enhanced thermal conductivity of nanofluids arise from static mechanisms. It can be inferred that the thermal conductivity of nanofluids is enhanced due to both static and dynamic mechanisms.

Papari et al. [142] presented a neural network method to estimate thermal conductivity of nanofluids consisting of MWCNTs suspended in oil (α-olfin), decene (DE), DW, EG, and single-walled carbon nanotubes (SWCNTs) in epoxy and poly methylmethacrylate (PMMA). Their predicted thermal conductivities values are in good agreement with the other theoretical models as well as experimental results. They mentioned that examining the neural network approach to predict other transport properties such as viscosity of nanofluids remains for future work.

Wang et al. [143] derived a new structural model of ETC for heterogeneous materials with multiple continuous phases by using mathematical deduction, a thermal field method, and an average field approximation. This new model has a distinctive structure which is substantially different from five conventional fundamental structural models (Series, Parallel, two forms of Maxwell–Eucken, Effective Medium Theory). The new model provides more structural models using the combinatory method proposed by literature. The model also provides narrower bounds of the ETC within the Hashin–Shtrikman bounds for heterogeneous materials where the physical structure can be characterized. The thermal conductivity of the CNTs composite consists the combined effect of CNT length, diameter, concentration, interface and matrix as

$$9(1-f)\frac{k_e-k_m}{2k_e+k_m}+f\left[\frac{k_e-k_{33}^C}{k_e+0.14(k_{33}^C-k_e)}+4\frac{k_e-k_{11}^C}{2k_e+(1/2)(k_{11}^C-k_e)}\right]=0 \tag{16}$$

where

$$k_{11}^C=\frac{k_C}{1+(2R_kk_c/d)},\quad k_{33}^C=\frac{k_C}{1+(2R_kk_c/L)} \tag{17}$$

The results of Koroteeva et al. [144] demonstrated that the numerical technique based on the extended Maxwell methodology works well for materials with periodic and random arrangement of spherical cavities. The analysis indicates that, for the face-centered cubic (FCC) and body-centered cubic (BCC) array of spherical pores, the Maxwell approximation provides relatively accurate estimate for the ETC up to large porosities. For the simple cubic (SC) array, the Maxwell methodology accurately predicts the k_{eff} only for the porosities that are less than 0.3. The SC, BCC, and FCC schematic diagram are shown in Fig. 23.

Li and Peterson [145] analyzed and modeled the mixing effect of the base fluid in the immediate vicinity of the nanoparticles caused by the Brownian motion. The simulation results indicate

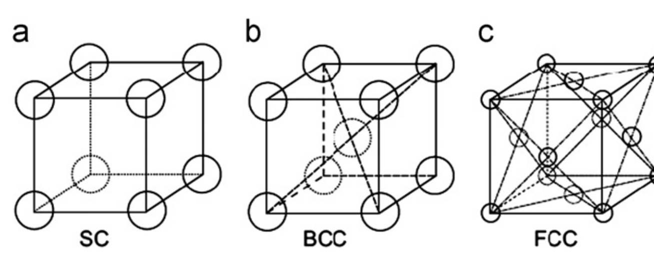


Fig. 23. (a) SC, (b) BCC, and (c) FCC [144].

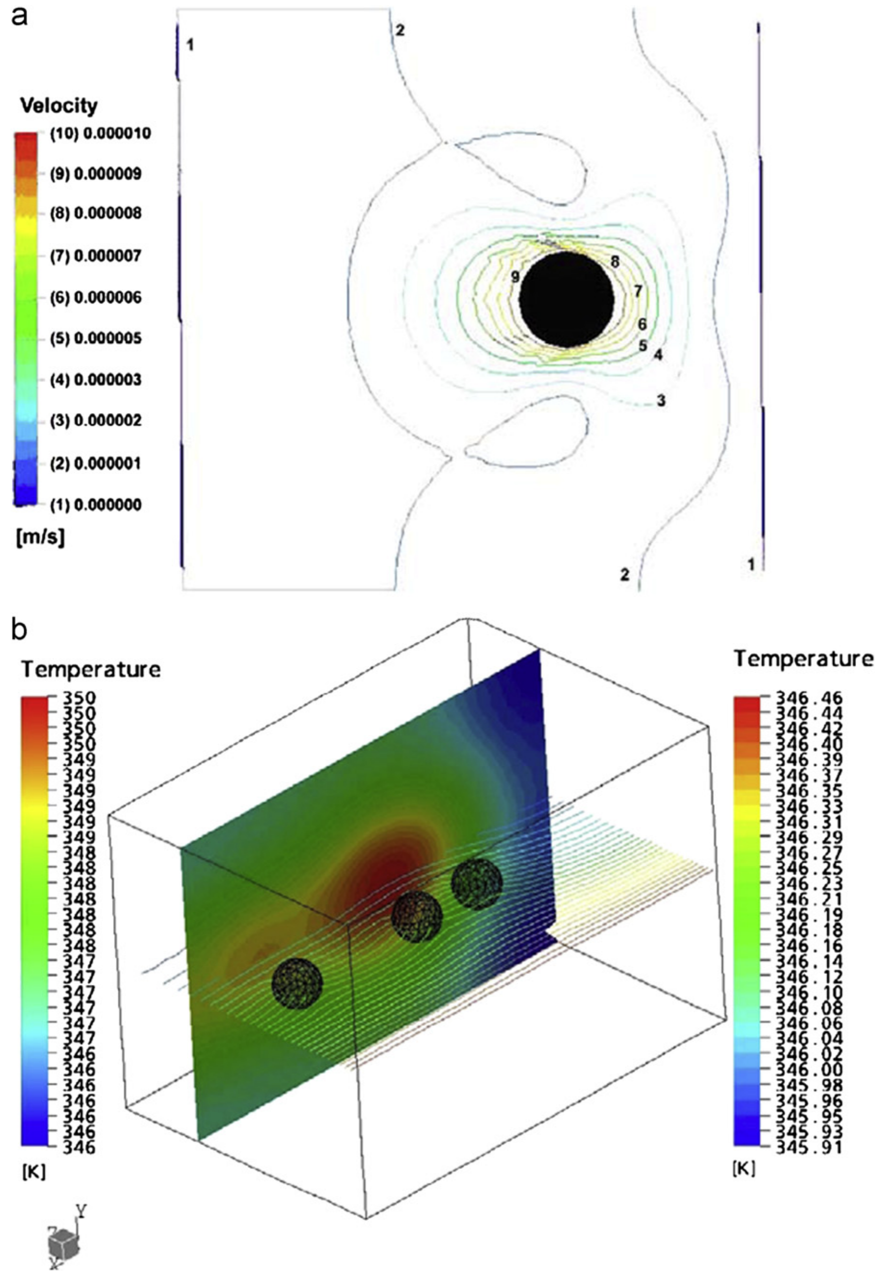


Fig. 24. (a) The velocity field of single nanoparticles simulation, (b) the comparison for simulated temperature field vertical plane (left, the temperature of *X–Z* plane; right, the temperature of *X–Y* plane) [146].

that this mixing effect can have a significant influence on the ETC of nanofluids as shown in Fig. 24.

Koo and Kleinstreuer [147] modeled a new equation to calculate the thermal conductivity for the nanofluid including the Brownian motion. Their formula depends upon the particle volume fraction, particle size, particle material and temperature. Their formula is

$$k_{eff} = k_{Static} + k_{Brownian} \tag{18}$$

where

$$k_{Static} = k_f \left[\frac{(k_{np}+2k_f) - 2\phi(k_f - k_{np})}{(k_{np}+2k_f) + \phi(k_f - k_{np})} \right] \tag{19}$$

$$k_{Brownian} = 5 \times 10^4 \beta \phi \rho_f C_{p,f} \sqrt{\frac{kT}{2\rho_{np} R_{np}}} f(T,\phi) \tag{20}$$

While β in Eq. (20) is a correlation that depends on the type of nanoparticles and shown in Table 2.

$$f(T,\phi) = -6.04\phi + 0.4705)T + (1722.3\phi - 134.63)$$

$$\text{for } 1\% \le \phi \le 4\% \text{ and } 300\ \text{K} < T < 325\ \text{K} \tag{21}$$

Vajjha and Das [148] developed the model of Koo and Kleinstreuer [147] by deriving new model for β and $f(T, \phi)$ from their set of experimental data from three nanofluids. Their new model of β is shown in Table 3.

And $f(T, \phi)$ is

$$f(T,\phi) = (0.028217\phi + 3.917 \times 10^{-3}) \left(\frac{T}{T_o} \right) + (-3.0669 \times 10^{-2}\phi - 3.91123 \times 10^{-3}) \tag{22}$$

Yurong et al. [149] correlated an equation for the thermal conductivity of TiO_2/water nanofluid as follows:

$$k_{nf} = k_l(125.62\phi^2 + 4.82\phi + 1.0) \quad (23)$$

4.5. Thermal stability

Kuznetsov [150] proposed a novel type of a nanofluid that contains both nanoparticles and motile (oxytactic) microorganisms to obtain enhanced mass transfer, micro-scale mixing, and anticipated improved stability of the nanofluid.

Sharma et al. [118] synthesized a silver nitrate-EG and poly nanofluids with different concentrations of silver nanofluid ranged from 1000 to 10,000 ppm. The results indicate a 10,000 ppm silver nanofluid exhibits rapid increase in the particle size with the passage of time as shown in Fig. 25. After 30 days of preparation, the thermal conductivity of 1000 and 5000 ppm silver nanofluids is observed to decrease slightly from 10% and 15% to 9% and 14%, respectively. In addition, the thermal conductivity of 10,000 ppm nanofluid was decreased from 18% to 14% after 30 days. It is noted that the silver particles were aggregated in early stage of preparation (up to 15 days), which leads to the increase in the size of silver particles. However, no significant change was observed after 15 days, which indicates the stability of silver nanofluids. The thickness of dispersion stabilizer surrounded each particle is reduced which might be the reason of increasing aggregation of silver particles as the time lapsed.

Sundar and Sharma [117] presented experimental results of heat retaining time of Al_2O_3 and CuO nanoparticles suspended in water with 0.8% nanoparticle volume fraction. Their measurements include measuring 50 ml in flask and heat up. The water, Al_2O_3 nanofluid, and CuO nanofluid have taken 17, 25 and 27.4 min, respectively to reach 35 °C. This analysis implies by adding some nano-size metallic oxide particles to the base fluid, these particles absorb heat and release heat to the adjacent liquid layers. But for a homogeneous fluid this will not be possible, because the entire liquid layer cool equally. Karthikeyan et al. [151] examined the behavior of thermal conductivity of CuO (8 nm) suspended in water and EG base fluid with 1 vol% nanoparticle concentration. They highlighted that the time dependent thermal conductivity in water based CuO nanofluid shows that the thermal conductivity decreases with elapsed time due to clustering of nanoparticles with time, as confirmed microscopically.

4.6. Viscosity

Viscosity as a physical property of fluids is significantly influenced by the volume fraction of nanoparticles and temperature of nanofluids. Viscosity is dramatically affected by *Re* number and friction factor of flowing fluid. Luciu et al. [152] found that the absolute viscosity of alumina/water nanofluid with volume fraction of 0.0–4.0% is reversely proportional to the temperature of the nanofluids as shown in Fig. 26. Whereas this viscosity is increasing as the nanoparticles concentration increases.

Einstein [153] established the following equation to calculate the viscosity:

$$\mu_{eff} = \mu_{bf}(1 + 2.5\phi) \quad (24)$$

Table 2
Correlations of β for different nanoparticles [147].

Type of particle	B	Remarks
Au-citrate, Ag-citrate and CuO	$0.0137(100\phi)^{-0.8229}$	$\phi < 1\%$
CuO	$0.0011(100\phi)^{-0.7272}$	$\phi > 1\%$
Al_2O_3	$0.0017(100\phi)^{-0.0841}$	$\phi > 1\%$

Table 3
Correlations of β for different nanoparticles [148].

Type of particle	β	Concentration (%)	Temperature (K)
Al_2O_3	$8.4407(100\phi)^{-1.07304}$	$1 < \phi < 10$	$298 \le T \le 363$
ZnO	$8.4407(100\phi)^{-1.07304}$	$1 < \phi > 7$	$298 \le T \le 363$
CuO	$9.881(100\phi)^{-0.9446}$	$1 < \phi > 6$	$298 \le T \le 363$

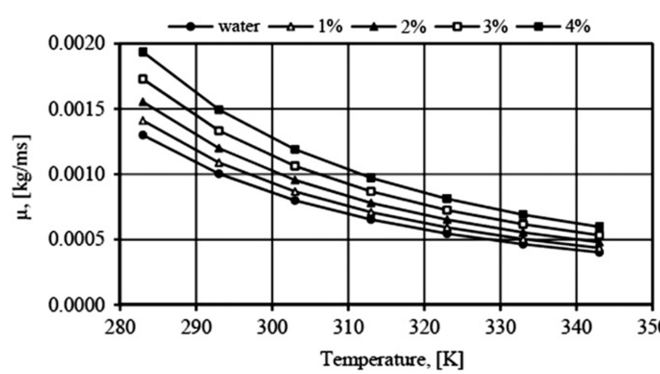


Fig. 26. Variation of viscosity [152].

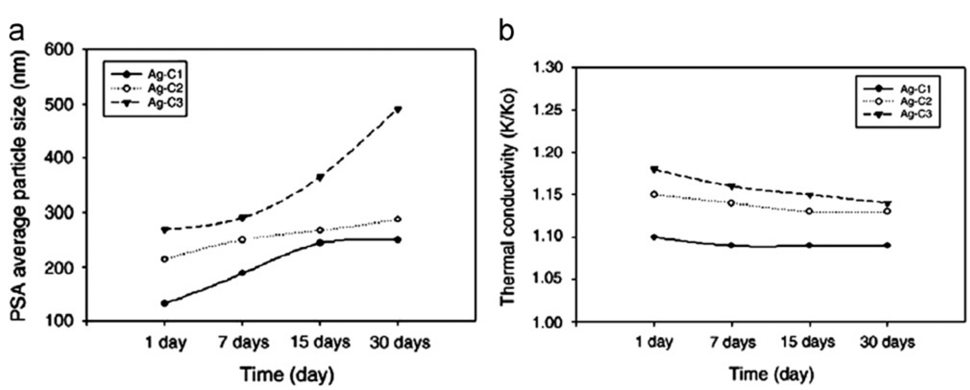


Fig. 25. (a) Average particle size of silver nanoparticles as a function of lapsed time and (b) thermal conductivity of silver nanoparticles for different concentrations of silver [118].

The correlations of viscosity of [131,132,134] are as follows, respectively:

$$\frac{\mu_{eff}}{\mu} = \frac{1}{1-34.87(d_p/d_f)^{-0.3}\varphi^{1.03}} \quad (25)$$

$$\mu_{eff} = \mu_{bf} + \mu_{app} \quad (26)$$

where μ_{app} is the apparent viscosity defined as

$$\mu_{app} = \frac{\rho_p v_B d_p^2}{72\delta C} \quad (27)$$

where C depends on the base fluid viscosity and mean diameter of the nanoparticles, δ depends on the mean diameter and volume fractions of the nanoparticles and v_B is the Brownian velocity of the nanoparticles that depends on temperature, diameter and density of particles [154].

$$\mu_{eff} = \mu_{Static} + \mu_{Brownian} \quad (28)$$

where

$$\mu_{Static} = \mu_f/(1-\phi)^{2.5} \quad (29)$$

$$\mu_{Brownian} = 5 \times 10^4 \beta\phi\rho_f \sqrt{\frac{kT}{2\rho_{np}R_{np}}} f(T,\phi) \quad (30)$$

Sommers and Yerkes [155] displayed that the viscosity of aluminum oxide (10 nm) dispersed in propanol exhibits non-linear behavior with concentration with the viscosity increasing sharply for concentrations greater than 1.0%. Torii [156] found experimentally that the viscosity of nano-diamond fluid increases with increasing the nanoparticles concentration. He observed that the experimental data is higher than the theoretical values over a wide range of volume fraction. While he studied three types of nanofluids which are alumina, copper oxide and diamond nanoparticles dispersed in conventional fluid of water [157]. He pointed out that the measured viscosities of nanofluids are much higher than that of predicted values using Batchelor equation which is

$$\frac{\mu_{nf}}{\mu_f} = 6.2\phi^2 + 2.5\phi + 1 \quad (31)$$

The viscosity of nanofluids increases with an increase in the volume fraction and this trend is different for three nanoparticles. He stated that the effective volume fraction including cluster in a nanofluid becomes higher than that in the ideal suspension fluid in which each particle is independently and homogenously dispersed in a fluid. He has seen that the viscosity of diamond nanofluid is the highest because diamond particles are strongly aggregated and cluster restricts a large amount of pure water. On the contrary, the viscosity of CuO nanofluid is relatively low because the CuO nanoparticles had already aggregated in the state of the powder.

Tavman et al. [112] illustrated that the effective viscosity of SiO_2/water and Al_2O_3/water has a similar behavior as water with the increase in temperature which ranged from 20 °C to 50 °C. Garg et al. [158] showed that the viscosity increase is almost fourfold of that predicted by the Einstein law of viscosity.

Due to the large increase in viscosity than the increase in thermal conductivity, nanofluids would be poorer coolants as compared to base fluids if they are used in the existing heat transfer hardware. Schmidt et al. [159] found that the measurements of longitudinal viscosity and the corresponding values of the particle size of alumina suspended in polyalphaolefin (PAO) are consistent with a picture of non-clustered particles in weakly shear-thinning viscous oligomeric oil.

Duangthongsuk and Wongwises [160] carried out experiments to investigate the effect of the thermophysical properties model on the predicted values of the convective heat transfer coefficient of TiO_2–water nanofluid flowing in a horizontal double-tube counter flow heat exchanger under turbulent flow conditions. They showed that the Brinkman equation Eq. (31) and Einstein equation Eq. (32) give similar results of viscosity, whereas the Wang et al. equation Eq. (33) gives a higher predicted viscosity than the preceding formulas.

$$\mu_{nf} = \frac{1}{(1-\phi)^{2.5}}\mu_w \quad (32)$$

$$\mu_{nf} = (1+\phi)\mu_w \quad (33)$$

$$\mu_{nf} = (1+7.3\phi+123\phi)\mu_w \quad (34)$$

Chopkar et al. [120] presented experimentally that $CaCO_3$-distilled water nanofluid with different nanoparticle concentrations is advantageous to reducing aggregation of primary nanoparticles. The effective viscosities and effective thermal conductivities of the nanofluid are related to the aggregates of nanoparticles and can be well predicted by the modified Krieger and Dougherty formula and the modified Hamilton and Crosser model, respectively. Whereas the modified Krieger and Dougherty formula for viscosity is

$$\eta_{eff}/\eta_f = (1-\varphi_a/\varphi_m)^{-2.5\varphi_m}$$
$$\varphi_a = \varphi(a_a/a)^{3-D} \quad (35)$$

where a_a and a are the ratio of aggregates and primary particles, respectively, D is the fractal index, has a typical value of 1.8 for nanofluids.

Murshed et al. [128] conducted the combined experimental and theoretical study on the effective thermal conductivity and viscosity of titanium oxide and aluminum oxide nanoparticles within 1–5 vol% dispersed in DIW and EG. The viscosity of nanofluids is observed to be substantially higher than the values of the base fluids. Both thermal conductivity and viscosity of nanofluids increase with the nanoparticle concentration. Corcione [132] presented empirical correlation for predicting the dynamic viscosity of nanofluids, based on a high number of previous experimental data.

$$\frac{\mu_{eff}}{\mu_f} = \frac{1}{1-34.87(d_p/d_f)^{-0.3}\varphi^{1.03}} \quad (36)$$

where d_f is given by

$$d_f = \left(\frac{6M}{N\pi\rho_{fo}}\right)^{1/3} \quad (37)$$

In which M is the molecular weight of the base fluid, N is the Avogadro number, and ρ_{fo} is the mass density of the base fluid calculated at temperature T_o=293 K. Corcione [161] and Cianfrini et al. [162] developed Eq. (36) by multiplying it by a factor of 0.1.

In addition, the (μ_{nf}/μ_f) increases as the nanoparticle volume fraction is increased, and the nanoparticle diameter is decreased, being practically independent of temperature for a wide regions of the dynamic viscosity equation of validity (i.e., 25–200 nm in diameter, 0.0001–0.071 volume fraction and 293–323 K temperature), makes such equation useful by the engineering point of view. Sundar et al. [163] experimentally and theoretically examined the effect of temperature variation on several flow characters such as density, specific heat and kinematic viscosity. They demonstrated that the density and viscosity of nanofluids decreases with the temperature for various concentrations of nanoparticles. While the specific heat increases with the temperature.

Yurong et al. [149] presented their experimental data of viscosity of the TiO_2/water nanofluid at about 22 °C by the

following correlation:

$$\mu_{nf} = \mu_{bf}(199.21\phi^2 + 4.62\phi + 1.0 \quad (38)$$

While Nguyen et al. [164] proposed a formula for 4 vol% of CuO nanoparticles suspended in water base fluid as follows:

$$\mu_{nf} = \mu_{water}(2.1275 - 0.0215T + 0.0002T^2) \quad (39)$$

And for Al_2O_3/water with $dp = 47$ nm and volume fraction ranges from 0% to 13%

$$\frac{\mu_{nf}}{\mu_{bf}} = 0.904e^{(14.8\phi)} \quad (40)$$

where T is the temperature in °C. Vajjha [165] developed a general correlation for viscosity of Al_2O_3, CuO and SiO_2 nanoparticles suspended in (60%EG/40%W) as follows:

$$\frac{\mu_{nf}}{\mu_{bf}} = A_1 e^{(A_2\phi)} \quad (41)$$

where A_1 and A_2 are constants. This equation works with specifications of nanoparticles diameters and volume fraction ranges.

4.7. Temperature dependence of thermal conductivity enhancement

Most measurements of the former investigators have been done at room temperature without attention to that the temperature has an important effect on the particle movement which tremendously affects on the thermal conductivity. Das et al. [166] were the first one to experimentally examine the thermal conductivity dependence on the temperature oscillation. They carried out their tests on water as a base fluid with particles of Al_2O_3 or CuO as suspension material. Their results bring out that a dramatic enhancement in thermal conductivity takes place with temperature. They obtained an enhancement of thermal conductivity up to 2% with 1% particles of Al_2O_3 at room temperature 21 °C, while a 10.8% enhancement was obtained at 51 °C. While a 24.3% enhancement was seen with a 4% volume fraction for the same previous range of temperature. They attributed this augmentation occurred in thermal conductivity of nanofluids to the increase occurred in the Brownian motion of particles. They stated that nanofluids can be made more attractive as cooling fluid for devices with high energy density where the cooling fluid is likely to work at a temperature higher than the room temperature. The temperature dependence of thermal conductivity enhancement of water–Al_2O_3 nanofluids can be seen in Fig. 27. This trend of thermal conductivity was also seen by Beck et al. [167] for alumina dispersed in either water or EG.

Minsta et al. [116] carried out experimental tests to study the relationship between the thermal conductivity and temperature oscillation. Particles of CuO with in 29 nm as well as 36 nm and 47 nm of Al_2O_3 particles is dispersed in water to produce nanofluids. The temperature range was from 20 °C to 40 °C. They found that the ETC of nanofluids increases with temperature for the three types of nanofluids. It is observed that the linear tendency fits of the measurements has slope more than 10°. They obtained 16% enhancement in thermal conductivity for each type of nanofluids when temperature ranged between 20 °C and 40 °C. The effect of temperature oscillation on thermal conductivity depends on the value of particles concentration. In comparison with distilled water, they found that an addition of nanoparticles gives a better enhancement with temperature for low volume fraction of particles.

Sundar and Sharma [168] stated that the ambient temperature thermal conductivity property of nanofluid is not sufficient for estimating the heat transfer coefficient. Thermal conductivity at different temperature is very important. They found that thermal conductivity of alumina/water and copper oxide/water nanofluids are relatively proportional with temperature shown in Fig. 28. Depend upon the increase of temperature, thermal conductivity of nanofluid increases with volume fraction.

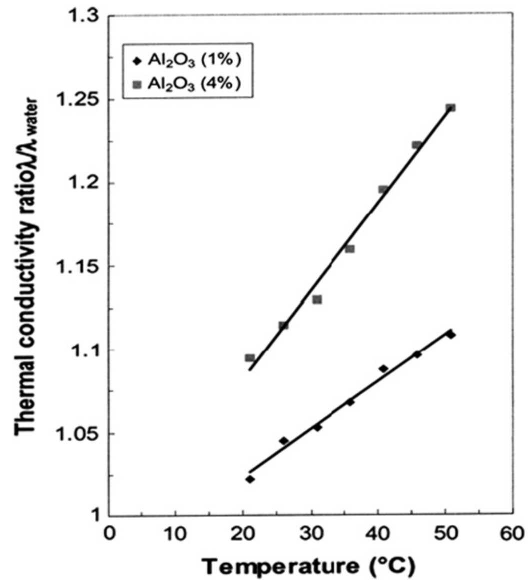


Fig. 27. Temperature dependence of thermal conductivity enhancement for water–Al_2O_3 nanofluids [167].

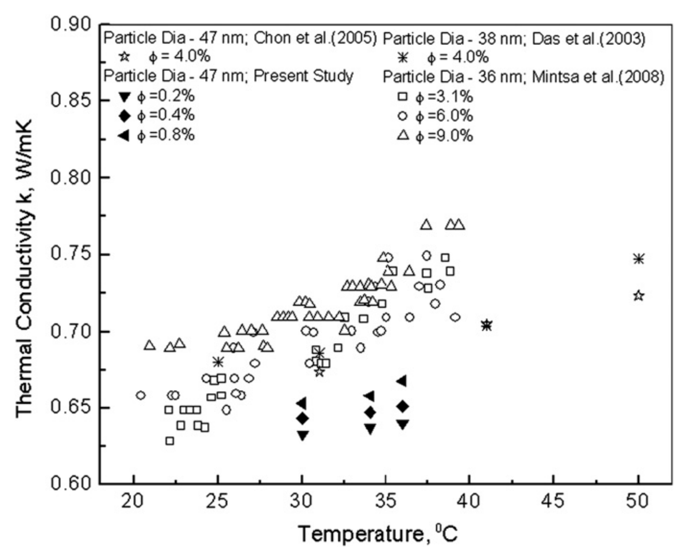


Fig. 28. Thermal conductivity of Al_2O_3 nanofluid at different temperature [168].

The same results were obtained by Izadi et al. [169] for the alumina–water nanofluid with temperature range from 300 K to 325 K. Liu et al. [97] obtained a maximum enhancement in thermal conductivity for TiO_2 nanoparticles dispersed in saturated $BaCl_2$ aqueous solution with pH 8 which was 15.65% with 1.13 vol% in higher temperature of 15 °C. They stated that the concentration of nano-particles and temperature are two important factors in improving thermal transport properties of nanofluids.

Li et al. [170] studied the effects of several parameters on the thermal conductivity of CuO (29 nm)/DW and Al_2O_3 (36 nm)/DW with 2–10 vol% of nanoparticles and nanofluid temperature ranged from 27.5 °C to 34.7 °C. Their results indicate that the temperature has a significant impact on the ETC. At temperature

of 34 °C and 6 vol%, they observed an enhancement in thermal conductivity by about 1.52 times for CuO/DW nanofluid greater than that of DW. At the same previous condition of temperature and with 10 vol%, they remarked 1.3 times of thermal conductivity enhancement for Al_2O_3/DW nanofluid higher than that of the base liquid. Wei et al. [115] showed that the thermal conductivity of nanofluid exhibits a strong sensitivity to the temperature. Beck et al. [167] measured the thermal conductivity of alumina nanoparticles dispersed in water, EG, and (water+EG) mixture nanofluids over a temperature range from 296 K to 420 K. They predicted the thermal conductivity and the effects of particle size, volume fraction, temperature and changes in base fluid using a simple model. They showed that the thermal conductivity–temperature behavior follows closely that of the base fluid. The maximum in thermal conductivity occurs near 380 K, which is close to the maximum in thermal conductivity–temperature behavior for pure EG or (water+EG) mixture. These results confirm the hypothesis that the temperature dependence of the effective thermal conductivity of nanofluids is due mostly to that of the base fluid.

Bianco et al. [171] studied numerically the turbulent forced convection flow of Al_2O_3/water nanofluid in a circular tube subjected to a constant and uniform temperature at the wall. To simulate the nanofluid convection, two-phase mixture model is considered taking in account appropriate thermophysical properties. They assumed that the particles are spherical with a 38 nm in diameter. They obtained a good agreement with the experimental correlation proposed in literature. They stated that the accuracy of the model could be improved by using a better description of nanofluid thermophysical properties taking into account the temperature dependence. Murshed et al. [128] conducted a combined experimental and theoretical study on the effective thermal conductivity of titanium oxide and aluminum oxide nanoparticles suspended in DIW and EG. They found that the thermal conductivity of nanofluids is strongly dependent on temperature. The same results are observed by Yu et al. [172] for the copper (5–10 nm)/EG nanofluids with 0.5 vol% and at 50 °C. They have seen that the thermal conductivity strongly depends on the temperature of fluid, and the enhancement ratios of the thermal conductivity of nanofluid increase along with the increasing temperatures. Brownian motions of Cu nanoparticles would play the key role in determining the effect of the temperature on thermal conductivity enhancement of nanofluids.

Temperature dependence of thermal conductivity of Al_2O_3/EG nanofluid was studied by Beck et al. [136] for a wide range of temperature from 298 K to 411 K. The k of the nanofluid was measured by liquid metal transient hot wire apparatus. They confirmed that additional temperature contributions inherent in Brownian motion models are not necessary to describe the temperature dependence of the thermal conductivity of nanofluids. They showed that the effect of mass or volume fraction of nanoparticles on the thermal conductivity of nanofluids can be correlated using the Hamilton and Crosser or Yu and Choi models with one adjustable parameter (the shape factor in the Hamilton and Crosser or the ordered liquid layer thickness in the Yu and Choi model).

Sundar and Sharma [117] presented the increase of thermal conductivity with temperatures for nanofluids with water as base fluid and particles of Al_2O_3 or CuO as suspension material. It is observed that a twofold to fourfold increase in thermal conductivity enhancement of nanofluids can take place over a temperature range of 30–60 °C. It was observed that nanofluids containing smaller CuO particles show more enhancement of conductivity with temperature. Sankar et al. [173] proposed a theoretical approach based on molecular dynamic modeling to estimate the thermal conductivity enhancement of platinum–water nanofluid. The results distinctly show that the enhancement of thermal conductivity increases as the volume fraction of nanoparticles increase from 1% to 7%. The enhancement is found to be more for higher temperatures. The temperature effect of thermal conductivity enhancement in Al_2O_3/water and CuO/water nanofluids was also presented by Sundar and Sharma [174]. They observed a dramatic increase in the enhancement of thermal conductivity occurs with temperature as shown in Fig. 29.

4.8. Effect of volume fraction

The previous studies demonstrated that there is a linear relationship between the thermal conductivity of nanofluids and the concentration of nanoparticles. But the increase in concentration of nanoparticles leads to undesirable consequents such as clogging, sedimentation, and pressure drop. Kumar et al. [175] found numerically a linear dependence of thermal conductivity enhancement on particle concentration of Au nanoparticle ($\varepsilon \ll 1$) with 4 nm in diameter. Liu et al. [97] found that the thermal conductivity of Ti_2O/saturated $BaCl_2$ aqueous nanofluids increases approximately linearly with the volume fraction of nanoparticles. A similar trend of thermal conductivity they observed with the changing the nanofluid temperature in different volume fraction of nanoparticles. This tendency of thermal conductivity with the volume fraction of nanoparticles is also observed by Jain et al. [176] which are similar to that of previous literature. Wei et al. [115] reported that the variation in the $CuSo_4$ molar concentration leads to a change in nanofluid thermal conductivity through changing the nanofluid microstructure. A linear relationship between the ratio of thermal conductivity of alumina/water

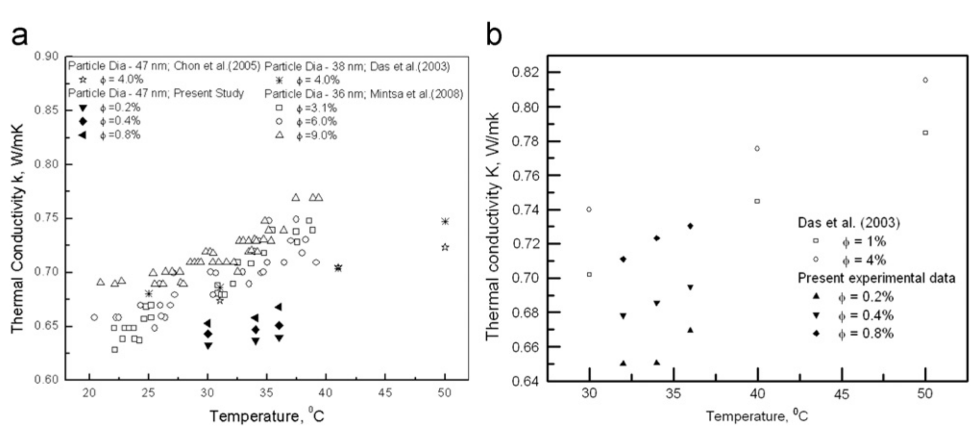


Fig. 29. Thermal conductivity of (a) Al_2O_3, (b) CuO nanofluid at different temperatures [174].

nanofluid and the concentration of nanoparticles was also proved by Izadi et al. [169]. Hu et al. [114] revealed that 20% enhancement in thermal conductivity of alumina/ethanol nanofluid can be obtained when 4.0% of nanoparticle is dispersed in the base liquid at 273.15 K. The same enhancement ratio in thermal conductivity was obtained by Hu et al. [108] where 4.0% volume fraction of AlN nanoparticles with 20 nm in diameter is dispersed in ethanol at 273.15 K.

Xie et al. [103] emphasized that the thermal conductivities of the SiC suspensions containing a small amount of solid particles are significantly higher than those of the base liquids. At low volume fraction range, the thermal conductivity enhancing ratios increase almost-linearly with the volume fraction of solid particles. The experimental results of Sunder and Sharma [168] showed that water containing a small amount of alumina or copper nanoparticles does not exceed 0.8% provides a substantially higher thermal conductivity than the same liquids without nanoparticles. Tavman et al. [112] have found experimentally that the ETC of alumina and silica nanoparticles dispersed in water increases as the volume fraction increases but not anomalously as indicated in literature. They claimed that this increase is independent on temperature. Labonté et al. [177] found numerically that for variable properties model, the enhancement in heat transfer is 20% where 1% particles concentration of alumina dispersed in a base liquid of water and 40% with 4% particles concentration. While for constant properties model, they obtained 5% and 20% for the same previous particles concentrations, respectively.

An increase of 1.52 times in the effective thermal conductivity of CuO nanoparticles with 6 vol% dispersed in DW was obtained by Li and Peterson [170]. This enhancement of the ETC of alumina nanoparticles was screened while 10% volume fraction is dispersed with water. The enhancements were at temperature of 34 °C.

Many parameters respect to the volume fraction were examined by Sundar et al. [163]. These parameters are the density, specific heat, and kinematic viscosity of alumina/water nanofluids with a volume fraction up to 0.8% of alumina particles. They screened that when metallic nanoparticles is added to the base fluid such as water those particles act as suspensions and the density of the water increases. This is because the density of the nanofluids is directly proportional to the mass of the fluid. They showed that the specific heat is reversely proportional to the volume fraction of nanoparticles. Their results revealed that the viscosity of the nanofluid increases with the increase of the nanofluid concentration. These results are shown in Fig. 30.

Das et al. [166] showed that the thermal conductivity of alumina–water and CuO–water nanofluid is directly proportional with the concentration of the nanoparticles at different temperatures. But this is stronger with alumna than with copper oxide. The same tendency of thermal conductivity with nanoparticle concentration was also seen by Jang and Choi [178] at volume fraction less than one percent for CNTs and less than 0.05% for an oxide and metallic nanoparticles. Sommers and Yerkes [155] showed that the enhancement of thermal conductivity of an alumina nanoparticles with 1 vol% dispersed in propanol was found to be slightly higher than that of base liquid for $1800 < Re < 2800$ and at room temperature. They attributed that to an earlier transition to turbulent flow. For 3% volume fraction, they observed that the thermal performance is deteriorated with respect to the baseline case.

The effective thermal conductivity of Ar–Cu nanofluid in shear field was calculated by equilibrium molecular dynamics (EMD) simulation using Green–Kubo formula was achieved by Sun et al. [179]. The relative thermal conductivity increases linearly as the flow shear rate increases for the enhanced "micro-convection" effect yielded by the rotation of the nanoparticle. The increase in the ETC at lower volume fraction with respect to the shear rate is larger than at higher volume fraction which is related to the slowed down rotation speed for the higher volume fraction of nanoparticle. The results exhibit that the shear flow did not affect the fluid structure and orderly fluid structure is not the reason for

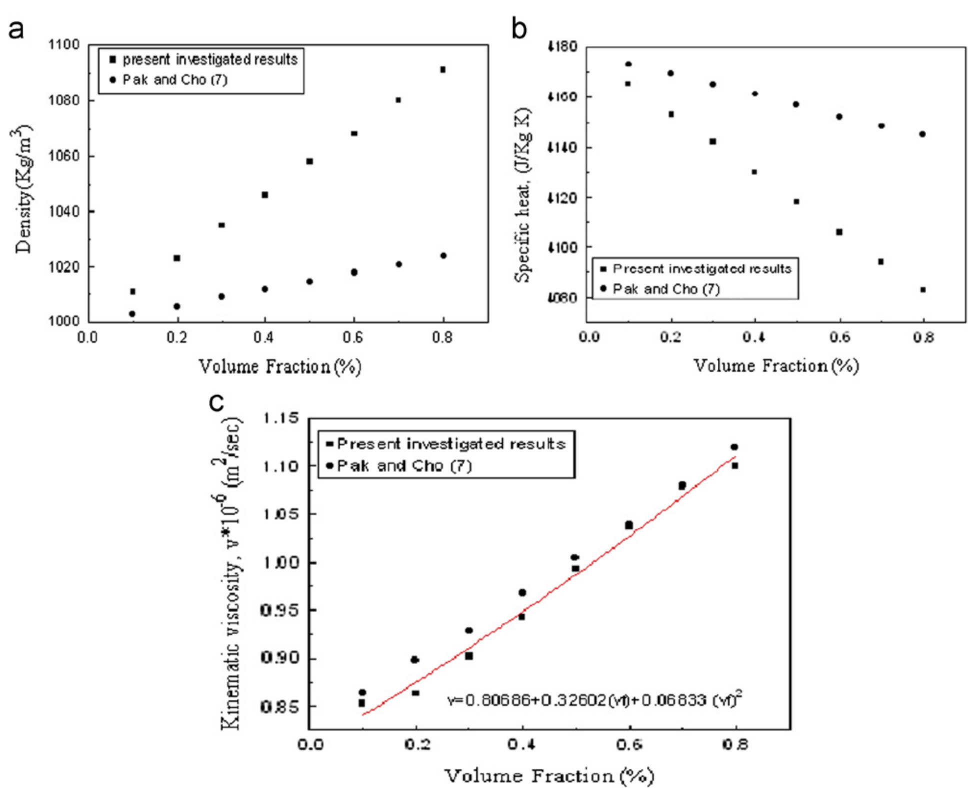


Fig. 30. (a) The density, (b) the specific heat, and (c) the Kinematic viscosity of nanofluid at different concentrations [163].

the enhancement in the thermal conductivity of shearing nanofluid. The effective thermal conductivity obtained from the conventional correlation:

$$\frac{\lambda_e}{\lambda_0} = 1 + BcPe_P^m \tag{42}$$

where λ_e is the effective thermal conductivity of the flowing suspension, λ_0 is the thermal conductivity of the suspension at static state, c is the volume fraction of the particles, B and m are constants, and Pe_P is the Peclet number of the particle expressed by

$$Pe_P = \frac{ed^2}{\alpha_f} \tag{43}$$

where e is the velocity gradient, d is the particle diameter, and α_f is the thermal diffusivity of the suspended fluid. It is obviously seen that the volume fraction effect is more explicit for the flowing suspensions containing micro-sized particles is significantly lower than their numerical results. Therefore, they stated that the conventional correlation is not suitable when the sizes of the suspended particles are reduced to nanometer.

Sundar and Sharma [117] reported that the thermal conductivity of Al_2O_3 and CuO nanofluids at 0.8 vol% increases by 6.52% and 24.6% when compared to base fluid of water. The enhancement is considerably increased for nanofluids with Al_2O_3 as well. Sharma et al. [118] synthesized nanofluids consisting silver nitrate (precursor), EG (reducing agent), and poly (acrylamide-co-acrylicacid) (dispersion stabilizer). The results illustrate an increase in thermal conductivity of silver nanofluids up to 10%, 16%, and 18% as the amount of silver particles in nanofluid is 1000, 5000, and 10,000 ppm, respectively. The effect of the nanoparticle concentration of Al_2O_3/water and CuO/water nanofluids was also implemented by Sundar and Sharma [174]. They highlighted that the thermal conductivity is directly proportional with the volume fraction as shown in Fig. 31. They presented that thermal conductivity of previous nanofluids for 0.8 vol% increase by 6.52% and 16.00%, respectively compared to the base fluid. They showed that nanofluids containing smaller amount of CuO particles show more enhancement of thermal conductivity compared to Al_2O_3 particles.

Karthikeyan et al. [151] reported that the increase in the enhancement of thermal conductivity of CuO (8 nm) suspended in water and EG base fluid with 1 vol% was observed to be 31.6% and 54%, respectively. They stated that the thermal conductivity nonlinearly increases with the volume fraction of nanoparticles.

4.9. Effect of particle size

The decrease in the nanoparticles size means an increase in the surface area of the nanoparticles exposed to the fluid. There is a significant effect of the nanoparticle size on the thermal conductivity of nanofluids as shown in the literature. Kumar et al. [175] displayed the increases in the enhancement of the effective conductivity with the reciprocal of the nanoparticles radius as shown in the following equation:

$$q^* = \frac{q}{-k_m A_m (dT/dx)} = 1 + \frac{k_p \varepsilon r_m}{k_m (1-\varepsilon) r_p} = \frac{k_{eff}}{k_m} \tag{44}$$

where the subscript m refers to the liquid and p refers to the nanoparticles. The results of Li and Peterson [170] reveal that the thermal conductivity of CuO (29 nm)/water is much higher than that of Al_2O_3 (36 nm)/water because the copper oxide nanoparticles is smaller than that of Al_2O_3 nanoparticles. It is greatly confirmed by the new model of Jang and Choi [178]. Their new model is

$$k_{eff} = k_{BF}(1-f) + \beta k_{particle} f + C_1 \frac{d_{BF}}{d_{nano}} k_{BF} Re_{d_{nano}}^2 Prf \tag{45}$$

where $C_1 = 18 \times 10^6$, f is the volume fraction, and k_{BF} is the thermal conductivity of the base fluid molecules. Fig. 32 shows the nanoparticle diameter decreases as the effective thermal conductivity of nanofluids increases.

As the particle size decreases, the Brownian motion of nanoparticles is greater and then nonconvection becomes dominant. This consequent is identical to the results of Vasu et al. [180]. They analytically observed that the effective thermal conductivity of nanofluids increases as the volume fraction increases, the nanofluid temperature increases and the nanoparticle size decreases as shown in Fig. 33. The same trend of nanofluid thermal conductivity was seen by Jain et al. [176]. The latter shows that the size effect is the most important effect in nanofluids, which traditional models fail to predict.

The results obtained by Izadi et al. [169] show that the effective thermal conductivity of alumina/water nanofluids is also dramatically affected by the size of nanoparticles until 5 nm in diameter of nanoparticles. At larger than this size, they claimed that the effect of the nanoparticle size becomes nil. Beck et al. [181] performed experiments on alumina/water and alumina/ethylene glycol nanofluids and they claimed that the thermal conductivity enhancement decreases as the particle size decreases below about 50 nm. The model made by Kumar et al. [126] showed that the Brownian motion contribution is higher at lesser particle size when particle volume fraction is held constant. As shown in Fig. 34, the changes in Brownian motion is in the range of 10–15 nm and this range is the critical size due to the considerable change in Brownian motion when the volume fraction and temperature are fixed. The Brownian motion is suppressed when the particle size and volume fraction are increased. This may be due to the fact that the

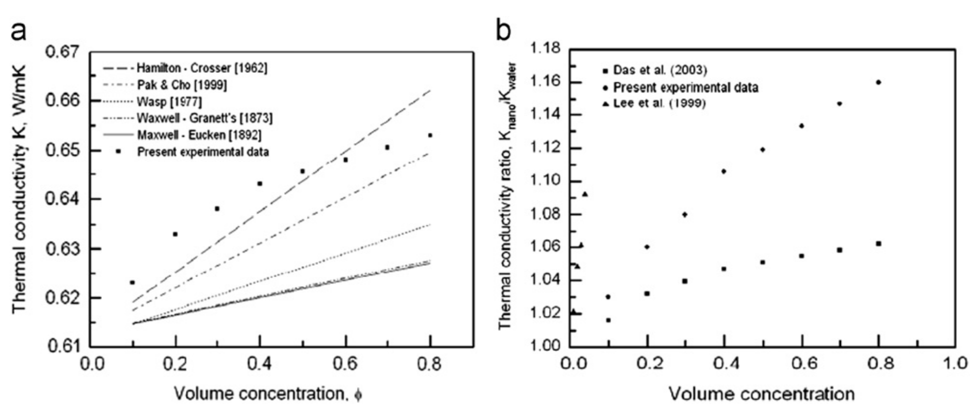


Fig. 31. (a) Thermal conductivity of Al_2O_3 nanofluid at ambient temperature and (b) thermal conductivity ratio of CuO nanofluid at ambient temperature [174].

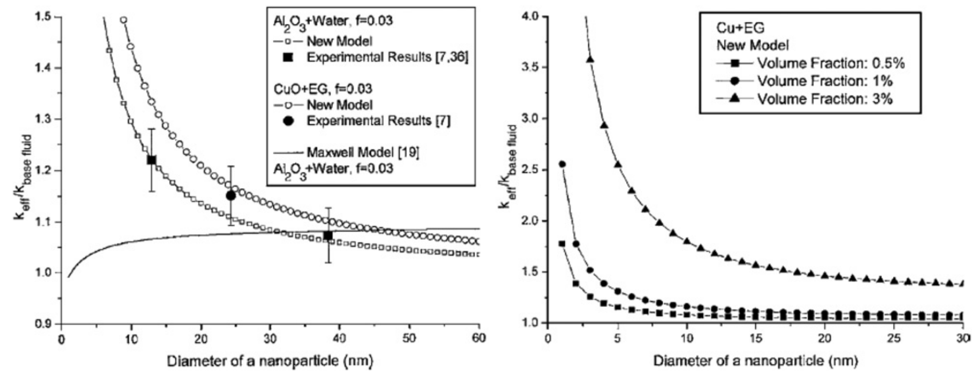


Fig. 32. Effect of diameter of nanoparticle on thermal conductivity of nanofluid [178].

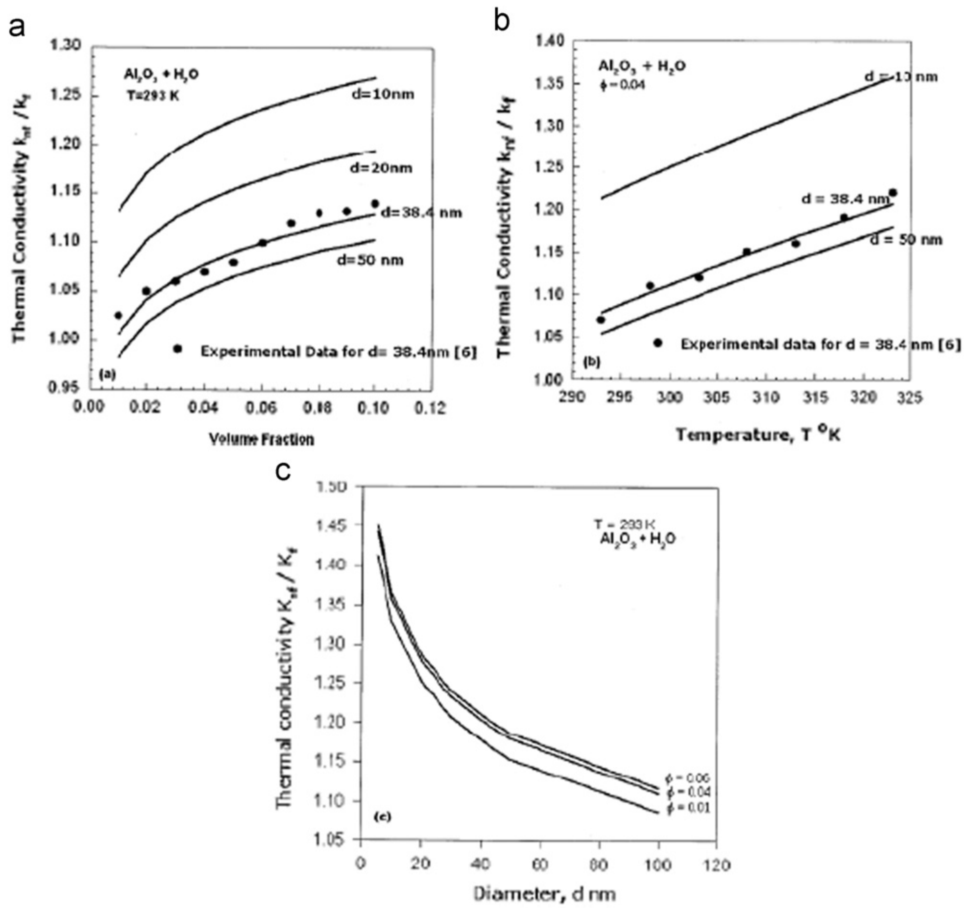


Fig. 33. The effect of (a) volume fraction, (b) temperature and, (c) diameter of nanoparticle on thermal conductivity of nanofluid [180].

Brownian motion velocity is inverse dependence with the particle diameter [126].

While Kondaraju et al. [182] studied the effect of multi-sized nanoparticle distribution on thermal conductivity of nanofluids ranged from 100 to 300 nm were considered while an initial diameter of 182.4 nm was considered for the single-sized nanofluid case. Their simulated results of Al_2O_3/DIW nanofluid revealed an increase in the effective thermal conductivity for the nanofluids with multi-sized nanoparticles when compared to that of the nanofluids with the corresponding single-sized nanoparticles. Sundar and Sharma [117] presented the increase of thermal conductivity with temperatures for nanofluids with water as base fluid and particles of Al_2O_3 or CuO as suspension material. However, the enhancement is considerably increased for nanofluids with Al_2O_3 as well. The measurements indicate that particle size is an important parameter for the observed behavior. Sundar and Sharma [174] confirmed that the thermal conductivities of Al_2O_3water and CuO/water nanofluids increase as the particle size decreases.

Lu and Fan [183] implied that the simplified dynamics simulation method is an effective method to forecast some thermal properties of nanofluids for volume fraction less than 8%. Their results give the effects of the volume fraction and the size of nanoparticles on the thermal conductivity and the viscosity of nanofluids. It is observed that the decrease in the nanoparticle size or increase in the volume fraction causes an increase in thermal conductivity and viscosity. For suitable volume fraction and size, increasing viscosity with improving heat transfer

capability is acceptable. For example, the largest enhancement of thermal conductivity is found to be 41% for Al_2O_3 (10 nm)/EG nanofluid with nanoparticle concentration of 5%. The effect of volume fraction on thermal conductivity is shown in Fig. 35.

Karthikeyan et al. [151] reported that the increase in the enhancement of thermal conductivity of CuO (8 nm) suspended in water and EG base fluid with 1 vol% nanoparticle concentration has observed to be 31.6% and 54%, respectively. They attributed this dramatic increase in thermal conductivity to the finer particle size and monodispersity of nanoparticles. Saterlie et al. [184] obtained an enhancement of thermal conductivity up to 22% over water for the 0.55 vol% Cu nanofluids. When the particle loading was increased to 1.0 vol%, the nanofluids of oleic acid-prepared Cu powders settled and clogged the test setup. A maximum increase was 48% for the 1.0 vol% copper nanofluid from the cetyl trimethylammonium bromide (CTAB) prepared Cu powders. This enhancement in thermal conductivity is attributable to the excellent dispersion of the nanoparticles in the fluid.

4.10. Effect of particle shape

The thermal conductivity enhancement of nanofluids is compared with the geometrical shape of the nanoparticles as shown in Figs. 36 and 37. As shown in these figures, a large difference is existed when the geometrical shape is varied. The whiskers particles of SiC exhibits a large enhancement of thermal conductivity compared to the spherical particles as shown in Fig. 36. In addition, the CNTs particles provides good enhancement of thermal conductivity with respect to spherical geometry particles, while the hybrid particles of sphere/CNTs particles provide better augmentation in thermal conductivity as shown in Fig. 37.

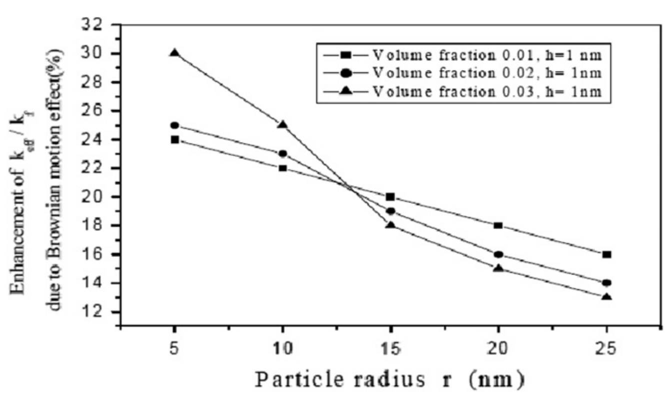


Fig. 34. Variation of particle size with thermal conductivity ratio due to Brownian motion [126].

4.11. Effect of particle material

The particle material has significant influence on the thermal conductivity enhancement based on the conductivity of the

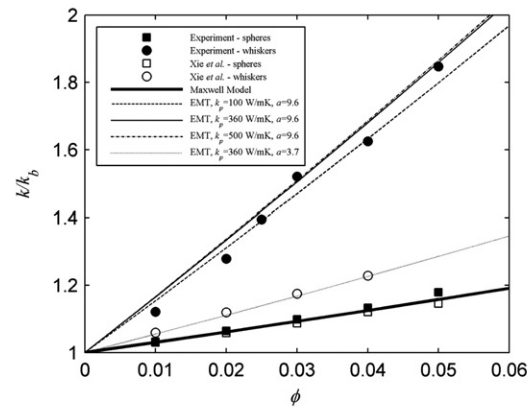


Fig. 36. Relative thermal conductivity enhancement in the suspensions containing SiC spherical particles (solid squares) and whiskers (solid circles) compared to the data calculated with the aid of Maxwell (dashed line) and EMT (solid line). Data by Xie et al. for spheres and cylinders are shown with hollow squares and circles correspondingly. EMT prediction for a=3.7 is shown with dotted line for comparison with the data on cylinders of Xie et al. [122].

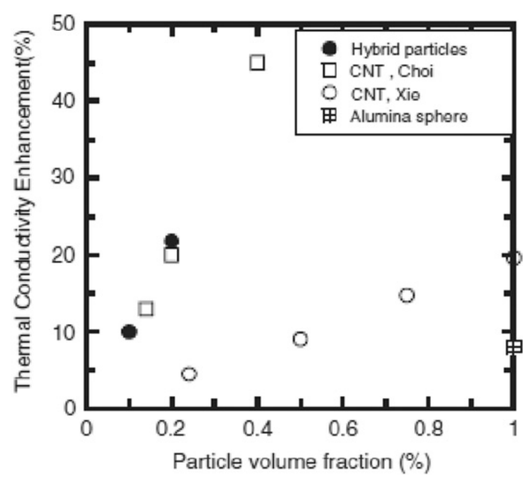


Fig. 37. Performance comparison of particles with different morphologies, e.g. spheres, carbon nanotubes (CNTs) and hybrid sphere/CNT particles (urchin-like), in nanofluids.

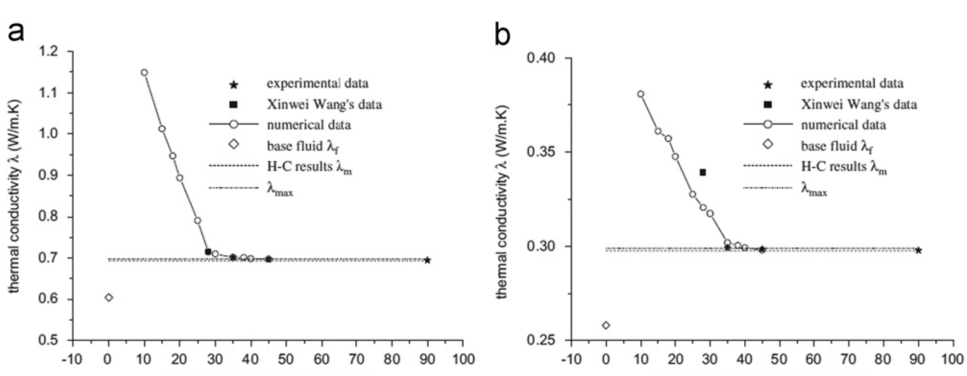


Fig. 35. Thermal conductivity as a function diameter of (a) Al_2O_3/water and (b) Al_2O_3/EG with 5 vol% [183].

material of nanoparticle. The effect of the particle material has been studied by [94,123,137,156,185–187]. As shown in Fig. 38, the thermal conductivity of Al_2O_3/EG, TiO_2/EG, and Al_2O_3/H_2O, Cu/H_2O and CuO/H_2O is varied depending on the particle material.

4.12. Effect of base fluid material

The base fluid material plays an important role in the enhancement of the thermal conductivity of nanofluids [107,143,187]. Fig. 39a, shows that the alumina–water provides a better enhancement in thermal conductivity than the EG, engine oil, and pump fluid, respectively. The same tendency can be seen with the CuO nanoparticles suspended in EG and water as shown in Fig. 39b.

The effect of the particle material and base fluid material as mentioned in the last two paragraphs can be concluded by the investigation done by Xie et al. [188]. They examined the enhancement of thermal conductivities of the DW, EG, glycerol, silicone oil, and the binary mixture of DW and EG as base fluids, and Al_2O_3 with different sizes, SiC with different shapes, MgO, ZnO, SiO_2, Fe_3O_4, TiO_2, diamond, and CNTs nanoparticles with different pretreatments were used as additives. The results demonstrate and confirm that the thermal conductivity enhancements of nanofluids could be influenced by multi-faceted factors including the volume fraction of the dispersed nanoparticles, the tested temperature, the thermal conductivity of the base fluid, the size of the dispersed nanoparticles, the pretreatment process, and the additives of the fluids. In addition, the k_{nf}/k_f decreases while the k_f increases.

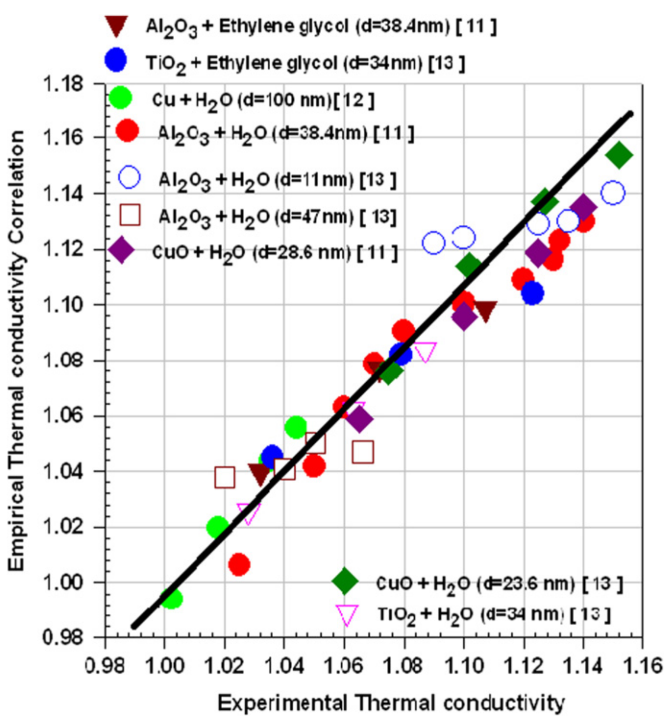


Fig. 38. Comparison of k_{nf} correlation with experimental data [187].

4.13. Convection heat transfer

An experimental study to investigate the increase in the thermal conductivity of the Al_2O_3/DIW nanofluid under developing convective boundary layer condition in tubes of 5 mm in diameter was performed by Kolade et al. [146]. Their experiments were done in a hydrodynamically fully developed laminar tube flow in the range $500 \le Re \le 1600$ with constant wall heat flux. In their study, the increase in effective thermal conductivity is 6% for 2% volume fraction. For a suspension of MWNTs in silicone oil, the thermal conductivity is increased by 10% over that of the base fluid for 0.2% particle concentration. Based on the results of the carbon nanotube (CNTs) experiments, they suggested that the structure of the nanomaterial is an important factor in the augmentation of thermal conductivity of a liquid by the means of nanoparticles.

Rostamani et al. [189] analyzed numerically the turbulent flow of mixture of CuO, Al_2O_3, and TiO_2 nanoparticles suspended in water with different nanoparticles concentrations flowing through a two-dimensional duct under constant heat flux condition. All the thermophysical properties of nanofluids are temperature-dependent. The results imply that by increasing the volume fraction, the wall shear stress and heat transfer rates increase. For a constant volume fraction and *Re* number, the effect of CuO nanoparticles to enhance the *Nu* number is better than Al_2O_3 and TiO_2 nanoparticles.The effect of nanoparticle volume concentration on *Nu* number can be seen in Fig. 40.

4.13.1. Forced convection heat transfer

Lotfi et al. [190] studied numerically the forced convective of Al_2O_3/water nanofluid flows in horizontal tubes. As a consequence, comparison of calculated results with experimental values shows that the mixture model is more precise than the single-phase and the Eulerian model. It is clearly shown that the rate of thermal enhancement decreases with the increase of nanoparticle concentration. Both single-phase and Eulerian approaches underestimate the *Nu* number in comparison with experimental results. Lai et al. [191] documented the results of heat transfer and pressure drop of alumina–water nanofluid flowing in a single 1.02 mm diameter stainless steel tube. The tube was electrically heated to provide a constant wall heat flux

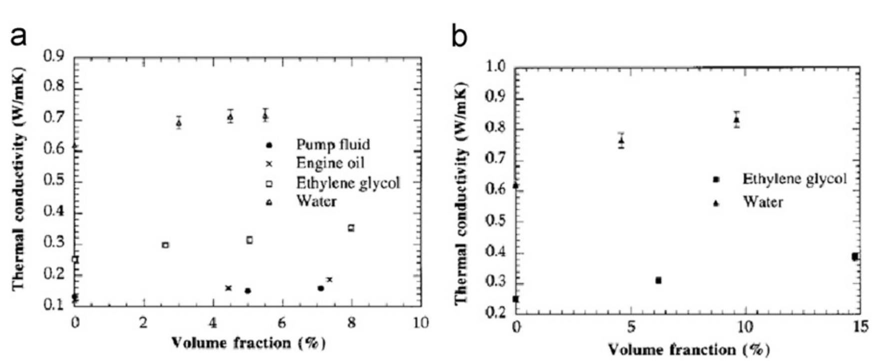


Fig. 39. (a) Thermal conductivity as a function of volume fraction of Al_2O_3 powders in different fluids, (b) thermal conductivity as a function of volume fraction of CuO powders in ethylene glycol and water [107].

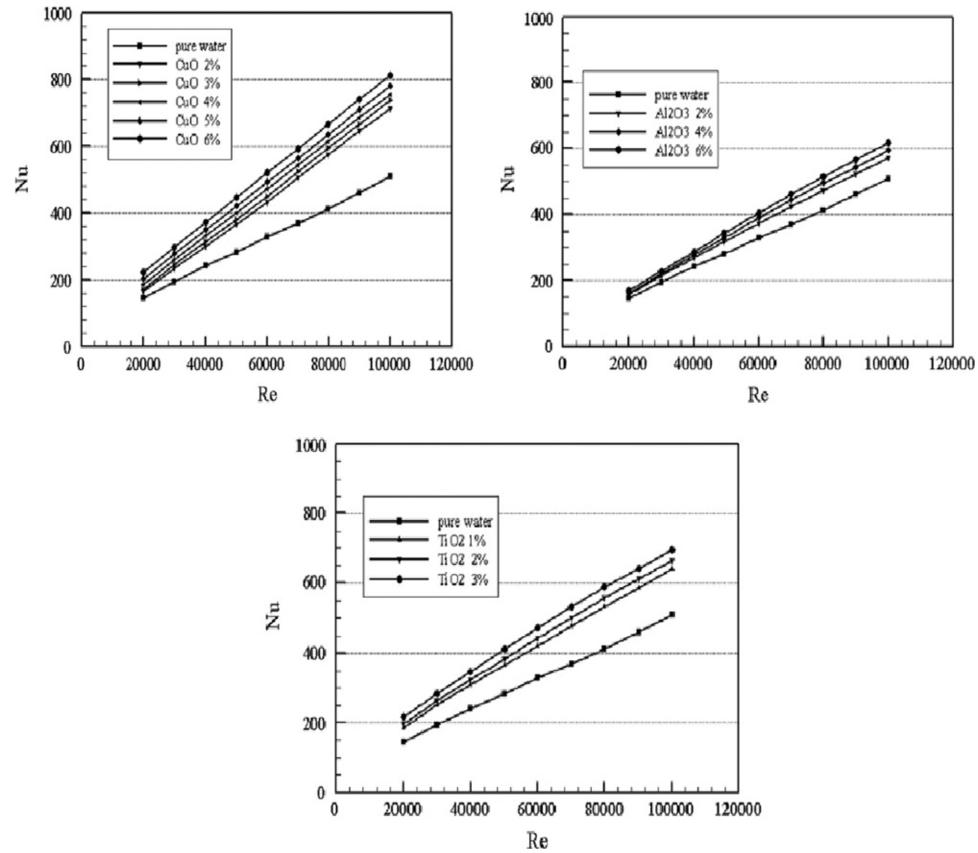


Fig. 40. The influence of the nanoparticle volume concentration on the Nusselt number over a range of the Reynolds numbers [189].

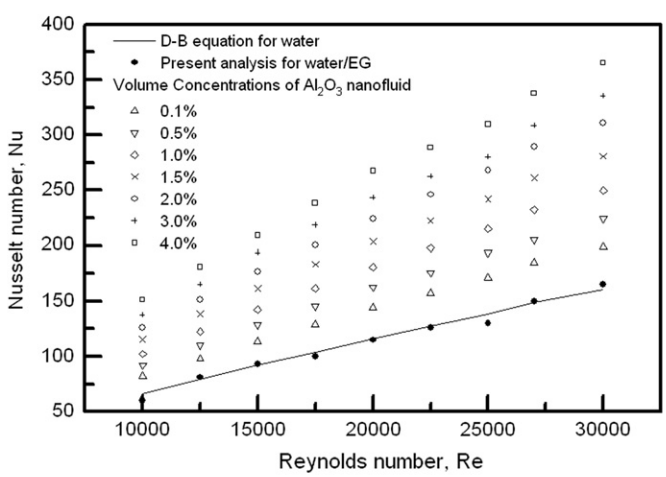


Fig. 41. The influence of Al_2O_3 nanoparticle volume concentration on the Nusselt number [192].

and the flow was under laminar flow condition. The heat transfer coefficient was measured in both developing and fully developed regions. Their experimental results illustrate that the heat transfer coefficient increases with the volume flow rate and nanoparticle volume fraction. In the developing region, the *h* enhancement decreases with increasing axial distance from the test section entrance. It is pronounced that the higher the volume fraction the longer the thermal entrance length.

Sundar and Sharma [192] emphasized that *Nu* number is relatively proportional with *Re* number as shown in Fig. 41. This trend of *Nu* number with Re number is also confirmed by Xuan and Li [193].

Maiga et al. [194] investigated the laminar forced convection flow of γAl_2O_3 suspended in the water and EG flows in a uniformly heated tube and a system of parallel coaxial and heated disks. It is pronounced that the inclusion of nanoparticles into the base fluids has produced an augmentation of the heat transfer coefficient that explicitly increases with an increase of the volume fraction. It is clearly shown that γAl_2O_3-EG nanofluid provides a better heat transfer enhancement than γAl_2O_3-water. The enhancement in heat transfer increases with *Re* number. They have proposed correlations based on the numerical results for computing the averaged *Nu* number as a function of the governing parameters *Re* and *Pr*:

$$\overline{Nu} = 0.086Re^{0.55}Pr^{0.5} \text{ for constant wall heat flux} \quad (46)$$

$$\overline{Nu} = 0.28Re^{0.35}Pr^{0.36} \text{ for constant wall temperature} \quad (47)$$

4.13.2. Natural convection heat transfer

Polidori et al. [185] studied the natural convection heat transfer of alumina/water nanofluid up to 4% volume fraction. As a result, it was found that natural convection heat transfer is not solely characterized by the nanofluid effective thermal conductivity and that the sensitivity to the viscosity model used plays a key role in the heat transfer behavior.

Jou and Tzeng [195] examined numerically the natural convection heat transfer enhancement utilizing nanofluids filled within a two-dimensional enclosure. The results indicate that increasing the buoyancy parameter and volume fraction of nanofluids cause an increase in the average heat transfer coefficient. The numerical predictions illustrate the enhancement is critical

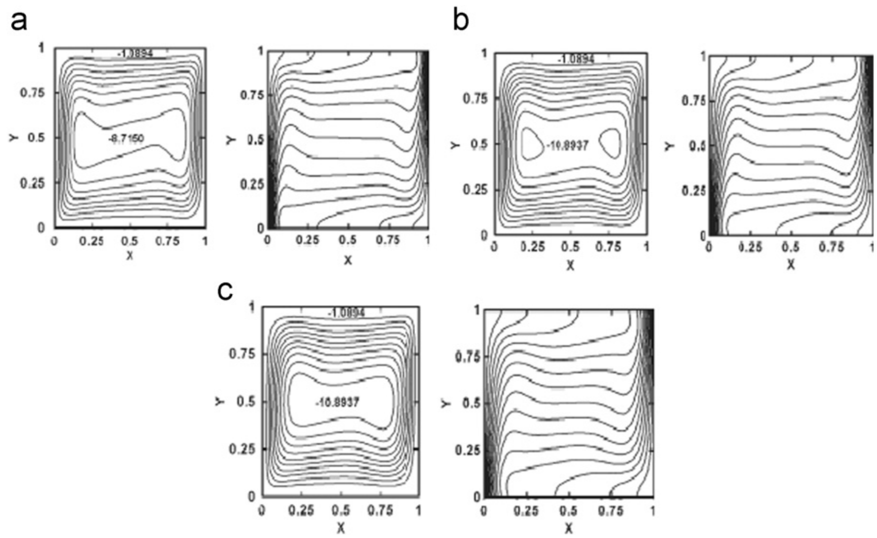


Fig. 42. Streamline and isotherm contours for different volume fraction ($Gr=10^5$, $Pr=6.2$) [195]. (a) $\phi=0$, (b) $\phi=0.1$ and (c) $\phi=0.2$.

for nanofluids than pure fluids. The stream line and isotherm contours for different volume fractions can be seen in Fig. 42.

Putra et al. [196] studied the natural convection of nanofluids inside horizontal cylinder heated from one end and cooled from the other. They apparently observed in their experimental study the paradoxical behavior of heat transfer deterioration. The fluid shows characters distinction from that of common slurries and it appears to behave more homogeneously compared to common slurries. They documented that no evidence of long initial flow instability or stratification of concentration layers was found. Unlike conduction or forced convection, a systematic and definite deterioration in natural convective heat transfer was found to occur. The deterioration is dependent on particle density, concentration as well as the aspect ratio of the cylinder. The reason for this effect is unclear. They stated that the role of particle–fluid slip and sedimentation seems to be important. Their study indicates the need for more investigations to understand the physical phenomenon completely before using these fluids in practical cooling applications.

4.13.3. Boiling heat transfer

Khandekar et al. [197] designed, fabricated and tested a two-phase gravity assisted thermosyphon with three nanofluids based on water with 1 vol% of Al_2O_3, CuO, and laponite clay. According to their results, it was observed that thermal performance deteriorates when nanofluids are used as working fluids. Maximum deterioration was observed with laponite while minimum deterioration was for aluminum oxide particles based nanofluids. Increased thermal conductivity of the nanofluids does not appear to be affecting the nucleate pool boiling heat transfer coefficient although single-phase heat transfer improves. Boiling characteristics of nanofluids seems to be more effected by the physical interaction of nanoparticles with the nucleating cavities.

Migration characteristics of nanoparticles in the pool boiling process of nanorefrigerant and nanorefrigerant–oil mixture are fundamental knowledge for the application of nanorefrigerants in refrigeration systems. Dinga et al. [198] experimentally studied and numerically simulated the migration characteristics of nanoparticles in the nanorefrigerant–oil mixture as well as in the nanorefrigerant. Experimental results show that the migrated mass of nanoparticles in the pool boiling process of both nanorefrigerant and nanorefrigerant–oil mixture increases with the increase of the original mass of nanoparticles and the mass of refrigerant. The migration ratio decreases with the increase of volume fraction of nanoparticles. The migrated mass of nanoparticles and migration ratio in the nanorefrigerant are larger than those in the nanorefrigerant–oil mixture. A numerical model, which qualitatively well predicted the migrated mass of nanoparticles, was established, and the deviations between the model predictions and experimental data were in the range of 7.7–38.4%.

4.14. Applications of nanofluids

The demand to thermal systems has an ultra-high performance encouraged the researchers to focus their efforts to improve the energy efficient by using such fluids have high convective heat transfer coefficients as nanofluids. Nowadays, the nanofluids are being used in a wide range of industrial and commercial applications. A high performance of heat exchanger means a small size of the exchanger, light weight, low cost and diminishing in the fuel consumption in vehicle industries.

Walsh et al. [199] demonstrated that μ-PIV measurements are feasible in nanofluids and can significantly aid in their understanding, either by validating/negate many theories put forward to explain their enhanced transport properties or by providing the direction to develop more informed ones.

4.14.1. Heat pipes

Tsai et al. [200] studied the performance of nanofluids of aqueous gold nanoparticles solution used as a working fluid in heat pipe with different sizes and shapes of nanoparticles. Their results indicate that the thermal resistance of heat pipe is 37% for a nanofluid contains 0.2 ml of Na_3 citrate, 2.5 ml of Tannic acid and 3 ml of $HAuCL_4$ lower than that using DIW. They attributed this reduction in thermal resistance to that the suspended nanoparticles tend to bombard the vapor bubbles formed at the liquid–solid interface during their formation. So they reported it is expected that the nucleation size of vapor bubble is much smaller for fluid with suspended nanoparticles than that without them.

Chen [201] examined the effectiveness of existence of silver nanoparticles with 35 nm in diameter suspended with pure water filled flat heat pipe (FHP). He found a small temperature difference of FHP when a small amount of Ag nanoparticles added in the pure water. A 0.6 °C, 0.79 °C, and 1.24 °C temperature difference is shown at 5 ppm of nanoparticles and 20–40 W was

utilized. These values are decreased when the nanoparticles concentration increases until 100 ppm as much as he tested. His results also illustrate that the thermal resistance of FHP filled with pure water is higher than nanofluid under 20–40 W.

The efficiency of a two-phase closed thermosyphon using Al_2O_3 (< 100 nm)/water nanofluid was improved by Noie et al. [202]. Different volume fractions of nanoparticles 1–3% are suspended within the two-phase closed thermosyphon (TPCT). The results inspire that nanofluids in all concentration studied show better thermal performance than pure water. The efficiency of the TPCT has improved up to 14.7%. It is distinctly seen that the temperature distribution on the TPCT are lower compared to pure water. Temperature differences between the evaporator and condenser sections with nanofluids are less than that pure water. On the other hand, thermal resistance of the TPCT when charged with nanofluids is less. This finding makes nanofluid attractive as working fluid in heat pipe and thermosyphon technology that further investigations are needed.

Naphon et al. [203] studied the performance of heat pipe with de-ionic water, alcohol, and titanium with 21 nm in diameter suspended in alcohol. They observed a significant effect of the nanofluids on the enhancement of heat transfer due to higher heat capacity, higher thermal conductivity of working fluid and higher mixing fluctuation. They demonstrated that the heat pipe thermal efficiency increases with increasing nanoparticles concentration. It was seen that 10.6% enhancement in heat pipe thermal efficiency is achieved while a 0.1 vol% of nanoparticles is used compared to that of the base fluid. When the volume fraction of nanoparticles exceeds 0.1%, the properties of the nanofluids seem to be a solid phase thereby lower evaporation rate of working fluid in the evaporator section. This in turn reduces the thermal efficiency of heat pipe.

Shafahi et al. [204,205] performed analytical models to study the thermal performance of a rectangular and disk-shaped heat pipes using Al_2O_3, CuO, and TiO_2/water nanofluids with particle diameter ranged from 10 to 40 nm. They claimed that the liquid pressure drop decreases by using the nanoparticles within the water due to an increase in density. After reaching a critical concentration level, a reversal effect occurs resulting in an increase in the pressure drop as the increase in viscosity of the nanofluid. They screened a decrease in the velocity in both disk and rectangular shaped heat pipe when the concentration level increases. They showed that as the nanoparticle concentration increases the thermal conductivity of the nanofluid increases and then in turn the evaporator temperature decreases. They remarked that the smaller nanoparticles or larger concentration level the more pronounced the reduction in the temperature difference between the evaporator and the condenser. They have seen that the thermal resistance becomes smaller when a nanofluid is utilized. It can be reduced up to 83% of its initial resistance. They stated that the CuO/water nanofluid provides 30% and 20% reduction in the size of the disk and rectangular shaped heat pipes, respectively. The removal heat capacity from the disk-shaped heat pipe is shown in Fig. 43.

The same previous nanofluids with a cylindrical heat pipe are tested by Shafahi et al. [205]. They found that the nanofluids enhance the heat pipe's thermal performance by reducing the thermal resistance as the concentration increases or as the particle diameter decreases. They reported that smaller particles have pronounced effect on the temperature gradient along the heat pipe. Wei et al. [206] used an Ag/water nanofluid as a working fluid in a grooved circular heat pipe with average diameter of 10 nm. Their test results show that the average decrease of 30–70% in the thermal resistance of the heat pipe

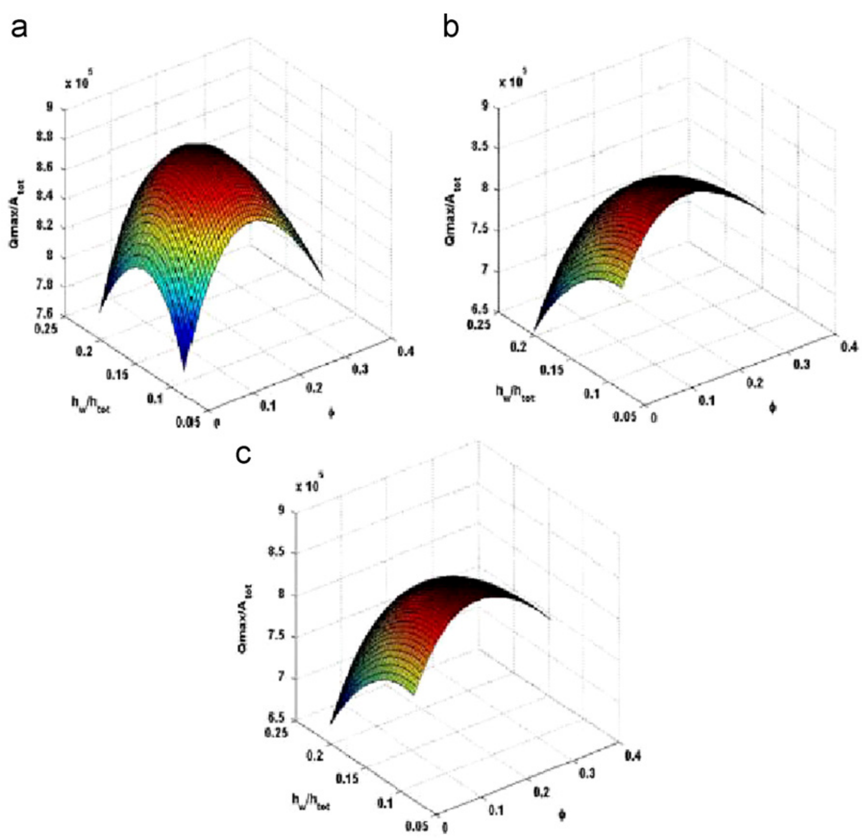


Fig. 43. Three dimensional representation of disk-shaped heat pipe maximum heat removal capability in terms of nanoparticles concentration levels and dimensionless thickness of the wick; (a) CuO, (b) Al_2O_3, and (c) TiO_2 [204].

with nanofluid as compared with pure water. Tsai et al. [200] examined a gold/water nanofluid as a working fluid in a conventional circular heat pipe. They designed the heat pipe as a heat spreader for CPU in a notebook or a desktop PC. They showed that at the same charge volume, there is a significant reduction in thermal resistance of heat pipe with nanofluid as compared with DI water. They reported that the thermal resistance of a vertical meshed heat pipe varies with the size of gold nanoparticles.

4.14.2. Electronics cooling

With the fast improvement of computer performance and the CPU chips become so small, a dramatic heat has been generated in the chips need to escape using such effective working fluid as nanofluids. Nguyen et al. [207] investigated experimentally the heat transfer performance by using the Al_2O_3–water nanofluid for a liquid system that is utilized for cooling of electronic components. They have found that convective heat transfer coefficient increases as much as 23% with respect to that of the base fluid with 4.5% nanoparticle volume concentration. It was observed from their results that an augmentation of particle concentration has produced a clear decrease of the junction temperature between the heated component and the water-cooling block. The results exhibit that for particular mass flow rate of 0.04 kg/s, the enhancement of the thermal performance is about 10% and 23% for nanofluids with 2.2% and 4.5% particle concentrations, respectively when compared to the corresponding results of distilled water.

Escher et al. [208] performed a systematic characterization of aqueous silica nanoparticle suspensions. They evaluated the potential of nanofluids for cooling of electronics by means of characterization of aqueous suspensions of silica nanoparticles for different volume fractions of 5–31%. They fabricated test-vehicles of microchannel heat sinks with three different channel widths. They found that an enlargement of the effective thermal mass which can be either achieved by increasing the heat capacity of the fluid or its density seems to be more promising to enhance the heat sink performance.

Jung and Yoo [209] proposed a novel expression for the thermal conductivity of nanofluids which incorporates the kinetic theory to describe the contribution of the Brownian motion of the nanoparticles with more realistic definition of the mean free path. Their expression also considers the contribution of the interparticle interaction due to the existence of the electrical double layer (EDL). They showed that this model is applied to Au/water nanofluids satisfactorily with respect to temperature, volume fraction and particle size. In the case of dense Al_2O_3/water, the effect of the interparticle interaction due to EDL on enhancing the thermal conductivity is more prominent than in the case of dilute Al_2O_3/water nanofluids. They outlined that this model shows that interparticle interaction due to EDL is the most responsible for the enhancement of thermal conductivity of nanofluids.

4.14.3. Microchannels

Tsai and Chein [210] performed an analytical study to examine the copper–water and carbon nanotube–water nanofluids as coolant in microchannel heat sink (MCHS). They found that the nanofluid reduces the temperature difference between the MCHS bottom wall and bulk nanofluid compared with that from pure fluid. This reduction of temperature is proportional to the particle volume fraction. This means a reduction will occur in conductive thermal resistance and an increase in convective thermal resistance when nanofluids are used due to the increase in viscosity and decrease in thermal capacity. They observed that the nanofluid has a significant effect on the MCHS performance when the channel aspect ratio and porosity are low. Shokouhmand et al. [211] studied analytically the influence of Cu–water nanofluid with various volume fraction on the thermal performance of a silicon MCHS. They emphasized that nanofluids could enhance MCHS performance compared with that using pure water as a coolant. The enhancement is due to the increase in thermal conductivity of coolant and the nanoparticle thermal dispersion effect. They observed that there is no extra pressure drop recorded as long as the nanoparticle is small and particle volume fraction is low.

Bhattacharya et al. [212] studied numerically the laminar forced convection heat transfer of Al_2O_3/H_2O nanofluid flowing in a silicon MCHS. They have seen that using nanofluid improves MCHS performance by reducing fin conductive thermal resistance. The improvement of MCHS performance becomes more pronounced with increase of nanoparticles concentration. However, they reported that there is an increase in pumping power by using nanofluids in MCHS which somewhat offsets the beneficial effect of using nanofluid. They revealed that the use the same nanoparticle concentration could give better synergy between velocity and temperature gradient vector at lower Reynolds number.

Ho et al. [213] conducted experiments to investigate the forced convective cooling performance of a copper MCHS with alumina/water nanofluid as the coolant in laminar regime. They remarked a significant high average heat transfer coefficient and markedly lower thermal resistance and wall temperature at high pumping power. Despite they marked increase in dynamic viscosity of nanofluid, the friction factor for the nanofluid was found slightly increased. It is observed an increase by about 70% in the average heat transfer coefficient with 1% nanoparticle concentration at $Re=1676$ compared with that with water. Lee and Mudawar [214] studied experimentally the effect of the same nanofluid implemented by Ho et al. [213] on the thermal performance of microchannel. Their results show a significant enhancement in thermal conductivity when nanofluid is used especially for laminar regime. High heat transfer coefficients were achieved mostly in the entrance region of microchannels. The enhancement was weaker in the fully developed region proving that nanoparticles have a remarked effect on thermal boundary layer development. Higher concentrations produced greater sensitivity to heat flux. They reported that despite this enhancement, the overall cooling effectiveness of nanoparticles was quite slight because of the large axial temperature rise associated with the decreased specific heat for the nanofluid compared to the base fluid.

Lee et al. [215] studied the effective convection coefficient and viscosity in microtubes ($D=0.5$ mm) along with stationary thermal conductivity measurements for (Al_2O_3, ZnO, and CuO) nanofluids and carbon nanotubes (CNT). They obtained an effective convection coefficient increase of 5% for 3 vol% of Al_2O_3/DIW nanofluid, 13.3% for 4 vol% of CuO/DIW nanofluid, and 11.6% for 0.2 vol% for CNT/DIW nanofluid.

Mohammed et al. [216] performed a 3-D simulation to study the effect of using Al_2O_3–H_2O nanofluids on heat transfer and fluid flow characteristics in rectangular microchannel heat sink (MCHS). Their results revealed that when the volume fraction of nanoparticles is increased under the extreme heat flux, both the heat transfer coefficient and wall shear stress are increased while the thermal resistance of the MCHS is decreased. Nanofluid with volume fraction of 5% could not be able to enhance the heat transfer or performing almost the same result as 0 vol% they found that a slight increase in the pressure drop in the MCHS compared with the pure water-cooled MCHS. While Gunnasegaran et al. [217] studied numerically in 3-D the effect of geometrical parameters which are rectangular, trapezoidal, and triangular on water flow and heat transfer characteristics in

microchannels. It is found that better uniformities in heat transfer coefficient and temperature can be obtained in the heat sinks having the smallest hydraulic diameter. It is also inferred that the heat sink having the smallest hydraulic diameter has better performance in terms of pressure drop and friction factor among other heat sinks studied. Mohammed et al. [218] performed a simulation to investigate the laminar flow and heat transfer characteristics of trapezoidal MCHS using various types of base nanofluids and various MCHS substrate materials on MCHS performance. they displayed that the best uniformities in heat transfer coefficient and temperature among the four mixture flows can be obtained using glycerin base nanofluid followed by oil-base nanofluid, EG-base nanofluid, and water-base nanofluid heat sinks. However, the heat transfer performance of water-base nanofluid can be greatly enhanced in steel made substrate heat sink.

4.14.4. Heat exchangers

Macro-compact heat exchangers have been widely used in various application thermal fluid systems including automotive thermal fluid systems, radiators for engine cooling systems, evaporators and condensers for HVAC systems, oil coolers and inter coolers. They are typical examples that can be found in vehicles have an important role in its weight and design of its front end module which has a strong impact on the car aerodynamic behavior [187].

Sundar et al. [219] studied experimentally the effect of the alumina/water nanofluid flowing through a copper tube subjected to constant heat flux boundary condition in the turbulent regime with and without tape insert. From their results, it was seen that further enhancement in heat transfer with twisted tape are achieved when compared to that in plain tubes using nanofluid at the same flow rate. Farajollahi et al. [186] measured the heat transfer characteristics of γ-Al_2O_3/water and TiO_2/water nanofluids in a shell and tube heat exchanger under turbulent flow condition. Based on the results, adding the nanoparticles to the base fluid causes a significant enhancement of heat transfer characteristics. For both nanofluids, two different optimum nanoparticle concentrations are found. Comparison of heat transfer behavior of two nanofluids indicates that at a certain Peclet number, heat transfer characteristics of TiO_2/water nanofluid at its optimum nanoparticle concentration are higher than those of γ-Al_2O_3/water nanofluid. Whereas the latter nanofluid possesses a better heat transfer behavior at higher nanoparticle concentrations.

Hwang et al. [220] examined experimentally the heat transfer and pressure drop characteristics of alumina/water nanofluids flowing through a uniformly heated circular tube in the fully developed laminar regime. From their results, it was shown that the results for nanofluid friction factor show a good agreement with analytical predictions from Darcy's equation for single-phase flow. However, the convective heat transfer coefficient of the nanofluids increases up to 8% at a concentration of 0.3 vol% compared with that of pure water and this enhancement cannot be predicted by the Shah equation. Furthermore, it is observed that the convective heat transfer enhancement exceeds the thermal conductivity enhancement.

Vasu et al. [187] performed a theoretical analysis with ε-NTU rating method using also Al_2O_3/water nanofluid as coolant on automobile flat tube plain fin compact heat exchanger. The results indicate that nanofluids possess higher heat transfer characteristics than conventional coolant water. The overall heat transfer coefficient is higher for nanofluids than water and increases with an increase in the nanoparticles concentration. They highlighted that with the increase of the volume fraction the cooling capacity in moderate manner and pressure drop increase with coolant inlet temperature. But cooling capacity is high when compared with pure water. It can be seen that in Fig. 44.

Chopkar et al. [120] prepared a nanofluid containing a small amount (<1 vol%) of nanocrystalline metallic particle ($Al_{20}Cu_{30}$) as a stable colloidal dispersion in EG. Their study showed that the thermal conductivity is significantly greater 1.2–2 times than that of the base fluid as well as that predicted by the models. They pointed out that this enhancement of thermal conductivity is a function of size, volume fraction and thermal property of the solid suspension. A simple quenching experiment demonstrates that the efficiency of the nanofluid is better than that of the base fluid particularly at lower temperature. Hence, this nanofluid could be useful in microthermal heat transfer applications including in MEMS and automobiles.

Mapa and Mazhar [221] performed an experimental study to investigate the effect of the nanofluid on heat exchanger thermal performance. The nanofluid implemented in their experiments was 99% pure copper oxide pre-dispersed in water with an average particle size of 29 nm. They found that this nanofluid enhances the heat transfer rate. An increase in heat transfer rate is observed at any given flow rate. For example, at a mass flow rate of 0.005 kg/s, 5.5% increase in heat transfer rate is observed. As the concentration of nanoparticles in the fluid increases, a further increase in the heat transfer rate is observed. The presence of nanoparticles in base fluid reduces the thermal boundary layer thickness. Khoddamrezaee et al. [222] studied the influence of Al_2O_3–EG nanofluid and EG fluid which flow in a rectangular arrangement of tubes in a shell and tubes heat exchanger. They indicated that the use of alumina/EG nanofluid increases the heat transfer coefficient ratio by about 3.25 on the first column and 3.16 on the second column.

Advancement in the electronics industry led to the development of micro-scale heat transfer devices which offered high heat transfer coefficient in a compact size. The amount of research done in this particular field is fairly new and limited. Most studies done on microchannel devices and nanofluids recently have reported enhanced heat transfer capabilities and results that challenge traditional theories and limitations on heat transfer devices and fluids [223]. Mohammed et al. [224] studied numerically the effects of using various types of nanofluids on heat transfer and fluid flow characteristics in a square shaped of an aluminum microchannel heat exchanger (MCHE). They reported that the thermal properties and performance of the heat exchanger were enhanced using nanofluids while a slight increase in pressure drop was observed. They added that increasing the *Re* number causes an increase in the pumping power and a decrease in the effectiveness. While Mohammed et al. [225] found that an enhanced performance with the usage of nanofluids and slight penalty in pressure drop. The increase in *Re* number caused an increase in the heat transfer rate and a decrease in the overall bulk temperature of the cold fluid. The increase in nanoparticle volume fraction results better performance at the expense of increased pressure drop.

4.14.5. Solar collector

Heat transfer enhancement in solar devices is one of the key issues of energy saving and compact designs. The use of the additives is a technique applied to enhance the heat transfer performance of base fluids [226]. Natarajan and Sathish [226] concluded that the thermal conductivity enhancement depends on the volume fraction of the suspended particles and thermal conductivities of the particles and base fluids. Their experiments proved that the nanofluid is more effective than the conventional fluids. If these fluids are used as a heat transport medium, they increase the efficiency of the traditional solar water heater.

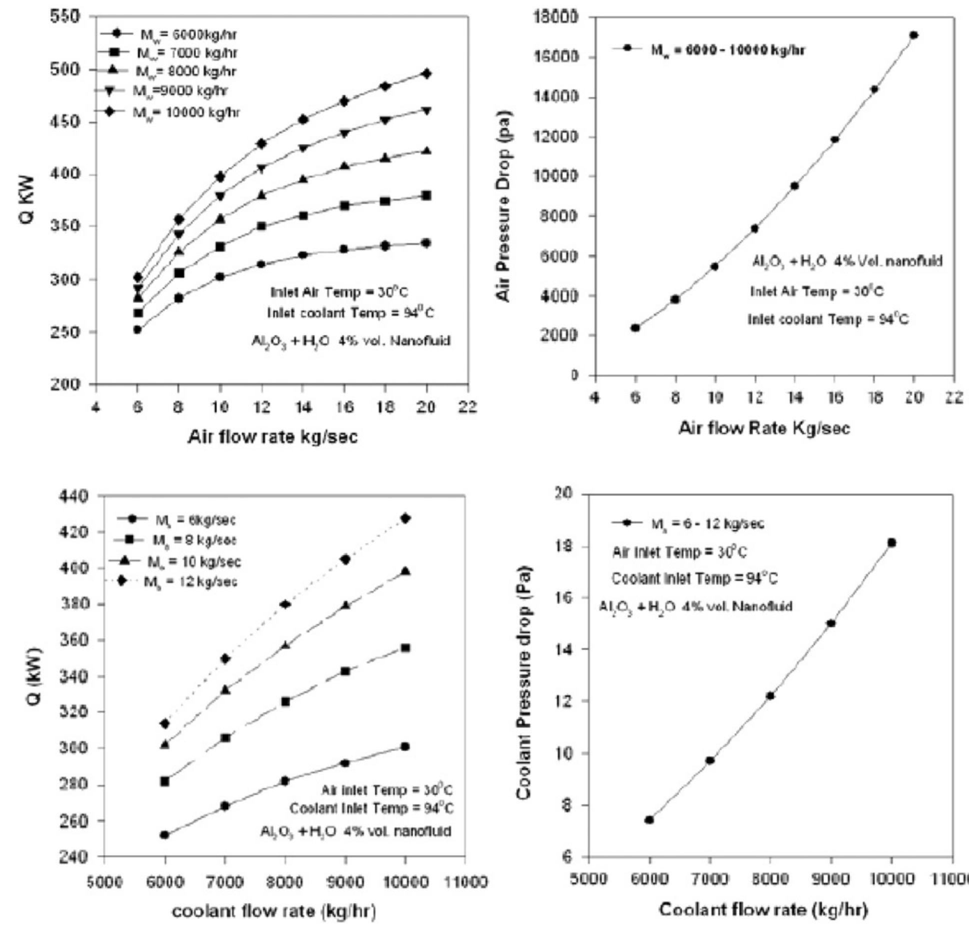


Fig. 44. Air and coolant flow influence on the thermal and fluid dynamic performance of compact heat exchanger [187].

Shahi et al. [227] numerically simulated the steady natural convictive flow and heat transfer in a single-ended tube with non-uniform heat input and with different inclination angle. This sample serves as a simplified model of the single-ended evacuated solar tube of a water-in-glass evacuated tube solar water heater. The sealed end of the tube is assumed to be adiabatic and the opening end is assumed to be subjected to copper–water nanofluid with particle concentration up to 0.05%. This study indicates that the maximum overall mean *Nu* number is obtained at 35° inclination angle, while the maximum output mass flow rate is increasing with the inclination angle. It is also obtained that both the *Nu* number and maximum output mass flow rate increasing function of solid concentration, but the presence of nanoparticles is more effective at the smaller inclination angles. Shin and Banerjee [228] tested two types of nanoparticles powder fine grained powders and coarse powders. They demonstrated that the electron microscopy of the samples reveal that the variation in thermophysical properties of the different samples was caused by the amount of the agglomeration of the nanoparticles as well as the formation of compressed phase. They showed that these nanomaterials can enable significantly reduction in the cost of solar thermal power.

4.15. Main problems of nanofluids

Despite the effectiveness of nanoparticles in enhancing the single-phase heat transfer coefficient by increasing the nanofluid thermal conductivity, especially for laminar flow, but there are some disadvantages of nanofluids such as; possible damage to flow loop by erosion, and inability to sustain flow boiling [214]. Other disadvantages can be summarized as follows:

4.15.1. Pressure drop

In 2002, Qiang and Yimin [229] carried out an experimental investigation to study the convection heat transfer and flow structure of the Cu–water nanofluid flows through a tube in laminar and turbulent regime. When the nanoparticles suspended in the water at lowervolume fraction the friction factor has not change. Therefore, they stated that nanofluid with so small nanoparticle concentration behaves like pure water as shown in Fig. 45 [229]. Compared with water, no significant augmentation in pressure drop for the nanofluid is found in all runs of the experiments [193].

The pressure drop of the CNTs suspended in distilled water and flows in a horizontal tube was also studied by Ko et al. [230]. They found that under the laminar flow conditions the friction factor of CNTs nanofluids stabilized by adding surfactant is much larger than that of CNTs nanofluids prepared by acid treatment, and both nanofluids show larger friction factors than distilled water. Under the turbulent flow conditions, the friction factor of both nanofluids becomes similar to that of the base fluids as the flow rate increases as can be seen in Fig. 46.

Sundar and Sharma [192] investigated numerically the turbulent fully developed flow heat transfer coefficient and friction factor of Al_2O_3/water and Al_2O_3/EG nanofluids in circular tube. They outlined that a 1.42 times of friction factor was achieved for a 4 vol% of nanoparticles and *Re* number of 30,000 over the base

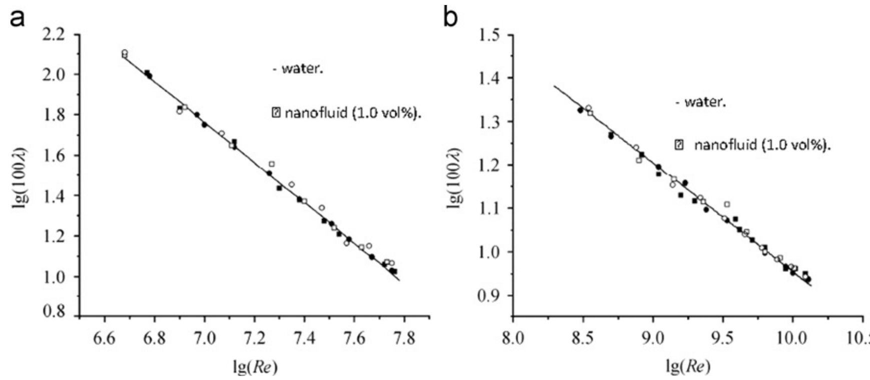


Fig. 45. (a) The friction factors of nanofluids for laminar flow and (b) the friction factors of nanofluids for turbulent flow [229].

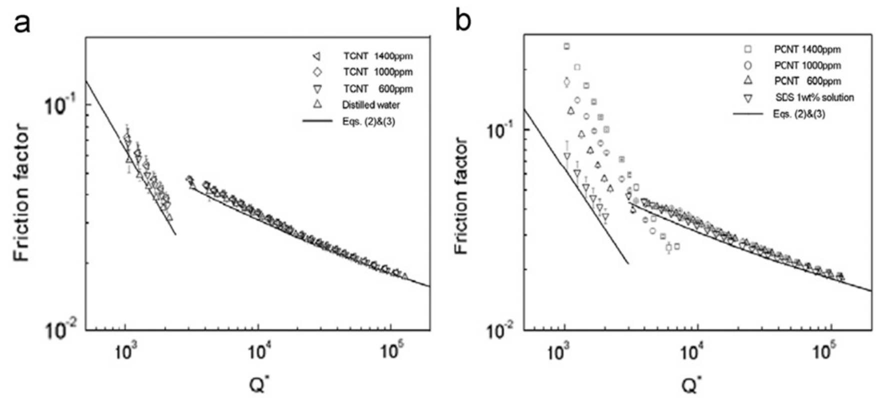


Fig. 46. Friction factor as a function of dimensionless flow rate [230].

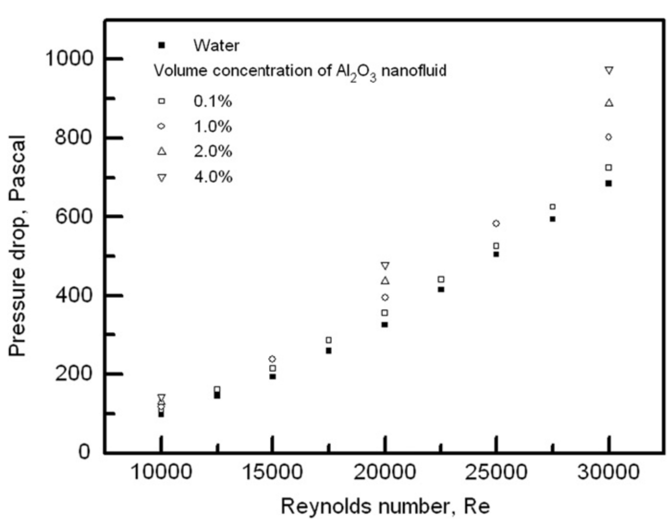


Fig. 47. Comparison of pressure drop of Al_2O_3 nanofluid in turbulent region [192].

fluid. They observed that pressure loss increases with increase in the volume fraction of the nanoparticles as shown in Fig. 47.

Bontemps et al. [231] performed experiments to investigate the behavior of SiO_2/water nanofluids inside a circular tube with imposed wall temperature. It was observed that high nanoparticle concentrations lead to surface modification probably due to particle deposition. This effect has to be confirmed for lower nanoparticle concentrations. In the turbulent regime, the pressure drop rapidly increased as a function of time to reach a maximum value. So they reported that Blasius law was not applicable anymore. They have seen an associated pressure drop to the presence of the nanoparticle in the base fluid. They observed the ageing effect just after loading the loop and after 40 h. Torii [157] revealed that the pressure drop of the nanofluids is slightly increased compared with that of the pure water, because an increase in the friction loss is caused by suspension of nanoparticles in the pure fluid. Lee and Mudawar [214] reported that the increasing in pumping power due to great pressure drop, and long-term fluid settling and potential clogging of flow passages are disadvantages of nanofluids.

4.15.2. High viscosity

The absolute viscosity of alumina/water nanofluid is increasing as the nanoparticles concentration increases and this trend is different for three nanoparticles [154–157]. Due to the large increase in viscosity than the increase in thermal conductivity, nanofluids would be poorer coolants as compared to base fluids if they are used in the existing heat transfer hardware [158]. The effective viscosities and effective thermal conductivities of the nanofluid are related to the aggregates of nanoparticles [232].

4.15.3. High cost of nanoparticles

Because of the ultra-fine techniques (nanotechnology) and high accurate equipment used to synthesize and produce nanometer size, the nanofluid has a high cost. So, the high price of the nanofluid is one of the major barriers to apply nanofluids in a wide range of applications up to date. Lee and Mudawar [214] reported the cost of nanofluids is one of the disadvantages. These factors restrain the researchers to enlarge the range of applications.

4.15.4. Low specific heat

As shown in literature, the specific heat of nanofluid is reversely proportional with the nanoparticles concentration [155,160,219]. If the concentration is more than the amount heat absorbed by the nanofluid [163]. Higher specific heat capacity of nanofluid, yields higher heat removal. An increased axial rise in wall temperature due to degraded specific heat is reported in negative side of nanofluids by Lee and Mudawar [160].

5. Conclusion

The heat transfer and flow structure characteristics are studied with the presence of vortex generators (VG). Different types of VGs are displayed. The VGs are embedded, attached, punched or mounted in laminar or turbulent boundary layer were investigated. The impact of VG on convective heat transfer coefficient and friction factor when VGs are present in rectangular channel, triangular duct, flat-plate, fin-tube heat sink, and plate heat exchanger were reviewed. Several arrangements for single, row, and two-dimensional array of VGs through the flow direction are summarized. The main conclusions can be briefly drawn as follows:

- Longitudinal vortices have as significant effective than the transverse vortices on heat transfer enhancement.
- Pointing down rectangular winglet vortex generators yield higher heat transfer rate than pointing up rectangular winglet vortex generators.
- Common flow-down VG gives better heat transfer characteristics than the common flow-up VG when a pair of DWVG is embedded in turbulent boundary layer of rectangular channel.
- Winglets provide better performance in heat transfer than wings. Delta-winglet pair performs slightly better than a rectangular-winglet pair for identical parameters.
- Maximum heat transfer for the case with rectangular winglet pair occurs at attack angle range between 45° and 65° and this maximum is smaller than that of delta–winglet pair of VG. While at 90° a sharp decrease in *Nu* number was observed.
- Combined ribs and delta-winglet vortex generator give significant increase in heat transfer rate over the smooth channel.
- A dramatic enhancement of heat transfer was observed when winglets placed on louvered of louvered fin heat exchanger.
- The position of VG plays an important role on the performance of heat transfer and Nu number decreases with the space between the LVG pair decreases.
- Longitudinal vortex generators can improve the synergy between the velocity and temperature field not only in the region near LVG but also in the large downstream region of LVG.
- Heat transfer becomes steady at lower *Re* number while it becomes unsteady at the higher *Re* number values when VG is used.
- The heat transfer rate and pressure drop directly increase with angle of attack, mass flow rate, length of vortex generator, and height of vortex generator (which should not be more than half of the channel height).
- VGs were successfully used in narrow and microchannels to improve the heat transfer rate.

This paper also presents an overview of recent developments in the experimental results and the numerical correlations on thermal conductivity using nanofluids. From literature, it can be summarized that nanofluids have high thermal conductivity compared to the conventional base fluids which is affected by several parameters. Nanoparticle concentration, nanoparticle size, nanoparticle type, nanoparticle shape, nanofluid temperature, base fluid type, and thermal stability are the parameters that influence the thermal conductivity of nanofluids. According to the high value of thermal conductivity of nanofluids, nanofluids are very suitable to be used as a working fluid in a wide range of applications especially when the pressure drop penalty accomplished the use of nanofluid is too small or nil. As a conclusion:

- A small amount of nanoparticles suspended in a base fluid provides substantially higher thermal conductivity than that of base fluid.
- In order to find out the temperature dependence of thermal conductivity of nanofluids, experiments were performed at room temperature up to 420 K. No paper has been yet published to report experiments dealing with low range of temperatures (<0 °C).
- For forced convection heat transfer, convective heat transfer coefficient increases with nanoparticle concentration when the mass flow rate is kept constant.
- Theoretically, viscosity, as well as the effective thermal conductivity of nanofluid, plays a key role in the natural convection heat transfer.
- Distinct deviations in the values of thermal conductivities of nanofluids obtained by models. Lack of theoretical understanding of the heat transfer mechanism using nanofluid. Therefore, further investigations are too necessary in future. Lack of agreement in the experimental results from different groups about the pressure drop associated to the suspension of nanoparticles in the base fluid.

Nanofluids open wide directions in the applications of thermal systems. Therefore, often research efforts are necessary to focus on the applications of nanofluids such as engineering, medical and space applications.

6. Outlook and future challenges

Further efforts are too necessary in future to focus on finding out new models and correlations to predict precise thermal conductivities with small deviation with the experimental results. Furthermore, future work should be done to give an explanation of heat transfer mechanism of nanofluids. The development in nanotechnology will be fruitful and helpful for nanofluid investigation. Combined VG and nanoparticles are new innovative idea in order to improve the performance of thermal systems which did not reported yet in the open literature. Wide opportunities will be opened when authors focus their efforts on using nanofluids combined with VGs in micro-scale heat exchangers and heat sinks. The results of the heat transfer and pressure drops of nanofluids in different shapes of compact heat exchangers and heat sinks gave high deviations compared to the results obtained by the theoretical correlations and experimental results obtained by using base fluids. So the behavior of the nanofluids is definitely different than the trend of the base fluids which motivate the investigators to concentrate their researches to perform a lot of experiments to study the characteristics of nanofluids in several micro-scale channels configurations to derive correlations for Nusselt number and friction factor particular for nanofluids to aid authors to compare the numerical data with the experiments.

References

[1] Wang C, Lo J, Lin Y, Liu M. Flow visualization of wave–type vortex generators having inline fin–tube arrangement. International Journal of Heat and Mass Transfer 2002;45:1933–44.

[2] Depaiwa N, Chompookham T, Promvonge P. Thermal enhancement in a solar air heater channel using rectangular winglet vortex generators. In: International conference on energy and sustainable development; 2010. p. 1–7.
[3] Min C, Qi C, Kong X, Dong J. Experimental study of rectangular channel with modified rectangular longitudinal vortex generators. International Journal of Heat and Mass Transfer 2010;53:3023–9.
[4] Shi B, Wang L, Gen F, Zhang Y. The optimal fin spacing for three–row flat tube bank fin mounted with vortex generators. Journal of Heat and Mass Transfer 2006;43:91–101.
[5] Wu JM, Tao WQ. Numerical study on laminar convection heat transfer in a rectangular channel with longitudinal vortex generator. Part A: Verification of field synergy principle. International Journal of Heat and Mass Transfer 2008;51:1179–91.
[6] Chang L, Wang L, Song K, Sun D, Fan J. Numerical study of the relationship between heat transfer enhancement and absolute vorticity flux along main flow direction in a channel formed by a flat tube bank fin with vortex generators. International Journal of Heat and Mass Transfer 2009;52:1794–801.
[7] Hernon, D, Hyde, MG, Patten, N. Comparison between time and averaged and instantaneous PIV and hotwire measurements downstream of a delta winglet pair. Summer of heat transfer conference; 2009. p. 1–8.
[8] Henze M, Wolfersdorf J von. Influence of approach flow conditions on heat transfer behind vortex generators. International Journal of Heat and Mass Transfer 2011;54:279–87.
[9] Torii K, Kwak KM, Nishino K. Heat transfer enhancement accompanying pressure–loss reduction with winglet-type vortex generators for fin–tube heat exchangers. International Journal of Heat and Mass Transfer 2002;45:3795–801.
[10] Zhang YH, Wang LB, Ke F, Su YX, Gao SD. The effect of span position of winglet vortex generator on local heat/mass transfer over a three–row flat tube bank fin. Journal of Heat and Mass Transfer 2004;40:881–91.
[11] Wang C, Lo J, Lin Y, Wei C. Flow visualization of annular and delta winglet vortex generators in fin-and-tube heat exchanger application. International Journal of Heat and Mass Transfer 2002;45:3803–15.
[12] Ahmed ST, Mohammed WS, Laith JH. Numerical investigation into velocity and temperature fields over smooth and rough ducts for several types of turbulators. Journal of Engineering Technology 2007;25(10):1110–28.
[13] Gorji M, Soleimani S, Hossein F. Pressure and heat transfer in staggered arrangement circular tubes with airfoil vortex generator. In: International conference on sustainable development; 2007. p. 1–5.
[14] Sanders PA, Thole KA. Effects of winglets to augment tube wall heat transfer in louvered fin heat exchangers. International Journal of Heat and Mass Transfer 2006;49:4058–69.
[15] Joardar A, Jacobi AM. A numerical study of flow and heat transfer enhancement using an array of delta–winglet vortex generators in a fin-and-tube heat exchanger. Journal of Heat Transfer 2007;129:1156–67.
[16] Yoo S, Park D, Chung M. Heat transfer enhancement for fin–tube heat exchanger using vortex generators. International Jourrnal of KSME 2002;16(1):109–15.
[17] Promvonge P, Chompookham T, Kwankaomeng S, Thianpong C. Enhanced heat transfer in a triangular ribbed channel with longitudinal vortex generators. Journal of Energy Conversion Management 2010;51:1242–9.
[18] Chompookham T, Thianpong C, Kwankaomeng S, Promvonge P. Heat transfer augmentation in a wedge–ribbed channel using winglet vortex generators. Intenational Journal of Communications in Heat and Mass Transfer 2010;37:163–9.
[19] Pauley WR, Eaton JK. The effect of embedded longitudinal vortex array on turbulent boundary layer heat transfer. Journal of Heat Transfer 1994;116:871–85.
[20] Wroblewski DE, Eibeck PA. Measurements of turbulent heat transfer in a boundary layer with an embedded streamwise vortex. International Journal of Heat and Mass Transfer 1991;34(7):1617–31.
[21] Kotcioğlu I, Ayhan T, Olgun H, Ayhan B. Heat transfer and flow structure in a rectangular channel with wing-type vortex generator. Journal of Engineering Environmental Science 1998;22:185–95.
[22] Allison CB, Dally BB. Effect of a delta–winglet vortex pair on the performance of a tube–fin heat exchanger. International Journal of Heat and Mass Transfer 2007;50:5065–72.
[23] Li Xiao-wei Yan H, Ji-an Meng, Li Zhi-xin. Visualization of longitudinal vortex flow in an enhanced heat transfer tube. Experimental Thermal and Fluid Science 2007;31:601–8.
[24] Kenan Y, Bayram S, Cafer C, Nihal A, Aslihan K. Effects of tapes with double-sided delta-winglets on heat and vortex characteristics. Applied Energy 2005;80:77–95.
[25] Kim E, Yang JS. An experimental study of heat transfer characteristics of a pair of longitudinal vortices using color capturing technique. International Journal of Heat and Mass Transfer 2002;45:3349–56.
[26] Qiuwang W, Qiuyang C, Ling W, Min Z, Yanping H, Zejun X. Experimental study of heat transfer enhancement in narrow rectangular channel with longitudinal vortex generators. Nuclear Engineering and Design 2007;237:686–93.
[27] Jian M, Yan PH, Jun H, Yan LW, Qiu WW. Experimental investigations on single-phase heat transfer enhancement with longitudinal vortices in narrow rectangular channel. Nuclear Engineering and Design 2010;240:92–102.
[28] Promvonge P, Khanoknaiyakarn C, Kwankaomeng S, Thianpong C. Thermal behavior in solar air heater channel fitted with combined rib and delta-winglet. International Communication on Heat and Mass Transfer 2011;38:749–56.
[29] Aris MS, McGlen R, Owen I, Sutcliffe CJ. An experimental investigation into the deployment of 3-D, finned wing and shape memory alloy vortex generators in a forced air convection heat pipe fin stack. Applied Thermal Engineering 2011;31:2230–40.
[30] Aris MS, Owen I, Sutcliffe CJ. The development of active vortex generators from shape memory alloys for the convective cooling of heated surfaces. International Journal of Heat and Mass Transfer 2011;54:3566–74.
[31] Mochizuki S, Kameda T, Yoneda H, Osaka H. Management of two-dimensional channel flow with a pair of streamwise vortices. Journal of Fluid Science Technology 2007;2(3):592–600.
[32] Charbel H, Serge R, Daniel B, Jean-Luc H, Thierry L, Dominique DV, et al. Enhancing heat transfer in vortex generator-type multifunctional heat exchangers. Applied Thermal Engineering 2012;38:14–25.
[33] Saraç BA, Bali T. An experimental study on heat transfer and pressure drop characteristics of decaying swirl flow through a circular pipe with a vortex generator. Experimental Thermal Fluid Science 2007;32:158–65.
[34] Wu JM, Tao WQ. Numerical study on laminar convection heat transfer in a channel with longitudinal vortex generator. Part B: Parametric study of major influence factors. International Journal of Heat and Mass Transfer 2008;51:3683–92.
[35] Yang JS, Lee DW, Choi GM. Numerical investigation of fluid flow and heat transfer characteristics by common-flow-up. International Journal of Heat and Mass Transfer 2008;51:6332–6.
[36] Biswas G, Chattopadhyay H. Heat transfer in channel with built-in wing-type vortex generators. International Journal of Heat and Mass Transfer 1992;35(4):803–14.
[37] Zhu JX, Fiebig M, Mitra NK. Numerical investigation of turbulent flows and heat transfer in a rib-roughened channel with longitudinal vortex generators. International Journal of Heat and Mass Transfer 1995;38(3): 495–501.
[38] Kaniewski M, Hahne HW, Mitra NK. Mass transfer enhancement by longitudinal vortices. Journal of Heat and Mass Transfer 1997;32:163–6.
[39] Rütten M, Krenkel L. Heat transfer enhancement by using vortex generators. ECCOMAS 2008. p. 1–2.
[40] Hiravennavar SR, Tulapurkara EG, Biswas G. A note on the flow and heat transfer enhancement in a channel with built-in winglet pair. International Journal of Heat and Fluid Flow 2007;28:299–305.
[41] Biswas G, Dep P, Biswas S. Generation of longitudinal streamwise vortices–a device for improving heat exchanger design. Journal of Heat Transfer 1994;116:588–97.
[42] Deb P, Biswas G, Mitra NK. Heat transfer and flow structure in laminar and turbulent flows in a rectangular channel with longitudinal vortices. International Journal of Heat and Mass Transfer 1995;38(13):2427–44.
[43] Sohankar A. Heat transfer augmentation in a rectangular channel with a vee–shaped vortex generator. International Journal of Heat and Fluid Flow 2007;28:306–17.
[44] Munish G, Kasana K, Vasudevan R. Heat transfer augmentation in a plate–fin heat exchanger using rectangular winglet. Journal of Heat Transfer—Asian Research 2010;2:1–43.
[45] Munish G, Kasana K, Vasudevan R. A numerical study of the effect on flow structure and heat transfer of a rectangular winglet pair in a plate fin heat exchanger. Journal of Mechanical Engineering Science 2009;223(Part C):2109–15.
[46] Nakod PM, Prabhu SV, Vedula RP. Heat transfer augmentation between impinging circular air jet and flat plate using finned surface and vortex generators. Experimental Thermal Fluid Science 2008;32:1168–87.
[47] Joardar A, Jacobi AM. Impact of leading edge delta-wing vortex generators on the thermal performance of the flat tube, louvered-fin compact heat exchanger. International Journal of Heat and Mass Transfer 2005;48: 1480–93.
[48] Gentry MC, Jacobi AM. Heat transfer enhancement by delta–wing vortex generators on a flat plate: vortex interactions with the boundary layer. Journal of Experimental Thermal and Fluid Science 1997;14:231–42.
[49] Chen TY, Shu HT. Flow structures and heat transfer characteristics in fan flows with and without delta-wing vortex generators. Experimental Thermal and Fluid Science 2004;28:273–82.
[50] Tiggelbeck S, Mitra NK, Fiebig M. Comparison of wing-type vortex generators for heat transfer enhancement in channel flows. Journal of Heat Transfer 1994;116:880–5.
[51] Wu JM, Tao WQ. Effect of longitudinal vortex generator on heat transfer in rectangular channels. Applied Thermal Engineering 2012;37:67–72.
[52] Guobing Z, Qiuling Y. Experimental investigations of thermal and flow characteristics of curved trapezoidal winglet type vortex generators. Applied Thermal Engineering 2012;37:241–8.
[53] Li-Ting T, Ya-Ling H, Yong-Gang L, Wen-Quan T. Numerical study of fluid flow and heat transfer in a flat-plate channel with longitudinal vortex generators by applying field synergy principle analysis. International Communications in Heat and Mass Transfer 2009;36:111–20.
[54] Akcayoglu A. Flow past confined delta-wing type vortex generators. Experimental Thermal Fluid Science 2011;35:112–20.
[55] Ferrouillat S, Tochon P, Garnier C, Peerhossaini H. Intensification of heat-transfer and mixing in multifunctional heat exchangers by artificially

generated streamwise vorticity. Applied Thermal Engineering 2006;26: 1820–9.
[56] Ahmad S, Lars D. Numerical study of heat and flow in a plate-fin heat exchanger with vortex generators. Turbulence Heat and Mass Transfer 2003;4:1155–62.
[57] Leu J, Wu Y, Jang J. Heat transfer and fluid flow analysis in plate-fin and tube heat exchangers with a pair of block shape vortex generators. International Journal of Heat and Mass Transfer 2004;47:4327–38.
[58] Jalil JM, Abdulla HK, Yousif AH. Effect of winglet shape on heat transfer from heated cylinder in cross flow. JKAU Engineering Science 2006;17(2): 119–30.
[59] Joardar A, Jacobi AM. Heat transfer enhancement by winglet-type vortex generator arrays in compact plain-fin-and-tube heat exchangers. International Journal of Refrigeration 2008;31:87–97.
[60] Kwak KM, Torii K, Nishino K. Heat transfer and pressure loss penalty for the number of tube rows of staggered finned-tube bundles with a single transverse row of winglets. International Journal of Heat and Mass Transfer 2003;46:175–80.
[61] Tang LH, Zeng M, Wang QW. Experimental and numerical investigation on air-side performance of fin-and-tube heat exchangers with various fin patterns. Experimental Thermal and Fluid Science 2009;33:818–27.
[62] Gorji M, Soleimani S, Jafari B. Numerical analysis of fluid flow in a duct around perpendicular cylinder with triangular cross section obstacle. Intrnational Journal of Dynamics of Fluids 2008;4(2):93–107.
[63] Lei Y, He Y, Tian L, Chu P, Tao W. Hydrodynamics and heat transfer characteristics of a novel heat exchanger with delta–winglet vortex generators. Journal of Chemical Engineering Science 2010;65:1551–62.
[64] Gorji M., Soleimani S. Two dimensional analyses of flow and heat transfer around compact heat exchanger equipped with a triangular obstacle. In: International conference on sustainable development, challenge and opportunities for GMS 2007. p. 1–8.
[65] Ünal UO, Gören Ö. Effect of vortex generators on the flow around a circular cylinder: computational investigation with two-equation turbulence models. Engineering Applications of Computational Mechanics 2011;5(1): 99–116.
[66] Li J, Wang S, Chen J, Lei Y. Numerical study on a slit fin-and-tube heat exchanger with longitudinal vortex generators. International Journal of Heat and Mass Transfer 2011;54:1743–51.
[67] Zeng M, Tang LH, Lin M, Wang QW. Optimization of heat exchangers with vortex-generator fin by taguchi method. Applied Thermal Engineering 2010;30:1775–83.
[68] Wu JM, Tao WQ. Investigation on laminar convection heat transfer in fin-and-tube heat exchanger in aligned arrangement with longitudinal vortex generator from the viewpoint of field synergy principle. Applied Thermal Engineering 2007;27:2609–17.
[69] Tiwari S, Maurya D, Biswas G, Eswaran V. Heat transfer enhancement in cross-flow heat exchangers using oval tubes and multiple delta winglets. International Journal of Heat and Mass Transfer 2003;46:2841–56.
[70] Chu P, He YL, Lei YG, Tian LT, Li R. Three-dimensional numerical study on fin-and-oval-tube heat exchanger with longitudinal vortex generators. Applied Thermal Engineering 2009;29:859–76.
[71] Chen Y, Fiebig M, Mitra NK. Heat transfer enhancement of finned oval tubes with staggered punched longitudinal vortex generators. International Journal of Heat and Mass Transfer 2000;43:417–35.
[72] Song K, Wang L, Fan J, Zhang Y, Liu S. Numerical study of heat transfer enhancement of finned flat tube bank fin with vortex generators mounted on both surfaces of the fin. Journal of Heat and Mass Transfer 2008;44: 959–67.
[73] Chen Y, Feibig M, Mitra NK. Conjugate heat transfer of a finned oval tube with a punched longitudinal vortex generator in form of a delta winglet–parametric investigations of the winglet. International Journal of Heat and Mass Transfer 1998;41:3961–78.
[74] Lemouedda A, Breuer M, Franz E, Botsch T, Delgado A. Optimization of the angle of attack of vortex generators in a plate-fin-and-tube heat exchanger. International Journal of Heat and Mass Transfer 2010;53:5386–99.
[75] O'Brien JE, Sohal MS, Foust TD, Wallstedt PC. Heat transfer enhancement for finned-tube heat exchanger with vortex generators: experimental and numerical results. INEEL/CON–01–01491, 2002.
[76] Dake T, Majdalani J. Improving flow circulation in heat sinks using quadrupole vortices. ASME summer heat transfer conference, 2009; p. 1–8.
[77] Kai-Shing Y, Jhih-Hao J, Yur-Tsai L, Kuo-Hsiang C, Chi-Chuan W. On the heat transfer characteristics of heat sinks: with and without vortex generators. IEEE Transactions on Components and Packaging Technologies 2010;33(2): 391–7.
[78] Kai-Shing Y, Shu-Lin L, Ing YC, Kuo-Hsiang C, Robert H, Chi-Chuan W. An experimental investigation of air cooling thermal module using various enhancements at low Reynolds number region. International Journal of Heat and Mass Transfer 2010;53:5675–81.
[79] Chomdee S, Kiatsiriroat T. Air-cooling enhancement with delta winglet vortex generators in entrance region of in-line array electronic modules. Journal of Heat Transfer Engineering 2007;28(4):372–9.
[80] Chomdee S, Kiatsiriroat T. Enhancement of air cooling in staggered array of electronic modules by integrating delta winglet vortex generators. International Communications in Heat and Mass Transfer 2006;33:618–26.
[81] Chao L, jyh-tong T, Jian-Cherng C, Yi-lang C, Suyi H, Shiping J, et al. Experimental investigation on liquid flow and heat transfer in rectangular microchannel with longitudinal vortex generators. International Journal of Heat and Mass Transfer 2011;54:3069–80.
[82] Sommers AD, Jacobi AM. Air-side heat transfer enhancement of s refrigerator evaporator using vortex generation. International Journal of Refrigeration 2005;28:1006–17.
[83] Sohal MS, O'Brien JE. Improving air-cooled condenser performance using winglet and oval tubes in a geothermal power plant. Geothermal resources council transactions, vol. 25; 2001. p. 1–7.
[84] Nsofor E. C. patents on nanofluids (nanoparticles in liquids) heat transfer. Recent Patents on Mechanical Engineering 2008;1:190–7.
[85] Xuan Y, Roetzel W. Concepts for heat transfer correlation of nanofluids. International Journal of Heat and Mass Transfer 2000;43:3701–7.
[86] Lazarus G, Raja B, Mohan LD, Wongwises S. Enhancement of heat transfer using nanofluids—an overview. Renewable and Sustainable Energy Reviews 2010;14:629–41.
[87] Weerapun D, Somchai W. A critical review of convective heat transfer of nanofluids. Renewable and Sustainable Energy Reviews 2007;11 797–17.
[88] Xiang-Qi W, Arun SM. A review on nanofluids—Part II: experimental and applications. Brazilian Journal of Chemical Engineering 2008;25(4):631–48.
[89] Kaufui VW, Omar DL. Review article applications of nanofluids: current and future. Advances in Mechanical Engineering 2010:1–11, http://dx.doi.org/10.1155/2010/519659.
[90] Visinee T, Somchai W. Critical review of heat transfer characteristics of nanofluids. Renewable and Sustainable Energy Reviews 2007;11:512–23.
[91] Xiang-Qi W, Arun SM. Heat transfer characteristics of nanofluids: a review. International Journalof Thermal Sciences 2007;46:1–19.
[92] Clement K, Yu F. Experimental and theoretical studies of nanofluid thermal conductivity enhancement: a review. Nanoscale Research Letters 2011;6(229): 1–13.
[93] Saidur R, Leong KY, Mohammad HA. A review on applications and challenges of nanofluids. Renewable and Sustainable Energy Reviews 2011;15:1646–68.
[94] Xuan Y, Li Q. Heat transfer enhancement of nanofluids. International Journal of Heat and Fluid Flow 2000;21:58–64.
[95] Yu W, France DM, Routbort JL, Choi SUS. Review and comparison of nanofluid thermal conductivity and heat transfer enhancements. Heat Transfer Engineering 2008;29(5):432–60.
[96] Romano JM, Parker JC, Ford QB. Application opportunities for nanoparticles made from condensation of physical vapor. Advances in Powder Metallurgy and Particulate Materials 1997;2:12–3.
[97] Liu Y, Zhou Y, Tong M, Zhou X. Experimental study of thermal conductivity and phase change performance of nanofluids PCMs, J. Microfluidics and Nanofluidics 2009;7 579–58.
[98] Zhu H, Han D, Meng Z, Wu D, Zhang C. Preparation and thermal conductivity of CuO nanofluid via a wet chemical method. Nanoscale Research Letters 2011;6(181):1–6.
[99] Sudhan EPJ, Meenakshi KS. Synthesis of silver nanofluid by a novel one pot method for heat transfer applications. Indian Journal of Science and Technology 2011;4(4):417–21.
[100] Keblinski P, Phillpot SR, Choi SUS, Eastman JA. Mechanisms of heat flow in suspensions of nano-sized particles (nanofluids). International Journal of Heat and Mass Transfer 2002;45:855–63.
[101] Nie C, Marlow WH, Hassan YA. Discussion of proposed mechanisms of thermal conductivity enhancement in nanofluids. International Journal of Heat and Mass Transfer 2008;51:1342–8.
[102] Ma K, Liu J. Nano liquid–metal fluid as ultimate coolant. Physica Letters 2007;361:252–6.
[103] Xie H, Wang J, Xi T, Liu Y. Thermal conductivity of suspensions containing nanosized SiC particles. International Journal of Thermophysics 2002;23(2):571–80.
[104] Assael MJ, Metaxa IN, Arvanitidis J, Christofilos D, Lioutas C. Thermal conductivity enhancement in aqueous suspensions of carbon multi-walled and double-walled nanotubes in the presence of two different dispersants. International Journal of Thermophysics 2005;26(3):647–64.
[105] Wu D, Zhu H, Wang L, Liu L. Critical issues in nanofluids preparation, characterization and thermal conductivity. Journal of Current Nanoscience 2009;5:103–12.
[106] Nagasaka Y, Nagashima A. Absolute measurement of the thermal conductivity of electrically conducting liquids by the transient hot wire method. Journal of Physics E: Scientific Instruments 1981;14:1435–40.
[107] Wang X, Xu X, Choi SUS. Thermal conductivity of nanoparticle–fluid mixture. Journal of Thermophysics and Heat Transfer 1999;13(4):474–80.
[108] Hu P, Shan W, Yu F, Chen Z. Thermal conductivity of ALN–ethanol nanofluids. International Journal of Thermophysics 2008;29:1968–73.
[109] Li CH, Williams W, Buongiorno J, Hu L, Peterson GP. Transient and steady-state experimental comparison study of effective thermal conductivity of Al2O3/water nanofluids. Journal of Heat Transfer 2008;130:1–7.
[110] Chen G, Yu W, Singh D, Cookson D, Routbort J. Application of SAXS to the study of particle-size-dependent thermal conductivity in silica nanofluids. Journal of Nanoparticle Research 2008;10:1109–14.
[111] Condreanu C, Condreanu N, Obreja VV. Experimental set-up for the measurement of the thermal conductivity of liquids. Brownian Journal of Information Science and Technology 2007;10(3):215–31.

[112] Tavman I, Turgut A, Chirtoc M, Schuchmann HP, Tavman S. Experimental investigation of viscosity and thermal conductivity of suspensions containing nanosized ceramic particles. International Journal of World Academy Materials Manufacturing Engineering 2008;34(2):99–104.
[113] Oh D, Jain A, Eaton JK, Goodson KE, Lee JS. Thermal conductivity measurement and sedimentation detection of aluminum oxide nanofluids by using the 3x method. International Journal of Heat and Fluid Flow 2008;29: 1456–61.
[114] Hu P, Shan W, Yu F, Chen Z. Thermal conductivity of ALN–Ethanol nanofluids. International Journal of Thermophysics 2008;29:1968–73.
[115] Wei X, Zhu H, Kong T, Wang L. Synthesis and thermal conductivity of Cu_2O nanofluids. International Journal of Heat and Fluid Flow 2009;52:4371–4.
[116] Mintsa HA, Roy G, Nguyen CT. New temperature dependent thermal conductivity data of water based nanofluids. In: International conference on heat transfer, thermal engineering and environment; 2007. p. 290–4.
[117] Sundar LS, Sharma KV. Thermal conductivity enhancement of nanoparticles in distilled water. International Journal of Nanoparticles 2008;1(1):66–77.
[118] Sharma P, Baek I, Cho T, Park S, Lee KB. Enhancement of thermal conductivity of ethylene glycol based silver nanofluids. Powder Technology 2011;208:7–19.
[119] Han ZH, Yang B, Kim SH, Zachariah MR. Application of hybrid sphere/carbon nanotube particles in nanofluids. Journal of Nanotechology 2007;18:1–4.
[120] Chopkar M, Das PK, Manna I. Synthesis and charactization of nanofluid for advanced heat transfer applications. Scripta Materialia 2006;55:549–52.
[121] Bonnecaze RT, Brady JF. A method for determining the effective conductivity of dispersions of particles. Proceedings of the Royal Society London 1990;430:285–313.
[122] Cherkasova AS, Shan JW. Particle aspect-ratio effects on the thermal conductivity of micro- and nanoparticle suspensions. Journal of Heat Transfer 2008;130:1–7.
[123] Kondaraju S, Jin EK, Lee JS. Direct numerical simulation of thermal conductivity of nanofluids: the effect of temperature two-way coupling and coagulation of particles. International Journal of Heat and Mass Transfer 2010;53:862–9.
[124] Yu W, Choi SUS. The role of interfacial layers in the enhanced thermal conductivity of nanofluids: a renovated Hamilton–Crosser model. Journal of Nanoparticle Research 2004;6:355–61.
[125] Shukla RK, Dhir VK. Numerical study of the effective thermal conductivity of nanofluids. In: Summer heat transfer conference. USA: ASME; 2005. p. 1–9.
[126] Kumar PC, Kumar J, Sendhilnathan S. Theoretical model to determine the thermal conductivity of nanofluids. International Journal of Engineering Science and Technology 2010;2(7):2846–52.
[127] Putnam SA, Cahill DG, Braun PV. Thermal conductivity of nanoparticle suspension. Journal of Applied Physics 2006;99:1–6.
[128] Murshed SMS, Leong KC, Yang C. Investigations of thermal conductivity and viscosity of nanofluids. International Journal of Thermal Science 2008;47:560–8.
[129] Wang B, Zhou L, Peng X. A fractal model for predicting the effective thermal conductivity of liquid with suspension of nanoparticles. International Journal of Heat and Mass Transfer 2003;46:2665–72.
[130] Emami M, Vafaie M, Rashidi A, amrollahi A, Tabasi M, Sid H. A model for thermal conductivity of nanofluids. Materials Chemistry and Physics 2010;123:639–43.
[131] Corcione M. Empirical correlating equations for predicting the effective thermal conductivity and dynamic viscosity of nanofluids. Energy Conversion and Management 2011;52:789–93.
[132] Corcione M. Heat transfer features of buoyancy-driven nanofluids inside rectangular enclosure differentially heated at the sidewalls. International Journal of Thermal Science 2010;49:1536–46.
[133] Chon CH, Kihm KD, Lee SP, Choi SUS. Emperical correlation finding the role of temperature and particle size for nanofluid (Al_2O_3) thermal conductivity enhancement. Applied Physics Letters 2005;87:1–3.
[134] Ghasemi B, Aminossadati SM. Brownian motion of nanoparticles in a triangular enclosure with natural convection. International Journal of Thermal Science 2010;49:931–40.
[135] Meibodi ME, Sefti MV, Rashidi AM, Amrollahi A, Tabasi M, Kalal HS. Simple model for thermal conductivity of nanofluids using resistance model approach. International Communications in Heat and Mass Transfer 2010;37:555–9.
[136] Beck MP, Sun T, Teja AS. The thermal conductivity of alumina nanoparticles dispersed in ethylene glycol. Fluid Phase Equilibria 2007;260:275–8.
[137] Hadjov KB. Modified self-consisted scheme to predict the thermal conductivity of nanofluids. Intrnational Journal of Thermal Science 2009;48:2249–54.
[138] Xue Q. Model for effective thermal conductivity of nanofluids. Physics Letters A 2003;307:313–7.
[139] Koo J, Kleinstreuer C. Impact analysis of nanoparticle motion mechanisms on the thermal conductivity of nanofluids. International Communications in Heat and Mass Transfer 2005;32:1111–8.
[140] Raykar VS, Singh AK. Dispersibility dependence of thermal conductivity of carbon nanotube based nanofluids. Physics Letters A 2010;374:4618–21.
[141] Murshed SMS, Leong KC, Yang C. A combined model for the effective thermal conductivity of nanofluids. Applied Thermal Engineering 2009;29:2477–83.
[142] Papari MM, Yousefi F, Moghadasi J, Karimi H, Campo A. Modeling thermal conductivity augmentation of nanofluids using diffusion neural networks. International Journal of Thermal Sciences 2011;50:44–52.
[143] Wang J, carson JK, North MF, Cleland DJ. A new structural model of effective thermal conductivity for heterogeneous materials with co-continuous phases. International Journal of Heat and Mass Transfer 2008;51:2389–97.
[144] Koroteeva O, Mogilevskaya S, Crouch S, Gordeliy A. A computational technique for evaluating the effective thermal conductivity of isotropic porous materials. Engineering Analysis with Boundary Elements 2010;34:793–801.
[145] Li CH, Peterson GP. Mixing effect on the enhancement of the effective thermal conductivity of nanoparticle suspensions (nanofluids). International Journal of Heat and Mass Transfer 2007;50:4668–77.
[146] Kolade B, Goodson KE, Eaton JK. Convective performance of nanofluids in a laminar thermal conductivity. Journal of Heat Transfer 2009;131:1–8.
[147] Koo J, Kleinstreuer C. A new thermal conductivity model for nanofluids. Journal of Nanoparticle Research 2004;6:577–88.
[148] Vajjha RS, Das DK. Experimental determination of thermal conductivity of three nanofluids and development of new correlations. International Journal of Heat and Mass Transfer 2009;52:4675–82.
[149] Yurong H, yubin M, Yunhua Z, Huilin L, Yulong D. Numerical investigation into the convective heat transfer of TiO_2 nanofluids flowing through a straight tube under the laminar flow conditions. Applied Thermal Engineering 2009;29:1965–72.
[150] Kuznetsov A. Nanofluid bioconvection in water-based suspensions containing nanoparticles and oxytactic microorganisms: oscillatory instability. Nanoscale Research Letters 2011;6(100):1–13.
[151] Karthikeyan NR, Philip J, Raj B. Effect of clustering on the thermal conductivity of nanofluids. Materials Chemistry and Physics 2008;109: 50–5.
[152] Luciu RS, Mateescu T, Cotorobai V, Mare T. Nusselt number and convection heat transfer coefficient for a coaxial heat exchanger using Al_2O_3–water pH=5 nanofluid. Buletinul Institutului Politehnic Din Iai 2009;2:71–80.
[153] Einstein A. A new determination of molecular dimensions. Annals of Physics 1906;19:289–306.
[154] Koo J, Kleinstreuer C. Laminar nanofluid in micro-heat sinks. International Journal of Heat and Mass Transfer 2005;48(13):2652–61.
[155] Sommers AD, Yerkes KL. Experimental investigation into the convective heat transfer and system-level effects of Al_2O_3–propanol nanofluid. Journal of Nanoparticle Research 2010;12:1003–14.
[156] Torii S. Experimental study on convection heat transfer of aqueous suspensions of nano-diamond particles. In: International symposium on eco topia science 2007; ISET07. p. 352–7.
[157] Torii S. Turbulent heat transfer behavior of nanofluid in a circular tube heated under constant heat flux. Journal of Advanced in Mechanical Engineering 2010:1–7.
[158] Garg J, Poudel B, Chiesa M, Gordon JB, Ma JJ, Wang JB, et al. Enhanced thermal conductivity and viscosity of copper nanoparticles in ethylene glycol nanofluid. Journal of Applied Physics 2008;103:1–6.
[159] Schmidt AJ, Chiesa M, Torchinsky DH, Johnson JA, Boustani A, McKinley GH, et al. Experimental investigation of nanofluid shear and longitudinal viscosities. Journal of Applied Physics 2008;92:1–3.
[160] Duangthongsuk W, Wongwises S. Effect of thermophysical properties models on the predicting of the convective heat transfer coefficient for low concentration nanofluid. International Communications in Heat and Mass Transfer 2008;35:1320–6.
[161] Corcione MRayleigh-Bénard. Convection heat transfer in nanoparticle suspensions. International Journal of Heat and Fluid Flow 2011;32:65–77.
[162] Cianfrini M, Corcione M, Quintino A. Natural convection heat transfer of nanofluids in annular spaces between horizontal concentric cylinders. Applied Thermal Engineering 2011;31:4055–63.
[163] Sundar LS, Ramanathan S, Sharma KV, Babu PS. Temperature dependent flow characteristics of Al_2O_3 nanofluid. International Journal of Nanotechnology Applications 2007;1(2):35–44.
[164] Nguyen CT, Desgranges F, Roy G, Galanis N, Mare T, Boucher S, et al. Temperature and particle-size dependent viscosity data for water based nanofluids—hysteresis phenomenon. International Journal of Heat and Fluid Flow 2007;28(6):1492–506.
[165] Vajjha RS. Measurements of thermophysical properties of nanofluids and computation of heat transfer characteristics. MS thesis, Mechanical Engineering Department, University of Alaska Fairbanks, Fairbanks, AK, 2008.
[166] Das s k, Putra N, Thiesen P, Roetzel W. Temperature dependence of thermal conductivity enhancement for nanofluids. Journal of Heat Transfer 2003;125:567–74.
[167] Beck MP, Yuan Y, Warrier P, Teja AS. The thermal conductivity of alumina nanofluids in water, ethylene glycol, and ethylene glycol+water mixtures. Journal of Nanoparticle Research 2010;12:1469–77.
[168] Sunder LS, Sharma KV. Experimental determination of thermal conductivity of fluid containing oxide nanoparticles. International Journal of Dynamics of Fluids 2008;4(1):57–69.
[169] Izadi M, Hossainpour S, Jalali DV. Effects of nanolayer structure and Brownian motion of particles in thermal conductivity enhancement of nanofluids. International Journal of Mechanical Industrial and Aerospace Engineering 2009;3(4):201–4.

[170] Li CH, Peterson GP. Experimental investigation of temperature and volume fraction variations on the effective thermal conductivity of nanoparticle suspensions (nanofluids). Journal of Applied Physics 2006;99:1–8.
[171] Bianco V, Manca O, Nardini S. Numerical simulation of water/Al_2O_3 nanofluid turbulent convection. Journal of Advances in Mechanical Engineering 2010:1–10.
[172] Yu W, Xie H, Chen L, Li Y. Investigation on the thermal transport properties of ethylene glycol-based nanofluids containing copper nanoparticles. Journal of Powder Technology 2010;197:218–21.
[173] Sankar N, Mathew N, Sobhan CB. Molecular dynamics modeling of thermal conductivity enhancement in metal nanoparticle suspensions. International Communications in Heat and Mass Transfer 2008;35:867–72.
[174] Sundar LS, Sharma KV. Experimental determination of thermal conductivity of fluid containing oxide nanoparticles. International Journal of Dynamics of Fluids 2008;4(1):57–69.
[175] Kumar DH, Patel HE, Kumar VR, Sundararajan T, Pradeep T, Das SK. Model for heat conduction in nanofluids. The American Physical Society 2004;93(14):1–4.
[176] Jain S, Patel HE, Das SK. Brownian dynamic simulation for the prediction of effective thermal conductivity of nanofluid. Journal of Nanoparticle Research 2009;11:767–73.
[177] Labonte J, Nguyen CT, Roy G. Heat transfer enhancement in laminar flow using Al_2O_3–water nanofluid considering temperature-dependent properties. In: International conference on heat transfer, thermal engineering and environment; 2006. p. 331–36.
[178] Jang SP, Choi SUS. Effects of various parameters on nanofluids thermal conductivity. Journal of Heat Transfer 2007;129:617–23.
[179] Sun C, Lu W, Liu J, Bai B. Molecular dynamics simulation of nanofluid's effective thermal conductivity in high-shear-rate couette flow. International Journal of Heat and Mass Transfer 2011;54:2560–7.
[180] Vasu V, Krishna KR, Kumar ACS. Analytical prediction of forced convective heat transfer of fluids embedded with nanostructured materials (nanofluids). Journal of Physics 2007;69(3):411–21.
[181] Beck MP, Yuan Y, Warrier P, Teja AS. The effect of particle size on the thermal conductivity of alumina nanofluids. Journal of Nanoparticle Research 2009;11:1129–36.
[182] Kondaraju S, Jin EK, Lee JS. Effect of multi-sized nanoparticle distribution on the thermal conductivity of nanofluids. Journal of Microfluidics and Nanofluidics 2011;10(1):133–44.
[183] Lu W, Fan Q. Study for the particle's scale effect on some thermophysical properties of nanofluids by a simplified molecular dynamics method. Engineering Analysis with Boundary Elements 2008;32:282–9.
[184] Saterlie M, Sahin H, Kavlicoglu B, Liu Y, Graeve O. Particle size effects in the thermal conductivity enhancement of copper-based nanofluids. Nanoscale Research Letters 2011;6(217):1–7.
[185] Polidori G, Fohanno S, Nguyen CT. A note on heat transfer modeling of Newtonian nanofluids in laminar free convection. International Journal of Thermal Sciences 2007;46:739–44.
[186] Farajollahi B, Etemad SGh, Hojjat M. Heat transfer of nanofluids in a shell and tube heat exchanger. International Journal of Heat and Mass Transfer 2010;53:12–7.
[187] Vasu V, Krishna KR, Kumar ACS. Application of nanofluids in thermal design of compact heat exchanger. International Journal of Nanotechnology Applications 2008;2(1):75–87.
[188] Xie H, Yu W, Li Y, Chen L. Discussion on the thermal conductivity enhancement of nanofluids. Nanoscale Research Letters 2011;6(124):1–12.
[189] Rostamani M, Hosseinizadeh SF, Gorji M, Khodadadi JM. Numerical study of turbulent forced convection flow of nanofluids in a long horizontal duct considering variable properties. International Communications in Heat and Mass Transfer 2010;37:1426–31.
[190] Lotfi R, Saboohi Y, Rashidi AM. Numerical study of forced convective heat transfer of nanofluids: comparison of different approaches. International Communications in Heat and Mass Transfer 2010;37:74–8.
[191] Lai WY, Phelan PE, Vinod S. Convective heat transfer for water-based alumina nanofluids in a single 1.02-mm tube. Journal of Heat Transfer 2009;131:1–9.
[192] Sundar LS, Sharma KV. Numerical analysis of heat transfer and friction factor in a circular tube with Al_2O_3 nanofluid. Intrenational Journal of Dynamics Fluids 2008;4(2):121–9.
[193] Xuan Y, Li Q. Investigation on convective heat transfer and flow features of nanofluids. Journal of Heat Transfer 2003;125:151–5.
[194] Maïga SEB, Palm SJ, Nguyen CT, Roy G, Galanis N. Heat transfer enhancement by using nanofluids in forced convection flows. International Journal of Heat and Fluid Flow 2005;26:530–46.
[195] Jou R, Tzeng S. Numerical research of nature convective heat transfer enhancement filled with nanofluids in rectangular enclosures. International Communications in Heat Transfer 2006;33:727–36.
[196] Putra N, Roetzel W, Das SK. Natural convection of nano-fluids. Journal of Heat and Mass Transfer 2003;39:775–84.
[197] Khandekar S, Joshi YM, Mehta B. Thermal performance of closed two-phase thermosyphon using nanofluids. International Journal of Thermal Sciences 2008;47:659–67.
[198] Dinga G, Penga H, Jianga W, Gaob Y. The migration characteristics of nanoparticles in the pool boiling process of nanorefrigerant and nanorefrigerant–oil mixture. International Journal of Refrigeration 2009;32:114–23.
[199] Walsh PA, Egan VM, Walsh EJ. Novel micro-PIV study enables a greater understanding of nanoparticle suspension flows: nanofluids. Journal of Microfluidics and Nanofluidics 2010;8:837–42.
[200] Tsai CY, Chien HT, Ding PP, Chan B, Luh TY, Chen PH. Effect of structural character of gold nanoparticles in nanofluid on heat pipe thermal performance. Materials Letters 2004;58:1461–5.
[201] Chen Y. Experimental study of silver nanofluid on flat heat pipe thermal performance. Journal of Marine Science and Technology 2010;18(5):731–4.
[202] Noie SH, Heris SZ, Kahani M, Nowee SM. Heat transfer enhancement using Al_2O_3/water nanofluid in a two-phase closed thermosyphon. International Journal of Heat and Fluid Flow 2009;30:700–5.
[203] Naphon P, Assadamongkol P, Borirak T. Experimental investigation of titanium nanofluids on the heat pipe thermal efficiency. International Communications in Heat and Mass Transfer 2008;35:1316–9.
[204] Shafahi M, Bianco V, Vafai K, Manca O. Thermal performance of flat-shaped heat pipes using nanofluids. International Journal of Heat and Mass Transfer 2010;53:1438–45.
[205] Shafahi M, Bianco V, Vafai K, Manca O. An investigation of the thermal performance of cylindrical heat pipes using nanofluids. International Journal of Heat and Mass Transfer 2010;53:376–83.
[206] Wei W, Tsai S, Yang S, Kang S. Effect of nanofluid on heat pipe thermal performance. In: International conference on heat transfer, thermal engineering and environment; 2005. p. 115–7.
[207] Nguyen CT, Roy G, Galanis N, Suiro S. Heat transfer enhancement by using Al_2O_3–water nanofluid in a liquid cooling system for microprocessors. In: International conference on heat transfer, thermal engineering and environment; 2006. p. 103–8.
[208] Escher W, Brunschwiler T, Shalkevich N, Shalkevich A, Burgi T, Michel B, et al. On the cooling of electronics with nanofluids. Journal of Heat Transfer 2011;133:1–11.
[209] Jung J, Yoo J. Thermal conductivity enhancement of nanofluids in conjunction with electrical double layer (EDL). International Journal of Heat and Mass transfer 2009;52:525–8.
[210] Tsia T, Chein R. Performance analysis of nanofluid-cooled microchannel heat sinks. International Journal of Heat and Fluid Flow 2007;28:1013–26.
[211] Shokouhmand H, Ghazvini M, Shabanian J. Performance analysis of using nanofluids in microchannel heat sink in different flow regimes and its simulation using artificial neural network. In: Proceeding of the world congress on engineering, vol. 3, III, 2008. p. 1–6.
[212] Bhattacharya P, Samanta A, Chakraborty S. Numerical study of conjugate heat transfer in rectangular microchannel heat sink with Al_2O_3/H_2O nanofluid. Journal of Heat and Mass Transfer 2009;45:1323–33.
[213] Ho CJ, Wei LC, Li ZW. An experimental investigation of forced convective cooling performance of a microchannel heat sink with Al_2O_3/water nanofluid. Journal of Applied Thermal Engineering 2010;30:96–103.
[214] Lee J, Mudawar I. Assessment of the effectiveness of nanofluids for single-phase and two-phase heat transfer in micro-channels. International Journal of Heat and Mass Transfer 2007;50:452–63.
[215] Lee J, Gharagozloo PE, Kolade B, Eaton JK, Goodson KE. Nanofluid convection in microtubes. Journal of Heat Transfer 2010;132:1–5.
[216] Mohammed HA, Gunnasegaran P, Shuaib NH. Heat transfer in rectangular microchannels heat sink using nanofluids. Intrenational Communications in Heat and Mass Transfer 2010;37:1496–503.
[217] Gunnasegaran P, Mohammed HA, Shuaib NH. The effect of geometrical parameters on heat transfer characteristics of microchannels heat sink with different shapes. International Communications in Heat and Mass Transfer 2010;37:1078–86.
[218] Mohammed HA, Gunnasegaran P, Shuaib NH. Influence of various base nanofluids and substrate materials on heat transfer in trapezoidal microchannel heat sinks. International Communications in Heat and Mass Transfer 2011;38:194–201.
[219] Sundar LS, Sharma KV, Ramanathan S. Experimental investigation of heat transfer enhancements with Al_2O_3 nanofluid and twisted tape insert in a circular tube. International Journal of Nanotechnology Applications 2007;1(2):21–8.
[220] Hwang KS, Jang SP, Choi SUS. Flow and convective heat transfer characteristics of water-based Al_2O_3 nanofluids in fully developed laminar flow regime. International Journal of Heat and Mass Transfer 2009;52:193–9.
[221] Mapa LB, Mazhar S. Heat transfer in mini heat exchanger using nanofluids. In: Conference of American Society for Engineering Education; 2005. p. 1–6.
[222] Khoddamezaee F, Motallebzadeh R, Vahid DJ. Simulation of ($EG+Al_2O_3$) nanofluid through the shell and tube heat exchanger with rectangular arrangement of tubes and constant heat flux. Journal of Applied Science 2010;10(6):500–5.
[223] Mohammed HA, Bhaskaran G, Shuaib NH, Saidur R. Heat transfer and fluid flow characteristics in microchannels heat exchanger using nanofluids: a review. Renewable and Sustainable Energy Reviews 2011;15:1502–12.
[224] Mohammed HA, Bhaskaran G, Shuaib NH, Abu-Mulaweh HI. Influence of nanofluids on parallel flow square microchannel heat exchanger performance. International Communications in Heat and Mass Transfer 2011;38:1–9.
[225] Mohammed HA, Bhaskaran G, Shuaib NH, Saidur R. Numerical study of heat transfer enhancement of counter nanofluids flow in rectangular microchannel heat exchanger. Superlattices and Microstructures 2011;50:215–33.
[226] Natarajan E, Sathish R. Role of nanofluids in solar water heater. International Journal of Manufacturing Technology 2009:1–5.

[227] Shahi M, Mahmoudi AH, Talebi F. Numerical simulation of steady natural convection heat transfer in a 3-dimentional single-ended tube subjected to a nanofluid. International Communications in Heat and Mass Transfer 2010;37:1535–45.

[228] Shin D, Banerjee D. Effects of silica nanoparticles on enhancing the specific heat capacity of carbonate salt eutectic (work in progress). International Journal of Structural Changes in Solids-Mechanics and Applications 2010;2(2):25–31.

[229] Qiang L, Yimin X. Convective heat transfer and flow characteristics of Cu–water nanofluid. Science in China, Series E 2002;45(4):408–16.

[230] Ko GH, Heo K, Lee K, Kim DS, Kim C, Sohn Y, et al. An experimental study on the pressure drop of nanofluids containing carbon nanotubes in a horizontal tube. International Journal of Heat and Mass Transfer 2007;50:4749–53.

[231] Bontemps A, Ribeiro J, Ferrouillat S, Gruss J, Soriano O, Wang B. Experimental study of convective heat transfer and pressure loss of SiO_2/water nanofluids; Part 1: nanofluid characterization-imposed wall temperature. In: Thermal Issue in Engineering Technologies, ThETA 2; 2008. p. 261–70.

[232] Tao ZH, Jiang LC, Xiong WD, Ying ZC, Sheng 500YY. Preparation, characterization, viscosity and thermal conductivity of $CaCO_3$ aqueous nanofluids. Science China, Technological Science 2010;53(2):360–8.